UNIVERSITY OF CALIFORNIA

Santa Barbara

Developing a New Array of Sustainable Hydrotalcites as Catalysts for the Selective Reductive Disassembly of Lignin Model Compounds

A dissertation submitted in partial satisfaction of the

requirements for the degree Doctor of Philosophy

in Chemistry

by

Megan Amanda Chui

Committee in charge:

Professor Peter C. Ford, Chair

Professor Steven K. Buratto

Professor Alison Butler

Professor R. Daniel Little

September 2017

The dissertation of Megan Amanda Chui is approved.

_____
Steven K. Buratto

_____
Alison Butler

_____
R. Daniel Little

_____
Peter C. Ford, Committee Chair

September 2017

Developing a New Array of Sustainable Hydrotalcites as Catalysts for the Selective Reductive Disassembly of Lignin Model Compounds

ACKNOWLEDGEMENTS

I would like to acknowledge the National Science foundation for funding the Center for Sustainable Use of Renewable Feedstocks (CenSURF, NSF CHE-1240194), and the UCSB Partnership for International Research and Education in Electron Chemistry and Catalysis Interfaces (PIRE-ECCI, OISE-0968399). I would also like to acknowledge Duncan and Suzanne Mellichamp for the Mellichamp Sustainability Fellowship, and Mrs. Shawn Byers for the Women In STEM Fellowship.

I am forever grateful to have been surrounded by so many driven, creative, loving, hilarious people throughout graduate school. All of my fellow Ford Group members, especially Chris Bernt and Agustin Pierri, I would not have gotten this far without you. My wonderful undergraduates, Danielle Hamann, Anthony Tran, Grace Hubbell, and Lanja Karadagi, without you all, I would literally not have been able to run any reactions. I would also like to thank all of the CenSURF collaborators, visiting post docs, and professors for their help and guidance. Naku, Gustavo Metzker, your, ideas, support, and dedication made our paper come alive. Mauricio Boscolo, thank you for bringing me to Brazil and showing me the most beautiful country. I have never felt greater sense of strength and peace travelling alone in Rio de Janeiro. Alexei Iretski, thank you for coming back each summer and offering advice for every new project. I would also like to thank my dissertation committee: Dr. Buratto, Dr. Butler, and Dr. Little, thank you for your patience and support. Most importantly, I am thankful for my advisor Dr. Ford. I feel as though I have become a better scientist and person over the past five years because of your guidance and encouragement.

Words cannot express my gratitude for my friends and family, and their unconditional love and support. My Clay Bay Bay, we lived together for four years and I can't imagine going through graduate school without you by my side, keeping me sane and always laughing. My Ride or Dies: Nichole Antilla, Jessi Bryant, Erica Hord, and Nicole Wright, any time, day or night, you have all been there for me. Laura Robertson and Shannon Van Gundy, I will always cherish our 15-minute phone calls that always turn into three hours. Thank you to Michelle Quirico, for loving my horse and me as though we were your own. Thank you to my Mom, Dad, and big brother for loving and believing in me, when I didn't believe in myself. You have supported me through every endeavor I've pursued, with unwavering faith and enthusiasm. I am so lucky and proud to be your daughter and little sister.

Curriculum Vitae of Megan A. Chui

September 2017

SKILLS

Solid Characterization	Liquid/Gas Characterization	Software and Data Analysis
• BET	• GC-FID/MS/TCD	• Chemdraw
• TGA-MS	• GPC	• Graphpad Prism
• High Temp XRD	• ICP-OES	• Igor
	• LC-MS	• Microsoft Office
	• MALDI	
	• NMR	
	• UV-VIS/IR	

EDUCATION

Ph.D. University of California, Santa Barbara, Santa Barbara, CA — September 2017
Inorganic Chemistry

B.S. University of Miami, Coral Gables, FL — May 2012
Chemistry, minor in mathematics

RESEARCH EXPERIENCE (UNIVERSITY OF CALIFORNIA, SANTA BARBARA)

Graduate Student Researcher, Dr. Peter C. Ford — September 2012 - Present

- Designed, synthesized, and characterized a series of sustainable catalysts using BET, ICP-OES, TGA-MS, and powder XRD tuning the ideal surface area, pore size, volume, and metal composition towards the selective reduction of lignin model compounds and biomass to commodity chemicals.
- Researched the effects of the addition Lewis and Brønsted acids on hydrogenolysis, hydrodeoxygenation, methylation, and aromatic hydrogenation of lignin model compounds using GC and LC techniques. Extensive method development was necessary for good product separation and identification, resulting in a publication in ACS Sustainable Chemistry and Engineering.

Visiting Scholar, Dr. Mauricio Boscolo
Universidade Estadual Paulista, São José do Rio Preto — August - October 2015

- Developed a catalyst with varying copper and niobium concentrations to modify the conversion of lignin model compounds and sugarcane bagasse. Additional optimization of GC-FID/MS methods to identify a vast product distribution.

Visiting Scholar, Dr. Jinghong Zhou — April 2014
East China University of Science and Technology (Shanghai) — January- February 2015

- Utilized a high temperature and pressure flow reactor to tune reactivity and selectivity in order to probe the viability of scaling towards industrial processes with the established catalytic system.

RESEARCH EXPERIENCE (UNIVERSITY OF MIAMI)

Undergraduate Research Assistant, Dr. Carl D. Hoff January 2010 - July 2012

- Investigated the kinetics and thermodynamics of oxygen atom transfer to a vanadium complex. These studies were in collaboration with Dr. Rybak- Akimova, Dr. Temprado, and Dr. Cummins from Tufts University, Universidad of Alcalá, and Massachusetts Institute of Technology, respectively resulting in a publication in the Journal of the American Chemical Society.
- Measured the heat of bromination to a platinum complex in collaboration with Dr. Sharp at the University of Missouri resulting in a publication in Inorganic Chemistry.

Undergraduate Research Assistant, Dr. Rajeev Prabhakar May 2010 - July 2012

- Used Density Functional Theory (DFT) Computation to determine heat of reactions, entropy, and bond strengths of molecules found with Dr. Carl Hof

PUBLICATIONS

Chui, M., Metzker, G., Bernt, C.M., Tran, A.T., Burtoloso, C.B., Ford, P.C., 2016: Probing the Lignin Disassembly Pathways with Catalysts based on Cu-doped Porous Metal Oxides. *ACS Sus. Chem. & Eng.*, 2017, 5 (4), 3158-3169.

Barrett, J.A., Gao, Y., Bernt, C.M., **Chui, M.**, Tran, A.T., Foston, M.B., Ford, P.C. Enhancing Aromatic Production from Reductive Lignin Disassembly: *in Situ* O-methylation of Phenolic Intermediates. *ACS Sus. Chem. & Eng.*, 2016, 4 (12), 6877-6886.

Springer, S.D., He, J., **Chui, M.**, Little, R.D., Foston, M.B., Butler, A. Peroxidative Oxidation of Lignin and a Lignin Model Compound by a Manganese SALEN Derivative. *ACS Sus. Chem. & Eng.*, 2016, 4 (6), 3212-3219.

Pierri, A.E., Huang, P.J., Garcia, J.G., Stanfill, J.G., **Chui, M.**, Wu, G., Zheng, N., Ford, P.C. A PhotoCORM nanocarrier for CO release using NIR light. *Chem. Commun.*, 2015, 51, 2072-2075.

Palluccio, T.D., Rybak-Akimoca, E.V., Majumdar, S., Xiaochen, X., **Chui, M.**, Temprado, M., Silvia, J.S., Cozzolino, A.F., Tofan, D., Velian, A., Cummins, C.C., Captain, B., Hoff, C.D. Thermodynamic and Kinetic Study of Cleavage of the N-O Bond of N-Oxides by a Vanadium(III) Complex: Enhanced Oxygen Atom Transfer Reaction Rates for Adducts of Nitrous Oxide and Mesityl Nitrile Oxide. *J. Am. Chem. Soc.*, 2013, 135, 11357-11372.

Karikachery, A.R., Lee, H.B., Masjedi, M., Ross, A., Moody, M., Cai, X., **Chui, M.**, Hoff, C.D., Sharp, P.R. High Quantum Yield Molecular Bromine Photoelimination from Mononuclear Platinum(IV) Complexes. *Inorg. Chem.*, 2013, 52, 4113-4119.

PRESENTATIONS AND INVITED TALKS

Oral Presentation: Chui, M., Metzker, G., Bernt, C.M., Tran, A.T., Burtoloso, A.C.B., Ford, P.C. "Investigating Lignin Disassembly Pathways Through Modifications of Cu-doped Porous Metal Oxides". 253rd ACS National Meeting, *Division of Catalysis Science and Technology,* San Francisco, CA, April **2017**.

Invited Talk: "Enhancing the Reactivity of CuPMOs Towards Desired Products from Lignin Model Compounds". Renewable Carbon Workshop, University of California Santa Barbara, Santa Barbara, CA, September **2016**.

Oral Presentation: Chui, M., Metzker, G., Azumi, T., Bernt, C.M., Tran, A.T., Boscolo, M., Ford, P.C. Enhancing the reactivity of CuPMOs with Lewis and Bronstead Acids Towards Desired Products from Lignin Model Compounds and Biomass. 251st ACS National Meeting, *Division of Catalysis Science and Technology*, San Diego, CA, March **2016.**

Oral Presentation: Chui, M., Hamann, D., Tran, A.T., Brunner, F.M., Iretskii, A.V., Boscolo, M., Scott, S.S., Ford, P.C. Tuning the reductive disassembly of lignocellulosic biomass and model compounds using doped porous metal oxides. 248th ACS National Meeting, *Division of Inorganic Chemistry,* San Francisco, CA, August **2014.**

Oral Presentation: Chui, M., Johnson, B.N., Bernt, C.M., Ford. P.C., Van Koppen, P., Feldwinn, D.L. Partnership for elementary school outreach: Developing an inquiry-based module to investigate CO_2 production, consumption and levels of CO_2 in the environment. 248th ACS National Meeting, *Div. Chemical Education and Sci-Mix* San Francisco, CA, August **2014.**

FELLOWSHIPS AND AWARDS

Mellichamp Sustainability Fellowship	2016
Women in STEM Fellowship	2015-2016
University of California Santa Barbara Outstanding Service to the Chemistry Department	2014
The UCSB Partnership for International Research and Education in Electron Chemistry and Catalysis Interfaces (PIRE-ECCI) Fellowship	2013-2014
American Chemical Society Undergraduate Award in Inorganic Chemistry	2012
University of Miami Chemistry Department Award for Excellence in Inorganic Chemistry	2012
University of Miami College of Arts and Sciences Summer Research Fellowship For Underrepresented Minorities and Women	2011

ABSTRACT

Developing a New Array of Sustainable Hydrotalcites as Catalysts for the Selective Reductive Disassembly of Lignin Model Compounds

by

Megan Amanda Chui

Nearly completely reliant on petroleum for organic platform chemicals, we are in desperate need of a more sustainable source. Lignin, a renewable, abundant, oxygen and aromatic rich biopolymer, is an exceptional potential source of chemical feedstocks. Previous studies in our laboratory have shown that copper doped porous metal oxides (CuPMOs) in supercritical methanol (s.c.-MeOH) catalyze the conversion of lignins and lignocellulose composites such as sawdust to organic liquids without the formation of char. Due to the high complexity of lignin, maintaining aromatic content while achieving full conversion continues to be a challenge. Here we present the ongoing efforts towards understanding the reactivity and selectivity of lignin model compounds through catalyst modification.

First we examine the effects of doping the CuPMOs with a series of lanthanides (Pr, Nd, Sm, Eu, Gd, Tb, Dy, Ho, Er, Tm, Yb, Lu) with Phenyl β-D glucopyranoside (PDG), a model compound with a variety of linkages more reminiscent of cellulose. Then we discuss the effects of introducing samarium(III), homogenously and heterogeneously, and formic acid,

into the catalytic system. The models studied are benzyl phenyl ether, 2-phenylethyl phenyl ether, diphenyl ether, biphenyl, and 2,3-dihydrobenzofuran, which are respective mimetics of the α-O-4, β-O-4, 4-O-5, 5-5, and β-5 linkages characteristic of lignin. Also, briefly investigated as a substrate is poplar organosolv lignin. Next, we examine a niobium doped catalyst with α-O-4 benzyl phenyl ether, phenol, *o*-cresol, *m*-cresol, dimethylphenol and dimethylanisole towards selective methylation. Finally we investigate a molybdenum doped catalyst with α-O-4 linkage benzyl phenyl ether, β-5 linkage 2,3 dihydrobenzofuran, methyl p-toluene sulfonate and benzyl mercaptan to monitor the stability of the catalyst in the presence of sulfur. We discuss the aromaticity of the reaction products can be preserved through selective catalytic modifications.

TABLE OF CONTENTS

LIST OF FIGURES

Introduction*

A. Biomass: An Attractive Alternative to Petroleum

Plant biomass is often discussed as a renewable feedstock for production of chemicals and liquid fuels. However, its potential as an alternative to petroleum feedstocks is tempered by the difficulty in developing selective chemical transformations owing to the complexity and variability of this substrate.[1-6] Lignocellulose, the principal non-food biomass, is largely composed of three components, the carbohydrates cellulose and hemicellulose plus the aromatic biopolymer lignin. Selective conversion of the latter to higher-value chemicals is particularly challenging owing to its irregular and highly functionalized structure(s), variety of chemical linkages and source-dependent compositions. [6-11] As a consequence, the lignin rich black and red liquors, from Kraft and sulfite pulping, respectively, are often treated as waste byproducts by biomass-based industries such as paper manufacture and second-generation ethanol production from cellulose. Typically they are burned for low-grade heat. However, the high content of aromatic carbon also makes lignin an attractive target to develop as a feedstock for the production of chemicals, and that is one goal of this laboratory[12-16] as well as of numerous others.[17-30]

* Parts of this dissertation is reprinted with permission from Chui, M., Metzker, G., Bernt, C.M., Tran, A.T., Burtoloso, C.B., Ford, P.C., Probing the Lignin Disassembly Pathways with Catalysts based on Cu-doped Porous Metal Oxides. *ACS Sus. Chem. & Eng.*, 2017, 5 (4), 3158-3169. Copyright 2017 American Chemical Society.

Lignin is formed from three monolignol sub-units (p-coumaryl, sinapyl and coniferyl alcohols) linked randomly by free radical pathways. It displays a variety of linkages between the component units, the common ones being β-O-4 (aryl ether), α-O-4 (aryl ether), β-5(dihydrobenzofuran-like), 4-O-5 (diaryl ether) and 5-5 (biphenyl) (Fig. 1). Although exact percentages vary from species to species and even within individuals of the same species, the β-O-4 is by far the most abundant, representing ~60% of such linkages in hardwoods and ~46% in softwoods.[10] For comparison, the other aryl ether linkages α-O-4 and 4-O-5 represent ~6-8% and ~6.5%, while the C-C linkages β-5 and 5-5 represent ~6% and 4.5%, respectively, in hardwoods.[10] Depending on the biomass application, lignin is separated from the carbohydrate components of lignocellulose by methods that may also modify the lignin structure.[8]

Figure 1. Hypothetical lignin fragment illustrating the most common linkages. The β-O-4 linkages are by far the most plentiful in hardwoods and softwoods.

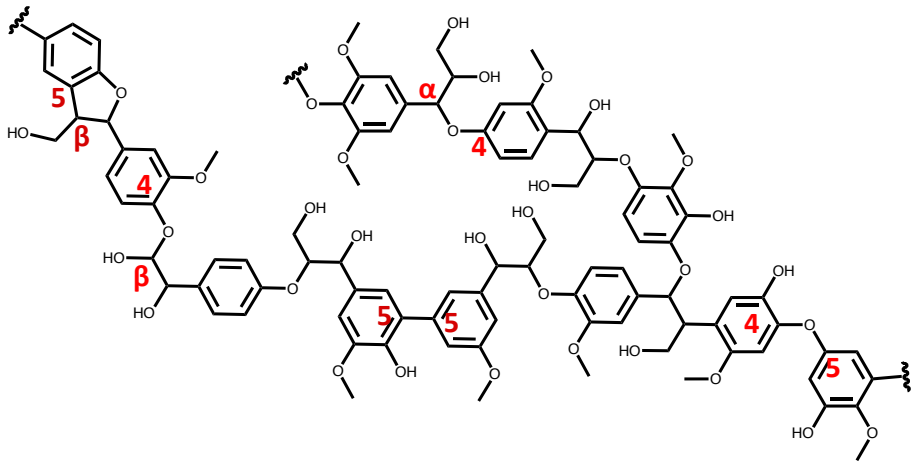

B. Developing New Heterogeneous Catalysts

Studies initiated at UCSB[12-14] developed a catalytic system using Cu-doped porous metal oxides (CuPMO) in super-critical methanol (sc-MeOH). The catalysts are based on Earth-abundant elements and are very effective in converting organosolv lignins, cellulose and even lignocellulose solids to organic liquids without forming intractable carbonaceous tars and chars. The sc-MeOH serves as the reaction medium *as well as* providing the H_2 reducing equivalents via reforming and water gas shift (eq 1 & 2).

$$CH_3OH \xrightleftharpoons{CuPMO} CO + 2\,H_2 \qquad \text{(eq. 1)}$$

$$CO + H_2O \xrightleftharpoons{CuPMO} CO_2 + H_2 \qquad \text{(eq. 2)}$$

These observations have stimulated subsequent studies that further demonstrated the utility of these and related Cu-doped catalysts in the reductive transformations of biomass-derived substrates. [31-38]

The CuPMOs are effective catalysts for the reductive disassembly of lignin in sc-MeOH owing to copper's multiple catalytic roles in alcohol reforming,[39,40] the water gas shift,[41] and the hydrogenolysis of lignin aryl ether linkages. This serendipity was first demonstrated in these laboratories with the model compound DHBF[12] and then extended to organosolv lignin[13] and lignocellulose[14] substrates. However, aryl ring hydrogenation and methylation are competitive with the desirable hydrogenolysis depolymerization and hydrodeoxygenation (HDO) pathways, resulting in product proliferation. Subsequent studies of temporal product distributions from several model substrates concluded that secondary

reactions of phenolic intermediates are largely responsible for this selectivity loss.[15,16] Simpler aromatics such as toluene are quite unreactive under these conditions.

The goal of this dissertation was to probe the effects of modifying the CuPMO catalyst on the hydrogenolysis reactions of model compounds representing key linkages noted above (Fig. 1). These model systems include organosolv poplar lignin (OPL) generated by moderate temperature extraction from Tulip poplar woodchips to give a methanol-soluble material with a molecular weight of ~3 kD [13,42,43] with a complexity representative of natural lignin was also studied.

The Cu_{20}PMO catalyst used in the earlier studies was prepared by calcining 3:1 Mg^{2+}:Al^{3+} hydrotalcite (HTC) in which 20% of the Mg^{2+} was replaced by Cu^{2+}. HTCs can be readily modified by doping with other M^{2+} and/or M^{3+} ions,[44-51] and such HTC-derived PMOs are solid bases that can catalyze the transesterification of triglyceride esters[52] and absorb atmospheric CO_2.[53] Furthermore, we have speculated[15] that deprotonation activates the phenolic intermediates of lignin disassembly toward secondary reactions; thus, it may be possible to enhance selectivity and/or reactivity by modifying the PMO support or by adding Brønsted or Lewis acids to the reaction medium. In this context are described catalysis studies with the substrates noted in which a variety of lanthanides (Pr^{3+}, Nd^{3+}, Sm^{3+}, Eu^{3+}, Gd^{3+}, Tb^{3+}, Dy^{3+}, Ho^{3+}, Er^{3+}, Tm^{3+}, Yb^{3+}, Lu^{3+}) have been incorporated into the PMO matrix of the CuPMO, Sm^{3+} simply added to the medium, and Nb^{5+} and Mo^{6+} deposited onto the surface of the PMO. We also describe analogous studies in which formic acid (FA) was added to the medium, since FA is of interest as a biomass-derived byproduct of chemical production from carbohydrates.[54]

C. References

1. Tuck, C. O.; Pérez, E.; Horváth, I. T.; Sheldon, R. A.; Poliakoff, M. Valorization of biomass: deriving more value from waste. Science **2012**, 337, 695-699.
2. Ruppert, A. M.; Weinberg, K.; Palkovits, R. Hydrogenolysis goes bio: from carbohydrates and sugar alcohols to platform chemicals. Angew. Chem. Int. Ed. **2012**, 51, 2564-2601.
3. Gallezot, P. Conversion of biomass to selected chemical products. Chem. Soc. Rev. **2012**, 41, 1538-1558.
4. Deuss, P. J.; Barta, K.; de Vries, J. G. Homogeneous catalysis for the conversion of biomass and biomass-derived platform chemicals. Catal. Sci. Technol. **2014**, 4, 1174-1196.
5. Gilkey, M. J.; Xu, B. Heterogeneous Catalytic Transfer Hydrogenation as an Effective Pathway in Biomass Upgrading. ACS Catal. **2016**, 6, 1420-1436.
6. Barta, K.; Ford, P. C. Catalytic conversion of nonfood woody biomass solids to organic liquids. Acc. Chem. Res. **2014**, 47, 1503-1512.
7. Boerjan, W.; Ralph, J.; Baucher. M. Lignin Biosynthesis. Annu. Rev. Plant Biol. **2003**, 54, 519-546.
8. Zakzeski, J.; Bruijnincx, P. C.; Jongerius, A. L.; Weckhuysen, B. M. The catalytic valorization of lignin for the production of renewable chemicals. Chem. Rev. **2010**, 110, 3552-3599.
9. Ragauskas, A. J.; Beckham, G. T.; Biddy, M. J.; Chandra, R.; Chen, F.; Davis, M. F.; Davison, B. H.; Dixon, R. A.; Gilna, P.; Keller, M.; Langan, P.; Naskar, A. K.; Saddler,

J. N.; Tschaplinski, T. J.; Tuskan, G. A.; Wyman, C. E. Lignin Valorization: Improving Lignin Processing in the Biorefinery. Science **2014**, 344, 709.

10. Pandey, M. P.; Kim, C. S.; Lignin Depolymerization and Conversion: A Review of Thermochemical Methods. Chem. Eng. Tech. **2011**, 34, 29-41.
11. Deuss, P. J.; Barta, K. From models to lignin: Transition metal catalysis for selective bond cleavage reactions. Coord. Chem. Rev. **2016**, 306, 510-532.
12. Macala, G. S.; Matson, T. D.; Johnson, C. L.; Lewis, R. S.; Iretskii, A. V.; Ford, P. C. Hydrogen transfer from supercritical methanol over a solid base catalyst: a model for lignin depolymerization. ChemSusChem, **2009**, 2, 215-217.
13. Barta, K.; Matson, T. D.; Fettig, M. L.; Scott, S. L.; Iretskii, A. V.; Ford, P. C. Catalytic disassembly of an organosolv lignin via hydrogen transfer from supercritical methanol. Green Chem. **2010**, 12, 1640-1647.
14. Matson, T. D.; Barta, K.; Iretskii, A. V.; Ford, P. C. One-pot catalytic conversion of cellulose and of woody biomass solids to liquid fuels. J. Am. Chem. Soc. **2011**, 133, 14090-14097.
15. Bernt, C. M.; Bottari, G.; Barrett, J. A.; Scott, S. L.; Barta, K.; Ford, P. C. Mapping reactivities of aromatic models with a lignin disassembly catalyst. Steps toward controlling product selectivity. Catal. Sci. Technol. **2016**, 6, 2984 - 2994.
16. Barrett, J. A.; Gao, Y.; Bernt, C. M.; Chui, M.; Tran, A. T., Foston, M. B.; Ford, P. C. Enhancing Aromatic Production from Reductive Lignin Disassembly: in Situ O-Methylation of Phenolic Intermediates. ACS Sustainable Chem. Eng. **2016**, 4, 6877-6886.

17. Hanson, S. K.; Wu, R.; Silks, L. A. C-C or C-O bond cleavage in a phenolic lignin model compound: selectivity depends on vanadium catalyst. Angew. Chem. Int. Ed. **2012**, 124, 3466-3469.
18. Sedai, B.; Baker, R. T. Copper Catalysts for selective C-C bond cleavage of b-O-4 lignin model compounds. Adv. Synth. Catal. **2014**, 356, 3563-3574.
19. Hanson, S. K.; Baker, R. T. Knocking on Wood: Base Metal Complexes as Catalysts for Selective Oxidation of Lignin Models and Extracts. Acc. Chem. Res. **2015**, 48, 2037-2048.
20. Rahimi, A.; Ulbrich, A.; Coon, J. J.; Stahl, S. S. Formic acid induced depolymerization of oxidized lignin to aromatics. Nature **2014**, 515, 249-252.
21. Zaheer, M. Kempe, R. Catalytic Hydrogenolysis of Aryl Ethers: A Key Step in Lignin Valorization to Valuable Chemicals. ACS Catal. **2015**, 5, 1675-1684.
22. Lohr, T. L.; Li, Z.; Marks, T. J. Selective Ether/Ester C−O Cleavage of an Acetylated Lignin Model via Tandem Catalysis. ACS Catal. **2015**, 5, 7004−7007.
23. Güvenatama, B.; Kursun, O.; Heeres, E. H. J.; Pidko, E. A.; Hensen, E. J. M. Hydrodeoxygenation of mono- and dimeric lignin model compounds on noble metal catalysts. Catal. Today **2014**, 233, 83-91.
24. Santos, R. S.; Hart, P. W.; Jameel, H.; Chang, H-M. Wood based lignin reactions important to the biorefinery and pulp and paper industries. BioRes. 2013, 8, 1456-1477.
25. Kong, J. He, M.; Lercher, J. A.; Zhao, C. Direct production of naphthenes and paraffins from lignin. Chem. Comm. **2015**, 51 17580-17583.
26. Rinaldi, R.; Schuth, F. Design of solid catalysts for the conversion of biomass. Energy Environ. Sci. **2009**, 2, 610-626.

27. Ferrini, P.; Rinaldi, R. Catalytic Biorefining of Plant Biomass to Non-Pyrolytic Lignin Bio-Oil and Carbohydrates through Hydrogen Transfer Reactions. Angew. Chem. Int. Ed. **2014**, 53, 8634-8639.
28. Trajano, H. L.; Engle, N. L.; Foston, M.; Ragauskas, A. J.; Tschaplinski, T. J.; Wyman, C. E. The fate of lignin during hydrothermal pretreatment. Biotechnol. Biofuels **2013**, 6, 110-116.
29. Ben, H.; Jarvis, M. W.; Nimlos, M. R.; Gjersing, E. L.; Sturgeon, M. R.; Foust, T. D.; Ragauskas, A. J.; Biddy, M. J. Application of a Pyroprobe-Deuterium NMR System: Deuterium Tracing and Mechanistic Study of Upgrading Process for Lignin Model Compounds. Energy & Fuels, **2016**, 30, 2968-2974.
30. Shuai, L.; Amiri, M. T.; Questell-Santiago, Y. M.; Héroguel, F.; Li, Y.; Kim, H.; Meilan, R.; Chapple, C.; Ralph, J.; Luterbacher, J. S. Formaldehyde stabilization facilitates lignin monomer production during biomass depolymerization Science, 2016 , 354, 329-333.
31. Hansen, T. S.; Barta, K.; Anastas, P. T.; Ford, P. C.; Riisager, A. One-pot reduction of 5-hydroxymethylfurfural via hydrogen transfer from supercritical methanol. Green Chem. **2012**, 14, 2457-2461.
32. Warner, G.; Hansen, T. S.; Riisager, A.; Beach, E. S.; Barta, K.; Anastas, P. T. Depolymerization of organosolv lignin using doped porous metal oxides in supercritical methanol. Bioresour. Technol. **2014**, 161, 78-83.
33. Barta, K.; Warner, G. R.; Beach, E. S.; Anastas, P. T. Depolymerization of organosolv lignin to aromatic compounds over Cu-doped porous metal oxides. Green Chem. **2014**, 16, 191-196.

34. Huang, X.; Koranyi, T. I.; Boot, M. D.; Hensen, E. J. M. Catalytic Depolymerization of Lignin in Supercritical Ethanol. ChemSusChem **2014**, 7, 2276-2288.

35. Huang, X.; Atay, C.; Koranyi, T. I.; Boot, M. D. Hensen, E. J. M. Role of Cu-Mg-Al Mixed Oxide Catalysts in Lignin Depolymerization in Supercritical Ethanol. ACS Catal. **2015**, 5, 7359-7370.

36. Chen, L.-C.; Cheng, H.; Chiang, C.-W.; Lin, S. D. Sustainable Hydrogen Production by Ethanol Steam Reforming using a Partially Reduced Copper-Nickel Oxide Catalyst. ChemSusChem **2015**, 8, 1787-1793.

37. Deutsch, K. L.; Shanks, B. H. Hydrodeoxygenation of lignin model compounds over a copper chromite catalyst. Appl. Catal. A-General, **2012**, 447, 144-150.

38. Strassberger, Z.; Alberts, A. H.; Louwerse, M. J.; Tanase, S.; Rothenberg, G. Catalytic cleavage of lignin beta-O-4 link mimics using copper on alumina and magnesia-alumina. Green Chem. **2013**, 15, 768-774.

39. Cunha, A. F.; Wu, Y. J.; Santos, J. C.; Rodrigues, A. E. Steam reforming of ethanol on copper catalysts derived from hydrotalcite-like materials. Ind. Eng. Chem. Res. **2012**, 51, 13132-13143.

40. Yong, S. T.; Ooi, C. W., Chai, S. P.; Wu, X. S. Review of methanol reforming-Cu-based catalysts, surface reaction mechanisms, and reaction schemes. Int. J. Hydrogen Energy **2013**, 38, 9541-9552.

41. Gokhale, A. A.; Dumesic, J. A.; Mavrikakis, M. On the Mechanism of Low-Temperature Water Gas Shift Reaction on Copper. J. Am. Chem. Soc. **2008**, 130, 1402–1414.

42. Azadi, R.; Inderwildi, O. R.; Farnood, R.; King, D. A. Renewable Liquid fuels, hydrogen and chemicals from lignin: A critical review. Sustainable Energy Rev. **2013**, 21, 506-523.
43. Li, M. F.; Sun, S. N.; Xu. F.; Sun, R. C. Organosolv Fraction of Lignocelluloses for Fuel, Chemicals and Materials. In Biomass Conversion: The Interface of Biotechnology, Chemistry and Materials Science, 1st ed.; Baskar, C.; Baskar, S.; Dhillon, R.; Eds., Springer Verlag, 2000, pp. 341-370.
44. Fan, G.; Li, F.; Evans, D. G.; Duan, X. Catalytic applications of double hydroxides: recent advances and perspectives. Chem. Soc. Rev. **2014**, 43, 7040-7066.
45. Wang, Q.; O'Hare, D. Recent Advances in the synthesis and application of layered double hydroxide (LDH) nanosheets. Chem. Rev. **2014**, 112, 4124-4155.
46. Sideris, P. J.; Nielsen, U. G.; Gan, Z.; Grey, C. P. Mg/Al ordering in layered double hydroxides revealed by multinuclear NMR spectroscopy. Science **2008**, 321, 113-117.
47. Debecker, D. P.; Gaigneaux, E. M.; Busca, G. Exploring tuning and exploiting the basicity of hydrotalcites for applications in heterogeneous catalysis Chem. Eur. J. **2009**, 15, 3920-3935.
48. Birjega, R.; Pavel, O. D.; Costentin, G.; Che, M.; Angelescu, E. Rare-earth elements modified hydrotalcites and corresponding mesoporous mixed oxides as basic solid catalysts. Appl. Catal. A **2005**, 288, 185-193.
49. Mitran, G.; Urda, A.; Tanchoux, N.; Fajula, F.; Marcu, I-C. Propane oxidative dehydrogenation over Ln–Mg–Al–O Catalysts (Ln = Ce, Sm, Dy, Yb). Catal. Lett. **2009**, 131, 250-257.

50. Wang, Z.; Yan, X.; Bi, X.; Wang, L.; Zhang, Z.; Jiang, Z.; Xiao, T.; Umar, A.; Wang, Q. Lanthanum-promoted copper-based hydrotalcites derived mixed oxides for NOx adsorption, soot combustion and simultaneous NOx soot removal. Mater. Res. Bull. **2014**, 51, 119-127.

51. Chen, C.; Xu, C.; Feng, L.; Li, Z.; Suo, J.; Qiu, F.; Yang, Y. Effect of rare earth doping on the catalytic activity of copper-containing hydrotalcites in phenol hydroxylation. Adv. Synth. Catal. **2005**, 347, 1848-1854.

52. Macala, G. S.; Robertson A. W.; Johnson, C. L.; Day, Z. B.; Lewis, R. S.; White, M. G.; Iretskii, A. V.; Ford, P. C. Transesterification catalysts from iron doped hydrotalcite-like precursors: solid bases for biodiesel production. Catal. Lett. **2008**, 122, 205-209.

53. Yavuz, C. T.; Shinall, B. D.; Iretskii, A. V.; White, M. G.; Golden, T.; Atilhan, M.; Ford, P. C.; Stucky, G. D. Markedly Improved CO2 Capture Efficiency and Stability of Gallium Substituted Hydrotalcites at Elevated Temperatures. Chem. Mater. **2009**, 21, 3473-3475.

54. Enthaler, S.; von Langermann, J.; Schmidt, T. Carbon Dioxide and formic acid – the couple for environmental-friendly hydrogen storage. Energy Environ. Sci. **2010**, 3, 1207-1217.

II. Screening Lanthanide Doped CuPMOs

A. Introduction

Comprising up to 40 % of lignocellulosic biomass is the organic biopolymer lignin. Due to the complexity of lignin, one of the main challenges in the practical conversion of biomass to chemicals and fuels is developing new catalysts to selectively cleave lignin aryl ether linkages while maintaining the oxygen content and aromatic functionality of the products from this resource. Copper doped porous metal oxides have previously shown to enhance the breakdown of biomass, organosolv lignin, and model compounds into smaller molecules, however, with little selectivity.[1-5] Normally the phenol/phenolate resonance structures regulates the stability of the molecule. But in the presence of a strong basic catalyst in superciticial methanol, phenol undergoes rapid hydrogenation. The experiments described here have focused on evaluating how the catalytic activity is affected by variations in the composition of the CuPMOs. The CuPMOs were doped with a series of lanthanides (Pr, Nd, Sm, Eu, Gd, Tb, Dy, Ho, Er, Tm, Yb, Lu) on the premise that increasing the acidic properties of the catalyst would activate C-O bond hydrogenolysis without forming the phenolate conjugate bases that were thought to activate the aromatic rings to hydrogenation.[6-8] The lanthanide doped CuPMOs were reacted with Phenyl β-D glucopyranoside (PDG), a model compound with a variety of linkages more reminiscent of cellulose (Figure 2).

Figure 2. Model compound phenyl β-D glucopyranoside

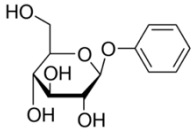

B. Experimental

Materials

Phenyl β-D glucopyranoside was purchased from Sigma Aldrich and methanol (99.5%, Aldrich) was dried over activated molecular sieves before use. Samarium triflate ($Sm(OTf)_3$•9 H_2O) was prepared by and gifted to us by J. Dethlefsen of the University of Copenhagen. The salts for the hydrotalcite synthesis, $Cu(NO_3)_2$•$3H_2O$, $Al(NO_3)_3$•$9H_2O$ and $Mg(NO_3)_2$•$6H_2O$, were purchased from Fisher Scientific and used without further purification.

Catalyst Preparation and Characterization

The Cu-doped porous metal oxide Cu_{20}PMO was prepared from Cu-doped HTC by calcining as described previously.[12-14] For all $Cu_{20}Ln_5$PMOs, (where Ln= Pr, Nd, Sm, Eu, Gd, Tb, Dy, Ho, Er, Tm, Yb, Lu) synthesis of the HTC precursor involved replacing 5 mol percent of the $Al(NO_3)_3$ component in the HTC preparation by $Ln(OTf)_3$. The procedure was otherwise the same as that employed for the synthesis of Cu_{20}PMOs.[2-4] A modified method for the preparation of all lanthanide and copper doped catalysts can be found in Appendix A. Both types of HTC precursors were calcined for 15 hours at 460 °C in air give the PMO within 24 hours prior to use in catalysis experiments. There was no difference in the reactivities of the PMO catalysts prepared by calcining freshly prepared HTCs and those that had been stored for up to 6 months before calcination.

Catalytic Reactions

The reactions in sc-MeOH were conducted in stainless steel mini-reactors as described before.[6] (*Caution! Under the reaction conditions, these vessels develop high internal pressures. Handle with care.)* For typical reactions with model compounds, the mini-

reactors (total volume 10 mL) were loaded with 3 mL of methanol, 100 mg of catalyst, and the substrate. The temporal evolution of the substrate phenyl β -D glucopyranoside and of each product was determined by preparing a series of 6 mini-reactors that were loaded identically and placed an oven thermostatted at 300 °C. After specific reaction intervals (1 to 18 hours), one of these mini-reactors was removed and cooled rapidly by immersing in a water bath to quench the reaction. The reactor was then opened to release the gases, and the volume released was measured by a water displacement method.[13,14] (*Warning: this step requires special care owing to the large volume of gas sometimes released*. *In addition, both H_2 and CO are released, so proper ventilation is required.*) After cooling, opening, and filtering the methanolic solution, the liquid was reduced to an oily residue under vacuum to remove the methanol. The residue was then dissolved in CD_3OD for analysis by ^1H NMR spectrometry on a Varian Unity Inova 500 MHz spectrometer The ^1H NMR spectra of the product mixtures were interpreted using the holistic analysis developed by Barta et al.[13] to evaluate relative quantities of aromatic (A_E), near oxygen (O_E) and aliphatic (H_E) protons. All NMR spectra were collected at room temperature with the d1 delay of 4.8 s. Although a longer d1 of 10 s gave slightly larger A_E values, this was not used owing to the much longer acquisition times required.

C. Results and Discussion

Prior to calcining, the precursor Cu_{20} and $Cu_{20}Sm_5$ HTCs were analyzed by XRD to check the hydrotalcite structure. The XRD patterns found for the Cu_{20} and $Cu_{20}Ln_5$ hydrotalcites (Appendix A) are consistent with the literature data for HTCs.[52]

Hollistic ^{1}H NMR anaylsis of products from phenyl β-D glucopyranoside

The product reaction mixtures were analyzed through a holistic interpretation of the proton NMR spectra developed by Barta et. al.[2] analyzing regions in the ^{1}H NMR spectrum. Aliphatic protons occur in the region 3.0-0.3 ppm, near oxygen protons in the region 5.0-3.0 ppm, and aromatic protons in the region7.2-5.0 ppm. The integrated peaks can be compared to determine a relative distribution.

Figure 3. Numerical indices to determine relative proton distribution

$$H_E = \left(\frac{R_H}{R_A + R_O + R_H}\right) \times 100$$

$$O_E = \left(\frac{R_O}{R_A + R_O + R_H}\right) \times 100$$

$$A_E = \left(\frac{R_A}{R_A + R_O + R_H}\right) \times 100$$

R_H is the integrated area of protons which resolve from 3.0 ppm, R_O is the integrated area of protons which resolve from 5.0-3.0 ppm, and R_A is the integrated area of protons which resolve from 7.2-5.0 ppm. H_E, O_E, and A_E are the experimentally calculated values.

Before reaction, PDG has 5 aromatic protons and 7 near oxygen protons, assuming the –OH protons exchange readily and do not resolve in the spectrum. In this case, the PDG spectrum would display 42 % A_E and 58 % O_E, which agrees with the measured values in Figure 4.

Figure 4: (Top) ^{1}H NMR of PDG in deuterated methanol. (Bottom) ^{1}H NMR of products from the reaction of PDG and methanol with the $Cu_{20}Lu_5PMO$ after 4 hours at 300 °C in CD_3O_D.

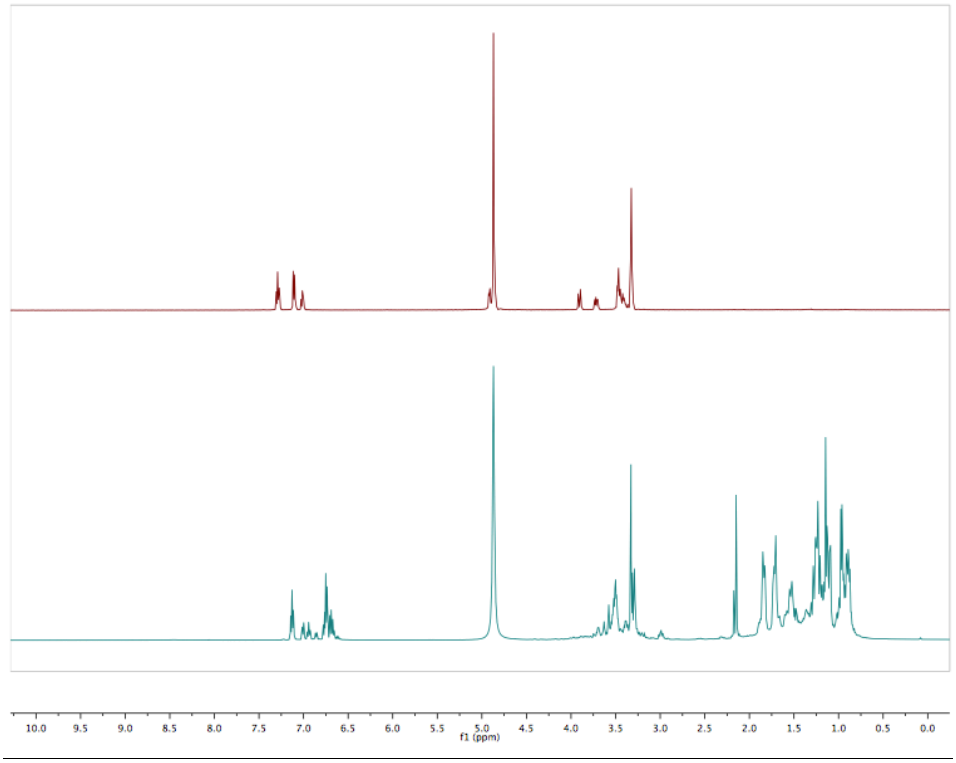

(Top) Before reaction the integrated areas aromatic protons and near oxygen protons are 56 % and 44 % respectively. Conditions: 100 mg catalyst, 100 mgs PDG, 3 mL of MeOH. (Bottom) After 4 hours at 300 °C, integrated areas for aliphatic protons, near oxygen protons, and aromatic protons are 71, 12, and 8 % respectively.

As expected, the pure PDG sample in deuterated methanol does not have any peaks in the region from 3.0-0.3 ppm as there are no aliphatic protons present in the sample. After the reaction, the increase in signal in the region from 3.0-0.3 ppm indicates that aliphatic carbons are being produced in the reaction. The decrease in the integrated signal in the 5.0-3.0 ppm region shows that oxygen is being removed from the substrate while the decrease in

the 7.2-5.0 ppm region and increase in the aliphatic region indicate that the aromatic carbons present are being hydrogenated. After 4 hours at 300 °C, the amount of oxygen removed reached a maximum of 12%. Decreases in O_E are very likely largely due to HDO of aliphatic carbons, while decreases in A_E can be attributed to ring hydrogenation and methylation. The catalyst is not capable of completely de-oxygenating the model compound, even after 18 hours. When developing new catalysts, it is not necessary for total deoxygenation. Some of the most widely used platform chemicals (succinic acid, terephthalic acid, and adipic acid) are all highly oxygenated species.[9]

Figure 5: ^{1}H NMR comparison of aliphatic (H) aromatic (A) and near oxygen (O) protons after reaction with Cu_{20} and $Cu_{20}Ln_5$ (where Ln= Pr, Nd, Sm, Eu, Gd, Tb, Dy, Ho, Er, Tm, Yb, Lu) catalysts after 6 hours reaction in sc-MeOH at 300 °C.

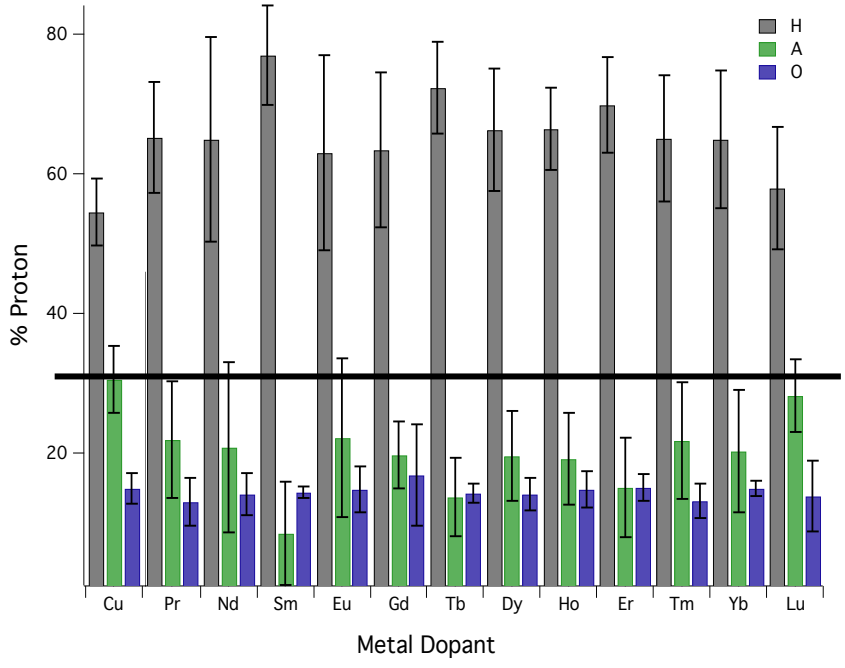

Figure 5 illustrates the distribution of aliphatic (H), aromatic (A) and near oxygen (O) protons after reacting at 300 °C for 6 hours with a variety of different catalysts. When reacting PDG with Cu_{20}PMO, the percentage of H, A, and O protons are 54, 31, 15 % respectively, and when reacted with a lanthanide, the average percentages were 66, 19, and 14 %, respectively, indicating a somewhat greater hydrogenation rates under these latter cases. This data is consistent with Figure 4, where we reached the maximum deoxygenation of this substrate possible under these conditions. We expected to observe a systematic trend in reactivity with the twelve different lanthanide dopants (Pr, Nd, Sm, Eu, Gd, Tb, Dy, Ho, Er, Tm, Yb, Lu) as their atomic radii decrease across the periodic table. Instead, we observed a seemingly random variation in reactivity with different lanthanide dopants in the catalyst. When compared to the original Cu_{20}PMO catalyst, the $Cu_{20}Sm_5$ exhibited the highest reactivity with the highest percentage of aliphatic protons and lowest percentage of aromatics. The $Cu_{20}Lu_5$PMO exhibited the lowest reactivity, similar to the original Cu_{20}PMO catalyst shown in Figure 5 and Appendix 13. $Cu_{20}Ho_5$PMO was seemingly one of the most active catalysts as determined by gas evolution. See Appendix A Table A1. Time-resolved experiments with PDG were conducted to compare the activity between normal Cu_{20} compared to $Cu_{20}Ho_5$PMOas shown below in Figure 6. When comparing the reaction of Cu_{20}PMO to $Cu_{20}Ho_5$PMO, the data was fit to an exponential curve. The rates of appearance of aliphatic protons, and of depletion of near oxygen and aromatic protons are all higher for the holmium doped catalyst as shown in Figure 6.

Figure 6. Temporal production aliphatic H_E protons (top left), near oxygen O_E protons (top right), and aromatic A_E protons from the reaction with Cu_{20}PMO (blue) and $Cu_{20}Ho_5$PMO with PDG over 18 hours at 300 °C.

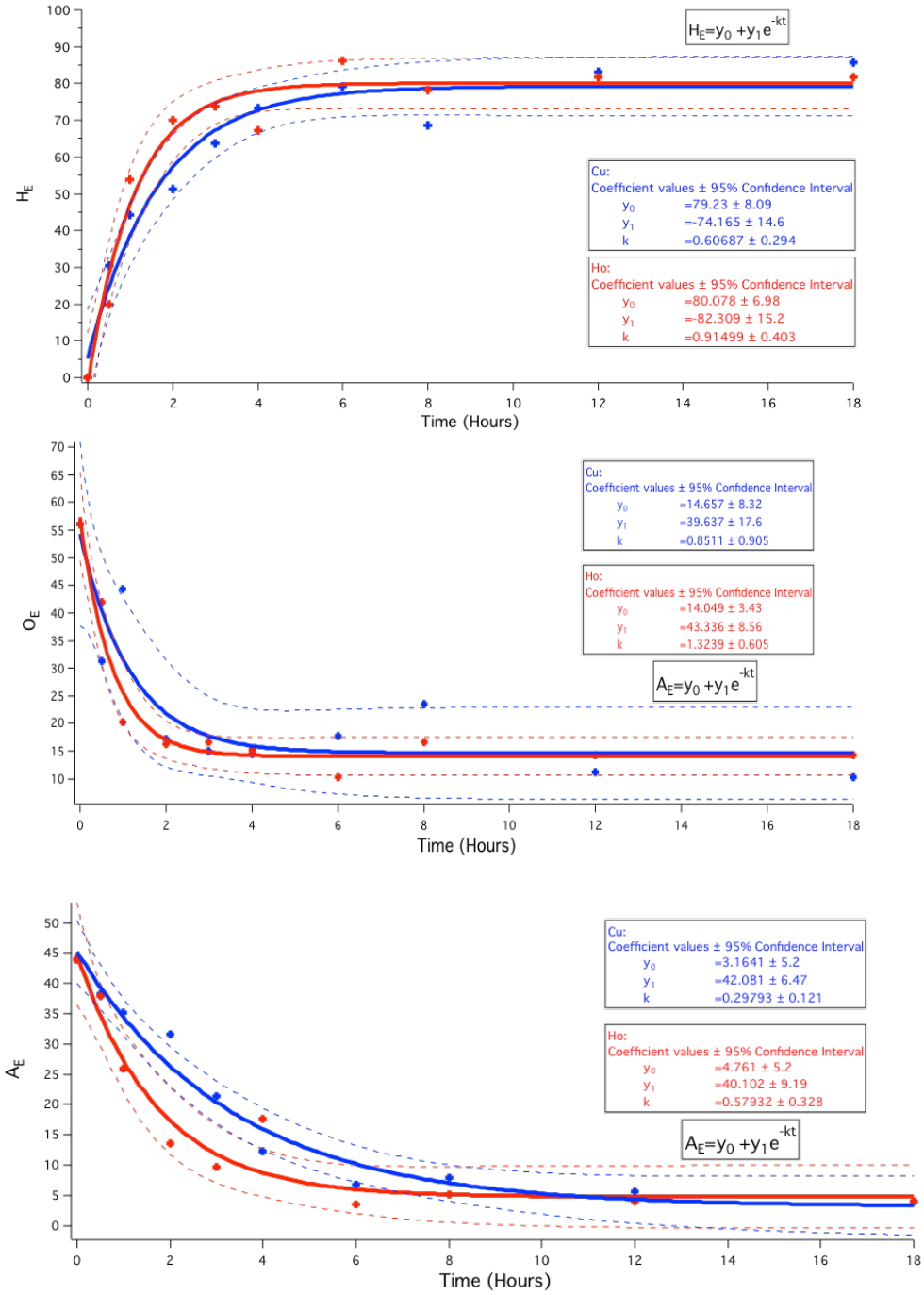

In the first few hours, the reactivity is much higher for the holmium CuPMO. However, at time points beyond six hours, the catalyst achieves maximum hydrodeoxygenation and hydrogenation, indicating that our reaction times do not need to be longer than 6 hours maximum.

D. Conclusion

A series of lanthanide doped CuPMOs were successfully synthesized and incorporated into the precursors of the CuPMOs forming a single phase catalyst confirmed by powder XRD. The catalysts were effective in enhancing the reductive disassembly and hydrodeoxygenation of PDG via hydrogen in supercritical methanol. However, catalytic activity did not increase systematically with the increase of Lewis acidity across the periodic table as expected. The presence of the lanthanide dopant in the matrix demonstrated in a higher catalytic activity in the first few hours of reaction than found for Cu_{20}PMO. These results provided the foundation for Chapter III, where the reactivity and selectivity of $Cu_{20}Sm_5$ is investigated with varying model compounds and additional acids.

E. References

1. Macala, G. S.; Matson, T. D.; Johnson, C. L.; Lewis, R. S.; Iretskii, A. V.; Ford, P. C. Hydrogen transfer from supercritical methanol over a solid base catalyst: a model for lignin depolymerization. ChemSusChem, 2009, 2, 215-217.
2. Barta, K.; Matson, T. D.; Fettig, M. L.; Scott, S. L.; Iretskii, A. V.; Ford, P. C. Catalytic disassembly of an organosolv lignin via hydrogen transfer from supercritical methanol. Green Chem. 2010, 12, 1640-1647.
3. Matson, T. D.; Barta, K.; Iretskii, A. V.; Ford, P. C. One-pot catalytic conversion of cellulose and of woody biomass solids to liquid fuels. J. Am. Chem. Soc. 2011, 133, 14090-14097.
4. Bernt, C. M.; Bottari, G.; Barrett, J. A.; Scott, S. L.; Barta, K.; Ford, P. C. Mapping reactivities of aromatic models with a lignin disassembly catalyst. Steps toward controlling product selectivity. Catal. Sci. Technol. 2016, 6, 2984 - 2994.
5. Barrett, J. A.; Gao, Y.; Bernt, C. M.; Chui, M.; Tran, A. T., Foston, M. B.; Ford, P. C. Enhancing Aromatic Production from Reductive Lignin Disassembly: in Situ O-Methylation of Phenolic Intermediates. ACS Sustainable Chem. Eng. 2016, 4, 6877-6886.
6. Tesin, A.C.; Ray, N.A.; Stair, P.C.; Marks, T.J. Etheric C–O Bond Hydrogenolysis Using a Tandem Lanthanide Triflate/Supported Palladium Nanoparticle Catalyst System. *Journal of the American Chemical Society*, 2012, 134 (36), 14682-14685.
7. Dzudza, A. and Marks, T.J. Efficient Intramolecular Hydroalkoxylation/Cyclization of Unactivated Alkenols Mediated by Lanthanide Triflate Ionic Liquids. *Organic Letters*, 2009, 11 (7), 1523-1526.

8. Kobayashi, S. and Hachiya, I. Lanthanide Triflates as Water-Tolerant Lewis Acids. Activation of Commercial Formaldehyde Solution and Use in the Aldol Reaction of Silyl Enol Ethers with Aldehydes in Aqueous Media. 1994, *J. Org. Chem.*, 59, 3590-3596.
9. Jang, Y-S.; Kim, B.; Shin, J.H.; Choi, Y.J.; Choi, S.; Song, C.W.; Lee, J.; Park, H.G.; Lee, S.Y. Bio-based Production of C_2-C_6 Platform Chemicals. **2012** *Biotechnology and Bioengineering*, 109, 2437-2459.

III. Tuning Catalytic Acidity: Heterogeneously and Homogenously

A. Introduction

Described are the reactivities and selectivities observed for reactions of organosolv poplar wood lignin (OPL) and of lignin model compounds with modifications of the copper-doped porous metal oxide (CuPMO) system previously shown to be a catalyst for lignin disassembly in super-critical methanol.[3] The models studied were benzyl phenyl ether, 2-phenylethyl phenyl ether, diphenyl ether, biphenyl and 2,3 dihydrobenzofuran, which are respective mimetics of the α-O-4, β-O-4, 4-O-5, 5-5 and β-5 linkages characteristic of lignin. The catalyst modifications included added samarium(III) (both homogeneous and heterogeneous) or formic acid. The highest activity for the hydrogenolysis of aryl ether linkages was noted for catalysts with Sm(III) incorporated into the solid matrix of the PMO structure. In contrast, simply adding Sm^{3+} salts to the solution suppressed the hydrogenolysis activity. Added formic acid suppressed aryl ether hydrogenolysis, presumably by neutralizing base sites on the PMO surface but at the same time improved the selectivity toward aromatic products. Acetic acid induced similar reactivity changes. While these materials were variously successful in catalyzing the hydrogenolysis of the different ethers, there was very little activity toward the cleavage of the 5-5 and β-5 C-C bonds that represent a small, but significant, percentage of the linkages between monolignols units in lignins.

B. Experimental

Materials

2-Phenylethyl phenyl ether (PPE), benzyl phenyl ether (BPE), diphenyl ether (DPE) and biphenyl (BP) were obtained from Acros Organics while 2,3 dihydrobenzofuran (DHBF) was obtained from Oakwood Chemical. All were used as received. Methanol (99.5%, Aldrich) was dried over activated molecular sieves before use. Samarium triflate ($Sm(OTf)_3 \bullet 9\ H_2O$) was prepared and gifted by J. Dethlefsen of the University of Copenhagen. Formic acid (88% in aq. solution), glacial acetic acid, and the salts for the hydrotalcite synthesis, $Cu(NO_3)_2 \bullet 3H_2O$, $Al(NO_3)_3 \bullet 9H_2O$ and $Mg(NO_3)_2 \bullet 6H_2O$, were purchased from Fisher Scientific and used without further purification.

Figure 7. Model compounds 2-phenylethyl phenyl ether (PPE), diphenyl ether (DPE), benzyl phenyl ether (BPE), biphenyl (BP) and 2,3 dihydrobenzofuran (DHBF).

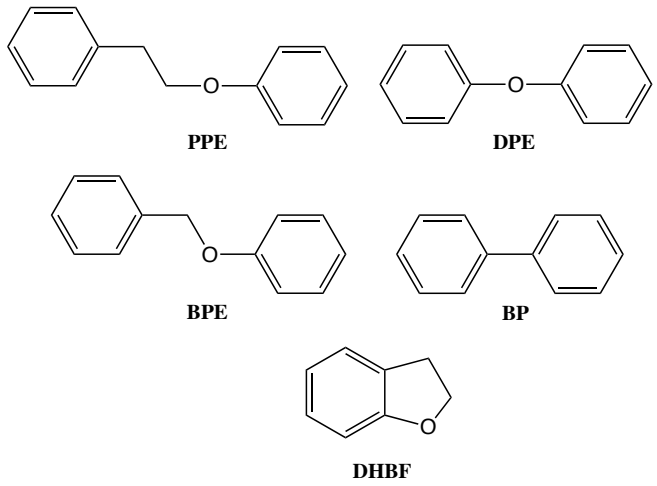

A modification of a procedure described in the Appendix of ref. 13 was used to prepare organosolv poplar lignin (OPL).[1] Woodchips and sawdust (1 kg) obtained by shaving down poplar wood planks from a local lumber yard were first pretreated by stirring in a

toluene/ethanol mixture of for 24 hours at ambient temperature. After filtration and drying, the wood chips (600 g) were added over a 3 hour period to a solution of MeOH (4.5 L) and concentrated HCl (12 mL) in a 12 L round bottom flask equipped with a reflux condenser and overhead stirrer while stirring at 200 rpm. The reaction mixture was heated with stirring at reflux for 9 days after which the solution was filtered and the solid washed with 2.5 L of MeOH. The solvent fractions were combined and the resulting mixture was reduced in volume to 1.5 L on a rotary evaporator and then poured over 9 kg of ice. The light beige precipitate that formed was collected by filtration and washed with excess cold water, and the resulting solid was dried in vacuum over P_4O_{10} until a constant weight was obtained. Yield: 13.7 g.

Catalyst Preparation and Characterization

The Cu-doped porous metal oxide Cu_{20}PMO was prepared from Cu-doped HTC by calcining as described previously.[2-4] For $Cu_{20}Sm_5$PMO, synthesis of the HTC precursor involved replacing 5 mol percent of the $Al(NO_3)_3$ component in the HTC preparation by $Sm(OTf)_3$. The procedure was otherwise the same as that employed for the synthesis of Cu_{20}PMOs. A modified method of all lanthanide and copper doped catalysts can be found in Appendix A. Both types of HTC precursors were calcined for 15 hours at 460 °C in air within 24 hours prior to give the PMO used in catalysis experiments. There was no difference in the reactivities of the PMO catalysts prepared by calcining freshly prepared HTCs and those that had been stored for up to 6 months before calcination.

The solid catalysis materials were analyzed by inductively coupled plasma optical emission spectroscopy (ICP-OES) using a Thermo iCAP 6300 ICP spectrometer equipped with a 6000 K argon plasma source and by powder X-ray diffraction (XRD) using a Bruker

D8 Advance High Temperature Powder Diffractometer. For ICP analysis, a weighed amount of the dry catalyst was digested overnight in concentrated nitric acid and the resulting solution was diluted with 18.2 MΩ deionized water to a known volume. The ICP standards were prepared by diluting commercial copper, aluminum, and magnesium standards (Sigma Aldrich) and by dissolving weighed quantities of dry Sm(III) triflate in 18.2 MΩ deionized acidified water. Reference emission lines were monitored at: 308.2 and 309.2 nm (Al), 324.7 and 327.3 nm (Cu), 330.6 and 359.2 nm (Sm) and 280.2 and 285.2 nm (Mg). Each reported measurement is the average of three replicates.

Surface areas of the Cu_{20}PMO and $Cu_{20}Sm_5$PMO catalysts, freshly calcined overnight at 460 °C, were measured using a Tristar 3000 porosimeter. A weighed sample (~150 mg) of each catalyst was loaded into an analysis tube and then degassed at 225 °C under a stream of N_2(g) overnight. A full isotherm was collected to determine surface area, pore volume, and pore size.

The number of basic sites for each catalyst was calculated by the methodology described by Parida and Das[5] and modified by Shuting et al.[6] A 50 mg sample of Cu_{20}PMO or $Cu_{20}Sm_5$PMO was added to solutions of 10 mL hexane with varying amounts of benzoic acid. The resulting solutions were filtered and analyzed by gas chromatography with flame ionization detection (GC-FID) on an Agilent Model 6890 programmable gas chromatograph to quantify the amount of benzoic acid that was not consumed by binding to base sites. By assuming the Langmuir isotherm, the number of moles of basic sites per gram of catalyst was calculated.

Catalytic Reactions

The reactions in sc-MeOH were conducted in stainless steel mini-reactors as described before.[7] (*Caution! Under the reaction conditions, these vessels develop high internal pressures. Handle with care.)* For typical reactions with model compounds, the mini-reactors (total volume 10 mL) were loaded with 3 mL of methanol, 100 mg of catalyst, the substrate plus 0.10 mmol of decane as an internal standard. The temporal evolution of the substrate and of each product was determined by preparing a series of 6 mini-reactors that were loaded identically and placed an oven thermostatted at the temperature of interest (generally 300 °C for PPE and BPE and 330 °C for DPE and BP and DHBF). After specific reaction intervals (1 to 6 hours), one of these mini-reactors was removed and cooled rapidly by immersing in a water bath to quench the reaction. The reactor was then opened to release the gases, and the volume released was measured by a water displacement method.[3,4] (*Warning: this step requires special care owing to the large volume of gas sometimes released*. *In addition, both H_2 and CO are released, so proper ventilation is required.*) The methanolic product solutions were separated from the solid catalysts by passing through a 0.2 μm filter to remove any suspended particles. Product analysis of the solution was conducted by GC-FID by comparing the retention times to those of known standards. Product quantification utilized the effective carbon number (ECN) as a weighting factor for identified species to evaluate the area of GC-FID peaks corrected by the area of the internal standard (decane).[8,9] GC-FID analysis parameters, effective carbon numbers (ECN) and response factors (Appendix Tables B1 and B2) for all compounds identified are summarized in the Appendix.

Temporal reactivity studies were carried out for each substrate with four different catalyst systems: (a) Cu_{20}PMO alone as the baseline; (b) Cu_{20}PMO plus different amounts of formic acid (FA); (c) $Cu_{20}Sm_5$PMO with ~5% of the Al^{3+} of the HTC precursor replaced by Sm^{3+}; (d) Cu_{20}PMO plus $Sm(OTf)_3$ dissolved in the medium. Control reactions were run without catalyst for each of the model substrates with the methanol solvent alone (3.0 mL) and with methanol solvent containing FA.

For reactions using OPL, the mini-reactors were loaded with 3 mL of methanol, 100 mg of catalyst, and 100 mg of OPL and heated at 300 °C for the desired reaction time. After cooling, opening, and filtering the methanolic solution, the liquid was reduced to an oily residue using a Smart Evaporator (Eicom USA) to remove the methanol. The residue was then dissolved in $CDCl_3$ for analysis by ^{1}H NMR spectrometry on a Varian Unity Inova 500 MHz spectometer and by gel permeation chromatography (GPC) using a Waters Alliance HPLC System having a 2690 Separation Module with Agilent PGEL 5 μm and MIXED-D 300 x 7.5 mm columns with Waters model 2410 differential refractometer and model 2998 photodiode array detector. The ^{1}H NMR spectra of the product mixtures were interpreted using the holistic analysis developed by Barta et al.[3] to evaluate relative quantities of aromatic (A_E), near oxygen (O_E) and aliphatic (H_E) protons. All NMR spectra were collected at room temperature with the d1 delay of 4.8 s. Although a longer d1 of 10 seconds gave slightly larger A_E values, this was not used owing to the much longer acquisition times required.

Catalyst Leaching

Leaching of metal ions from the PMO catalysts was evaluated by ICP-OES after a 6 hour reaction at 300 °C. The mini-reactors were loaded with 100 mg of $Cu_{20}Sm_5$PMO, 1000 μmol BPE, 0.10 mmol decane, and 3 mL of MeOH. Following cooling, the methanolic solution and catalyst were transferred from the reactor, which was then washed with additional methanol. The combined solutions and catalyst (~10 mL) were centrifuged (at 7000 rpm) after which the solution was decanted from the solid and passed through a 0.2 μm filter. The resulting solution was then evaporated to dryness to remove volatiles, and the resulting solid residue was digested in 10% nitric acid solution and subjected to ICP-OES analysis.

Catalyst Recycling

For catalyst recycling experiments, the mini-reactors were loaded with 100 mg OPL, 100 mg $Cu_{20}Sm_5$PMO, and 3.0 mL MeOH. They were then sealed and heated at 300 °C for 6 hours. The reactors were then rapidly cooled to quench the reaction, opened, and washed with 15 mL of methanol. The methanolic solution and catalyst slurry was centrifuged for 10 min at 7000 rpm. The solution was removed by decanting from the solids. The solid catalyst was dried under vacuum overnight and then was reloaded into the reactor for another run under the same conditions. The above procedure was repeated three more times. The less volatile organic products in the decanted methanolic solution were subjected to ^{1}H NMR and GPC analysis after evaporating the solvent.

C. Results and Discussion

Catalyst Characterization

Prior to calcining, the precursor Cu_{20} and $Cu_{20}Sm_5$ HTCs were analyzed by XRD to check the hydrotalcite structure and by ICP-OES to evaluate the catalyst composition. The XRD patterns found for the Cu_{20} and $Cu_{20}Sm_5$ hydrotalcites (Appendix B1) are consistent with the literature data for HTCs.[10] ICP-OES analysis of the Cu_{20}PMO catalyst gave the Al: Cu: Mg molar ratio of 1.0: 0.63: 2.40 consistent with an anticipated ratio of 1.0: 0.60: 2.40. Analysis of the $Cu_{20}Sm_5$PMO catalyst gave the Al: Sm: Cu: Mg ratio 1.0: 0.06: 0.66: 2.56, consistent with the anticipated ratio 1.0: 0.05: 0.63: 2.53. In addition, the surface areas and porosities of the calcined PMOs were determined using porosimetry, and the number of basic sites was quantitatively evaluated by a procedure that involves neutralizing benzoic acid.[5,6] These data are summarized in Table 1 and show that incorporation of Sm^{3+} has little effect on the surface area or porosity but increases the number of accessible base sites in the respective PMO. The latter observation can be rationalized in terms of the Sm^{3+} -oxide bonding having a more ionic character than the corresponding Al^{3+}-oxide interactions on the surface, thereby affecting the overall basicity of the catalyst.

Table 1. Surface area, pore volume, pore size, and number of basic sites for Cu_{20}PMO and $Cu_{20}Sm_5$PMO catalysts.

Catalyst	Surface Area[a] (m^2 g^{-1})	Pore Volume[b] (cm^3 g^{-1})	Pore Size[c] Å	Basic Sites[d] (mmols g^{-1})	Density of Basic sites[e] (μmols m^{-2})
Cu_{20}PMO	174	1.22	277	10.7	61.5
$Cu_{20}Sm_5$PMO	175	1.28	288	13.5	77.1

[a,b,c] Calculated using N_2 adsorption as described in the Experimental Section.

[d] Calculated using benzoic acid method as described in the Experimental Section.

[e] Basic sites divided by the surface area.

Benzyl Phenyl Ether (BPE)

BPE is a model for the α-O-4 lignin bond. The expected initial products of hydrogenolysis are toluene and phenol (eq. 3). As shown previously by Bernt

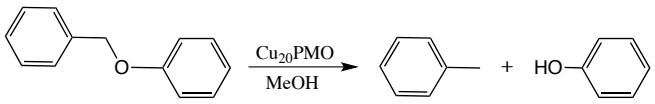

(3)

et al,[8] the reaction of BPE with Cu_{20}PMO under the conditions that are effective for lignocellulose disassembly (300 °C in sc-MeOH) leads to a number of products owing to the secondary methylation and hydrogenation of the phenol aromatic ring and to subsequent reactions of the secondary products. In contrast, the toluene is relatively unreactive. Appendix Fig. B2 illustrates phenol formation and consumption over the 6 hour course of the reaction of BPE with the four catalyst systems. The differences in final phenol concentrations are largely attributed to how rates of secondary reactions of phenol are influenced by the catalysts.

The reactions of BPE were studied under conditions described in the Experimental Section using each of the four catalyst systems. The quantitative numerical data are

summarized in Appendix Table B3. In each case, nearly stoichiometric quantities of the toluene co-product were found, while the benzene yield was <1%, indicating that the initial hydrogenolysis step primarily occurs at the PhO-CH_2Ph bond as depicted in eq. 1. However, the distributions of secondary products from the phenol co-product differ for the four catalysts. As we have shown previously,[11] BPE is also susceptible to solvolytic processes in sc-MeOH even in the absence of catalyst. Side by side comparison of BPE reactions in sc-MeOH and in sc-MeOH containing FA (1.17 mmol) indicated little reactivity difference with ~50% of the BPE consumed after 2 hours at 300 °C. For comparison, in the presence of Cu_{20}PMO, BPE would have been 97% consumed in sc-MeOH but only about 55% consumed in the sc-MeOH/FA medium. More importantly, in both cases intractable tars were formed, if catalyst was not present, thus leading to a poor material balance of analyzable products that included toluene, phenol, benzaldehyde, phenol, and unidentified dimers as detected by GC-MS.

Fig. 8 illustrates the temporal product evolution for the reaction of BPE catalyzed by Cu_{20}PMO in the presence of added FA (1.17 mmol). The data show that under these conditions, BPE hydrogenolysis is substantially slower than with Cu_{20}PMO alone. However, the added FA also appears to suppress the secondary reactions of phenol, especially ring hydrogenation. Thus, after 6 hours under these conditions, the toluene yield is essentially quantitative, while the yield of aromatics derived from the phenol co-product is ~80% with phenol (52% yield), cresols (19%) and anisole (6%) being the primary components itself.

Figure 8. Temporal BPE consumption and products from the reaction with Cu_{20}PMO+FA with BPE.

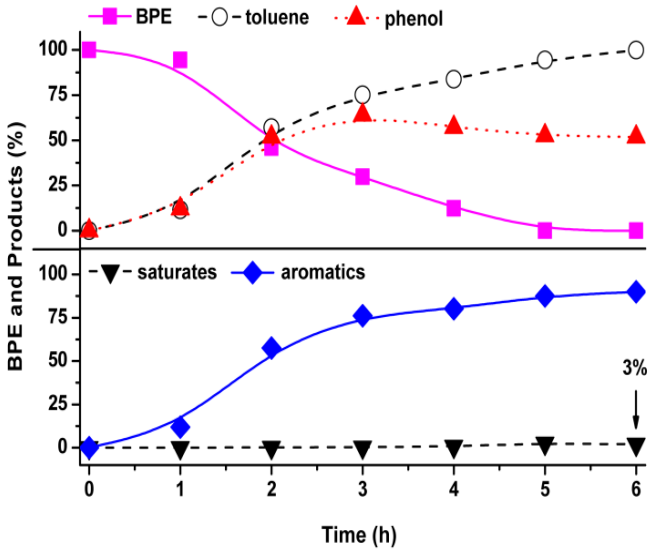

Top: evolution of BPE (magenta squares); toluene (black circles) and phenol (red triangles). *Bottom:* Aromatics (blue diamonds) mostly anisole, Me-anisole, cresols, benzene and xylenol and saturated products (black reverse triangles) mostly cyclohexanol and methylcyclohexanols, Conditions: BPE = 1041 mmols (initial), 100 mg Cu_{20}PMO, 50 µL 88% aq. FA (1.17 mmol), 3.0 mL of MeOH, decane as internal standard, T = 300 °C. Products quantified by GC-FID. For more details regarding aromatic and saturated products, see also Appendix Fig. B2 and Table B3. These data represent average of two catalysis experiments under identical conditions.

The yield of identified saturated products, mostly cyclohexanol and methycyclohexanol was <5%. For comparison, the reaction with Cu_{20}PMO alone gave a quantitative yield of toluene but only a 19% yield of the aromatics that might be derived from the phenol channel. Cyclohexanol and the methylcyclohexanols (77%) represent most of the remainder (Appendix Table B3A). If the shorter 3 hour reaction time is considered, only 70% of the

initial BPE substrate reacted in the Cu_{20}PMO+FA system, compared to 100% for Cu_{20}PMO, but the products from the phenol stream were nearly quantitatively aromatic.

When Sm^{3+} was incorporated in the PMO matrix ($Cu_{20}Sm_5$PMO) there was a moderate enhancement of the rate of BPE hydrogenolysis; however, the products are qualitatively similar to those from the catalysis by Cu_{20}PMO (Fig. 9 and Appendix Table B3).

Figure 9. Conversion and product distributions are shown for the reactions of BPE with the Cu_{20}PMO catalyst systems at 300 °C after 6 hours.

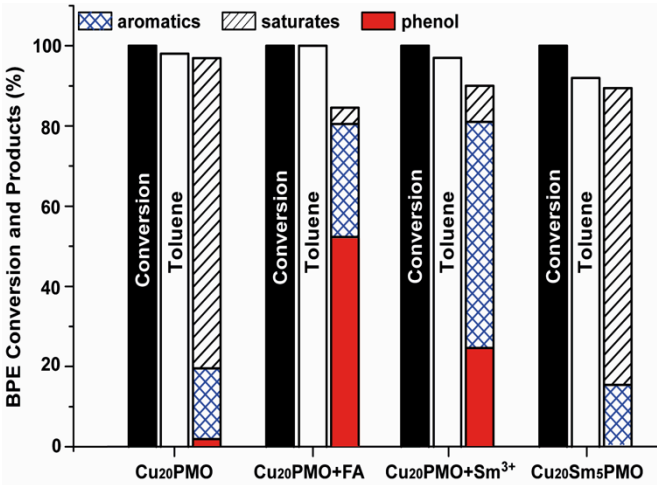

Unidentified products not included but estimated yields were small (<2%) in each case. The black bars indicate the substrate conversion; the center bars indicate toluene yields, while the bars on the right summarize other products (phenol, other aromatics and saturates), that are thought to arise mostly from the intermediacy of phenol. Conditions: 100 mg of catalyst, 3 mL of MeOH, 1041 μmols of BPE (initial). For Cu_{20}PMO+FA, 1.17 mmol of FA was added as 50 μL of 88% aq. formic acid. For Cu_{20}PMO+Sm^{3+}, $Sm(OTf)_3$ (5 mg) was added to the reaction medium. Products were determined by GC-FID. The mass balance (the sum of products divided twice by BPE_0) ranged from 90 to 97%. These data represent averages of two catalysis experiments under identical conditions. See also Appendix Table B3E.

There was somewhat increased benzene production, although this was only ~0.8%. In both cases, the yield of aromatic products from the phenol channel after 6 hour reaction was small (17 and 19%, respectively), and the principal components were saturated (83 and 81%). The yields of phenol itself were very small (~0.1 and ~1.5%, respectively).

In contrast, when Sm^{3+} (6.7 μmol) was instead added to the catalytic solution as a soluble salt, the product mixture with BPE was markedly different. After 6 hour reaction with Cu_{20}PMO and added $Sm(OTf)_3$, the yield of aromatics from the phenolic channel was ~80% in addition to the nearly stoichiometric yield of the toluene co-product. The identified saturated products, cyclohexanol and various methylcyclohexanols, represented <10% of the products (Fig. 9 and Appendix Fig. B2). Substantial amounts of phenol (24% yield) remained and two other phenolics, cresol (34%) and xylenol (15%), were major products. Thus, solution phase Sm^{3+} appears to suppress phenol hydrogenation and to enhance phenol ring methylation under these reaction conditions.

Bernt et al,[8] previously identified the secondary reactions of phenol in reactions with the Cu_{20}PMO catalyst in sc-MeOH that are outlined in Scheme 1.

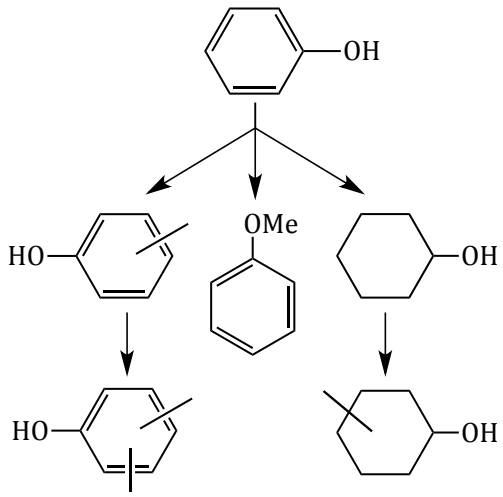

Scheme 1. Cu_{20}PMO catalyzed secondary reactions of the phenol product of BPE hydrogenolysis, showing aromatic ring methylation, O-methylation and ring hydrogenation followed by methylation. Since methylation was noted at all 3 sites (o, p & m), the structures indicate simply the number not the regiochemistry of added CH_3's.

The overall effect on these reactions upon substituting Sm^{3+} for 5% of the Al^{3+} in the PMO matrix was relatively minor; however, significant perturbations were seen upon adding either FA or Sm^{3+} to the solution. Both additives suppressed hydrogenation of the aromatic ring, but the latter accelerated ring methylation to give cresols and xylenols. In this context, Bernt et al[15] showed that cresol undergoes slower subsequent reactions with Cu_{20}PMOs including ring hydrogenation to methylcyclohexanol (MCH), ring methylation to xylenol and O-methylation to methylanisole, as well as hydrodeoxygenation to toluene. However, given that substantial phenol remains after 6 hour reaction with the Cu_{20}PMO + Sm^{3+} system, ring methylation does not fully explain the high yields of aromatics in this case.

A possible explanation of the modified reactivity when FA was added would be neutralization of base sites on the Cu_{20}PMO surface. According to Table 1, 100 mg of Cu_{20}PMO would have 1.07 mmol of base sites as measured using the benzoic acid

neutralization method, so the 1.17 mmol of FA should be sufficient to neutralize these sites. Such neutralization would likely reduce the strength of phenol binding to the catalyst surface and/or the affect nature of that substrate on that surface. This view gains support from the observation that when an equivalent amount of glacial acetic acid was used instead as an additive in the reaction of BPE with Cu_{20}PMO, the product mixture after 6 hours included a nearly stoichiometric amount of toluene (98%) plus phenol (27%) and, other aromatics (31%) in yields much higher than in an analogous reaction without the added acid (Appendix Table B3E). However, this behavior did not extend to all acids, since addition of aq. HCl in small amounts poisoned the catalyst giving very poor reactivity.

It is harder to explain the role of added Sm^{3+} given that it constitutes only 6.7 μmoles. A major effect is the apparent enhanced rate of phenol methylation. This laboratory has previously reported[8] that cresols and xylenols tend to be less easily hydrogenated than is phenol. However, the presence of Sm^{3+} (or its counter ions) also appears to suppress the hydrogenation of phenol itself.

2-Phenylethyl Phenyl Ether (PPE).

PPE is a model for the β-O-4 lignin linkage. In analogy to BPE, one might expect the initial products from hydrogenolysis to be ethylbenzene and phenol. Ethylbenzene is resistant to further reaction under these conditions,[8] so this would again leave secondary reactions of phenol to account for product proliferation. However, one key difference between the reactions of BPE and those of PPE is the extent of benzene formation. With each catalytic system, only traces of benzene were formed from BPE (0.1-0.8% after 6 hours reaction, Appendix Table B3). However, with PPE, benzene is formed in much higher yields (5-8% after 6 hours, Fig. 10 and Appendix Table B4).

Figure 10 Temporal PPE consumption and product formation from the reaction of PPE with $Cu_{20}Sm_5PMO$.

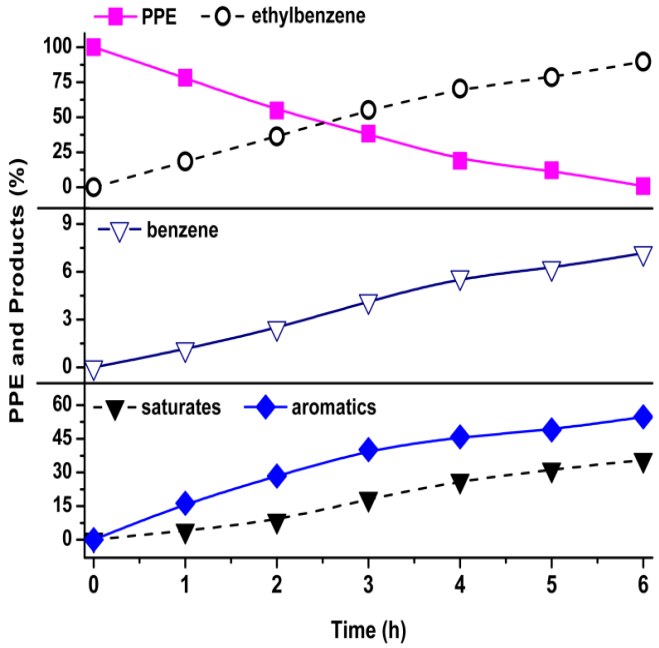

Top: evolution of PPE (magenta squares); ethylbenzene (black circles). *Middle*: Temporal formation of benzene (open triangles) showing how this parallels ethylbenzene production. *Bottom:* Total aromatic (blue diamonds: anisole, benzene cresols ethyl and other minor aromatics) and saturated products (black reverse triangles, cyclohexanol and methylcyclohexanols plus other minor saturates) as a function of time. Conditions: PPE = 530 μmols (initial), 3.0 mL of MeOH, decane as internal standard, T = 300 °C. Products quantified by GC-FID. For more details see Appendix Table B4. These data represent the average of two catalysis experiments under identical conditions.

Furthermore, the temporal runs for each catalyst showed an approximately constant ratio (within experimental uncertainty) of the benzene and ethylbenzene products throughout each run, although this differed somewhat from one system to another (~0.06 for $Cu_{20}PMO$ plus Sm^{3+} to ~0.09 for $Cu_{20}PMO$ plus FA). Although we have demonstrated[8] that benzene is very slowly formed under related conditions by the HDO of secondary products, the

constant ratio indicates that the benzene seen here is a direct product of phenyl-oxygen bond hydrogenolysis in competition with the faster $PhCH_2CH_2$-OPh hydrogenolysis (eq. 4).

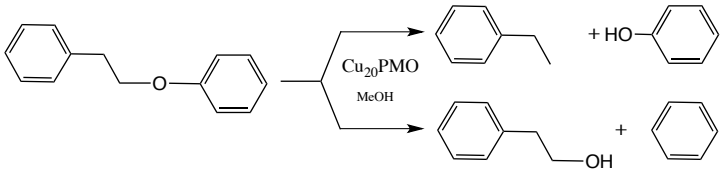

(4)

Any 2-phenylethanol formed according to eq. 4 would likely undergo HDO to ethylbenzene via dehydration to styrene followed by hydrogenation to ethylbenzene.[8] Thus, the rate of ethylbenzene formation serves as a monitor of the initial hydrogenolysis. Temporal studies showed that, for each of the catalytic systems, PPE is several fold less reactive than BPE, a feature that correlates with the calculated dissociation enthalpies (ΔH_d) of ~69 and ~56 kcal mol^{-1}, respectively, for the β-O-4 and α-O-4 bonds (somewhat substituent dependent).[12] The hydrogenolysis rates by Cu_{20}PMO and by $Cu_{20}Sm_5$PMO as followed by ethylbenzene production (Fig. 11) were comparable as were the product distributions for these two systems (Appendix Tables B4A and B4D). Other than the ethylbenzene and benzene predicted by eq. 2, the major products with both catalysts were cyclohexanol and methylcyclohexanol, presumably the results of secondary reactions of the phenol also predicted by eq. 4. Following the pattern found for BPE, Cu_{20}PMO gave more cyclohexanol while $Cu_{20}Sm_5$PMO gave more methylcyclohexanol (Fig. 12, Appendix Table B4).

The addition of Sm^{3+} (6.7 μmol) decreased the rate of hydrogenolysis catalyzed by Cu_{20}PMO by roughly a factor of two (Appendix Fig. B4 and Table B4C). Of the products identified after 6 hour reaction, only 14% were saturated, so this additive also suppressed hydrogenation of aryls, including phenol.

Figure 11. Temporal production of ethylbenzene from the reaction of PPE with various catalytic systems in sc-MeOH at 300 °C.

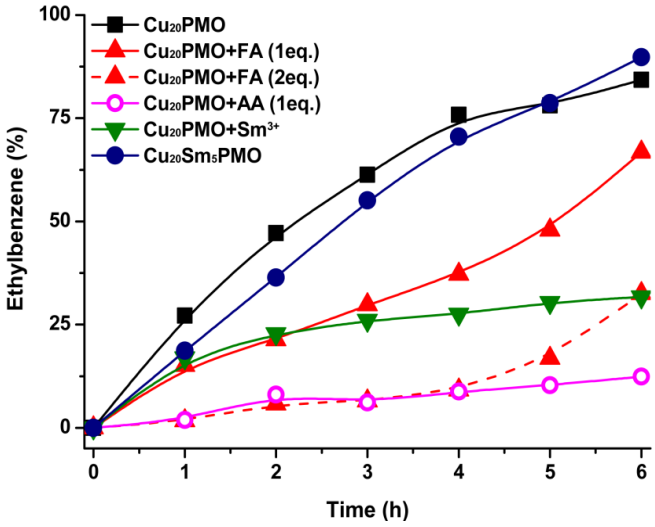

Again for PPE, adding FA slowed the hydrogenolysis reaction over Cu_{20}PMO and, the extent of this slowing depends on the quantity of FA added. When reactions with Cu_{20}PMO (100 mg) were run with 0.58 mmol of added FA, the initial hydrogenolysis rate as evidenced by the formation of ethylbenzene, was about two-fold slower (Appendix Table B4B). However, when the FA was increased to 1.17 mmol, the initial rate was nearly 10-fold slower than in the absence of the added FA. Notably, in both cases the rate seemed to pick up after 3 hours, perhaps due to catalyzed FA decomposition. With the higher FA, saturated products did not appear in the early reaction stages, but did appear in the later stages. When acetic acid (1.17 mmol) was used instead of FA, the rate of ethylbenzene production was again markedly suppressed, but there was no increase in the rate at longer reaction times. The primary products were ethylbenzene (50% of the products), anisole (17%) and phenol (11%), and the only saturated product identified was cyclohexanol (~1%), so the acetic acid suppresses both ether hydrogenolysis and aryl ring hydrogenation.

Fig. 12 illustrates the products found after 6 hour reaction of PPE with the four catalyst systems. The four catalysts display significant reactivity differences with substrate conversion ranging from 38 to 99%. $Cu_{20}Sm_5PMO$ again proved to be the most reactive. Added Sm^{3+} suppressed the secondary reactions of phenol but also suppressed ether hydrogenolysis.

Figure 12. Percent conversion and product distribution after 6 hours for the PPE reaction with the four catalyst systems at 300 °C.

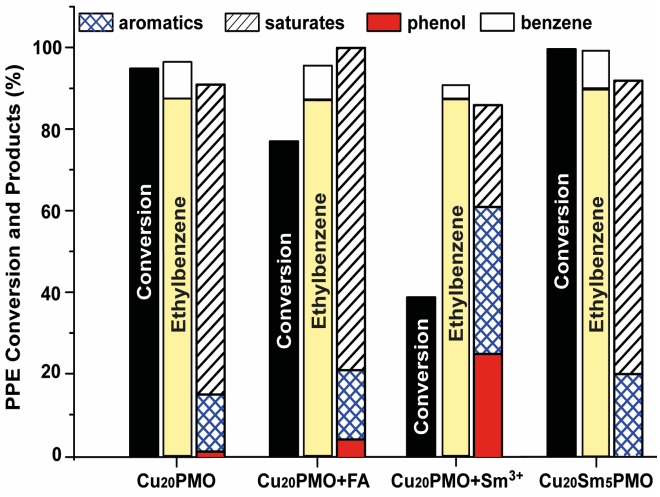

Unidentified products seen in the GC-FID are not included but estimated yields were small (<2%) in each case. The left bars indicate substrate conversion, the center bars the yield of ethylbenzene and benzene, and the right bars summarize the products (phenol, other aromatics and saturates), thought to arise from the intermediacy of phenol. Conditions: 100 mg catalyst, 3 mL MeOH, PPE= 530 μmol (initial), For $Cu_{20}PMO$+FA, 1 eq. FA relative to PPE_0 was added. For $Cu_{20}PMO+Sm^{3+}$, 5 mg $Sm(OTf)_3 \bullet 9\ H_2O$ was added. The mass balance (the sum of products divided by 2x PPE consumed) ranged from 91 to 96%. These data represent averages of two catalysis experiments under identical conditions.

Appendix Fig. B3 summarizes the major phenol-derived products after a 6 hour reaction. Hydrogenation and methylation products followed a trend similar to that observed with BPE. Notably, unlike BPE, PPE shows virtually no solvolytic reactivity in the absence of catalyst. When the catalyst-free reactions were run for 6 hours at 300 °C in either sc-MeOH or in sc-MeOH/FA, the respective recovery of substrate (GC analysis) was, within experimental uncertainty (±5%), quantitative.

Diphenyl Ether (DPE)

DPE is a model for the diaryl ether 4-O-5 linkages in lignin. The expected products from simple hydrogenolysis of this bond are benzene and phenol. (eq. 5). Benzene is relatively unreactive under these conditions, so further product proliferation would again be expected to result primarily from subsequent reactions of phenol or from reactions of the substrate prior to hydrogenolysis.

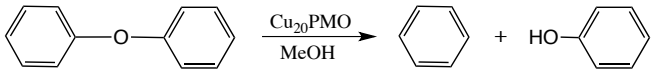

(5)

When studied under the previous reaction conditions, it was clear that DPE at 300 °C was much more recalcitrant than either BPE or PPE, a feature that can be attributed to the stronger 4-O-5 linkage (ΔH_d ~79 kcal mol^{-1}).[13] After 6 hours, the conversion of DPE was only 39% for the most active catalyst $Cu_{20}Sm_5PMO$, followed by $Cu_{20}PMO$+FA (27%), $Cu_{20}PMO$ (21%) and $Cu_{20}PMO+Sm^{3+}$ (10%) (Appendix Table B5).

Increasing the temperature to 330 °C led to greater rates of conversion with $Cu_{20}Sm_5PMO$ again being the most reactive and $Cu_{20}PMO+Sm^{3+}$ being the least (Appendix Table B6). At these temperatures, the principal aromatic product after 6 hour reaction is benzene, as predicted by eq. 5. The products formed along the phenol channel are largely

the saturated alcohols cyclohexanol and methylcyclohexanol. For example, the products from the reaction of DPE with $Cu_{20}Sm_5$PMO after 6 hours were benzene (97% based on amount of DPE consumed) and phenol-derived methylcyclohexanols (49%), cyclohexane (9.8%), methylcyclohexane (9.8%) methylanisole (7.1%), cyclohexanol (1.6%), anisole (1.2%), and toluene (0.8%). Only traces of phenol itself remained (0.4%) (Appendix Table B6) showing that under these catalytic conditions, phenol ring hydrogenation and/or methylation as well as O-methylation of phenol (Scheme 1) is rapid relative to hydrogenolysis of the ether. Fig. 13 depicts the temporal behavior for the reaction of DPE with $Cu_{20}Sm_5$PMO at 330 °C (see also Appendix Table B7).

Figure 13. Temporal behavior of DPE consumption and products formed from the reaction with $Cu_{20}Sm_5$PMO with DPE at 330 °C.

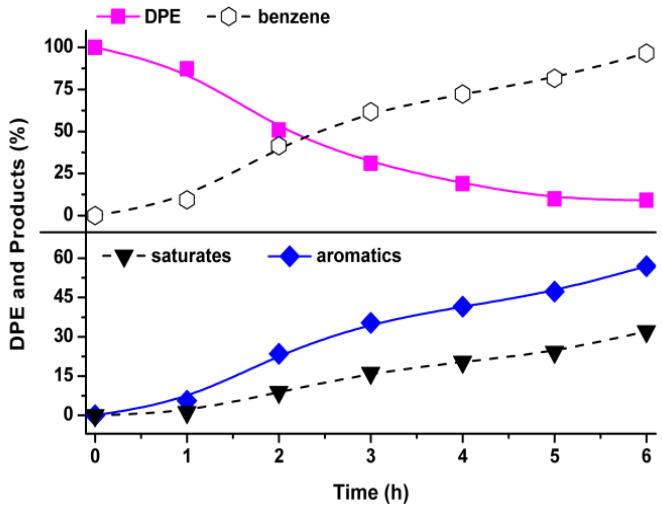

Top: DPE (magenta squares) and benzene (black hexagons). *Bottom*: Sum of aromatic products including benzene (blue diamonds) and saturated products (reverse triangles). Numerical data from Appendix Table B7. These data represent the average of two catalysis experiments under identical conditions

DPE shows no solvolytic reactivity in the absence of catalyst. When the catalyst-free reactions were run for 6 hours at 330 °C in either sc-MeOH or sc-MeOH/FA, the recovery of unreacted substrate was (within experimental uncertainty) quantitative.

2,3-Dihydrobenzofuran (DHBF)

A dihydrobenzofuran type ring system is typically formed with the β-5 type linkage in lignin, so DHBF was investigated as a reactivity model with the various catalysts. The hydrogenolysis of DHBF over Cu_{20}PMO catalysts would be expected to give 2-ethylphenol as the initial product as depicted in eq. 6, although in analogy to PPE, one must consider the possible cleavage of the phenyl-O bond as well. In the latter case the product would be 2-phenylethanol, which as noted above, should rapidly undergo HDO to give ethylbenzene. The latter was formed in modest yields with Cu_{20}PMO (6.0%) and $Cu_{20}Sm_5$PMO (8.0%), although, since one can also envision its formation by the HDO of 2-ethylphenol, there is some ambiguity regarding its origin.

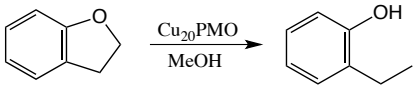

(6)

The reactions of DHBF proved to be relatively slow for all four catalysts at 300 °C, although again it was evident that $Cu_{20}Sm_5$PMO is the most reactive and Cu_{20}PMO+Sm^{3+} is the least reactive catalyst system (Appendix Table B8). Raising the reaction temperature to 330 °C increased DHBF conversion considerably in all four cases (Appendix Table B9) with $Cu_{20}Sm_5$PMO remaining the most active toward hydrogenolysis. Fig. 14 shows the DHBF and product time evolution for the reaction with $Cu_{20}Sm_5$PMO catalyst at this temperature.

Figure 14. Temporal substrate consumption and products from the reaction of DHBF with $Cu_{20}Sm_5$PMO at 330 °C.

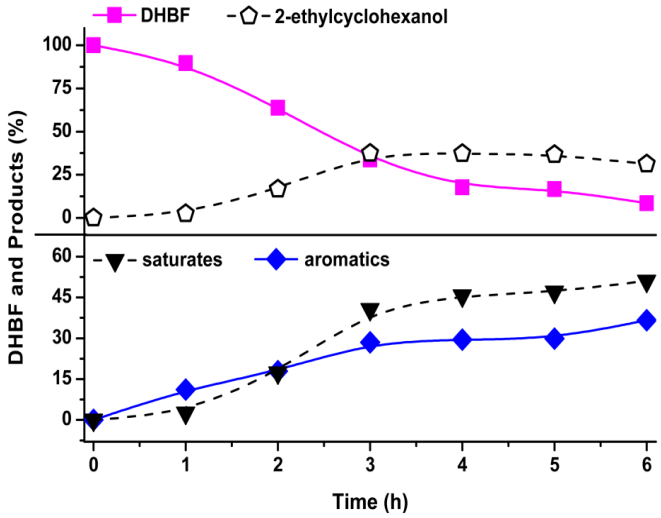

Top: Evolution of DHBF (magenta squares) and of 2-ethylcyclohexanol (black pentagons). *Bottom*: Evolution of the summed aromatic products consisting of methylethylphenol, ethylbenzene, 2-ethylphenol and other minor aromatics (blue diamonds) and of the summed saturated products consisting of 2-ethylcyclohexanol, methylethylcyclohexane, ethylcyclohexane, ethylcyclohexanol and other minor saturates (reverse triangles). Conditions: DHBF = 502 μmols (initial), 3.0 mL of MeOH, decane as internal standard. Products quantified by GC-FID; data from Appendix Table B10. These data represent the average of two catalysis experiments under identical conditions

The aromatic and saturated product distributions are illustrated in Fig. 15. After 6 hours, the major products identified were 2-ethylcyclohexanol followed by 2-ethylmethylphenol. These are likely hydrogenated or methylated byproducts, respectively, of the expected primary hydrogenolysis product 2-ethylphenol. This primary product is immediately evident in the initial stages of the reaction (e.g. at 1 hour, 2-ethylphenol represents 61% of the identified products), but progressively disappears during the reaction owing to secondary

reactions (Appendix Table B10). As noted above, some ethylbenzene was also observed, and while this could be the result of a primary, though minor, hydrogenolysis of the O-CH_2 bond of DHBF, there are other pathways, such as the HDO of ethyl phenol, that could also lead to this product.

Figure 15. DHBF conversion and products distribution for the reaction with $Cu_{20}Sm_5$PMO at 330 °C after 6 hours.

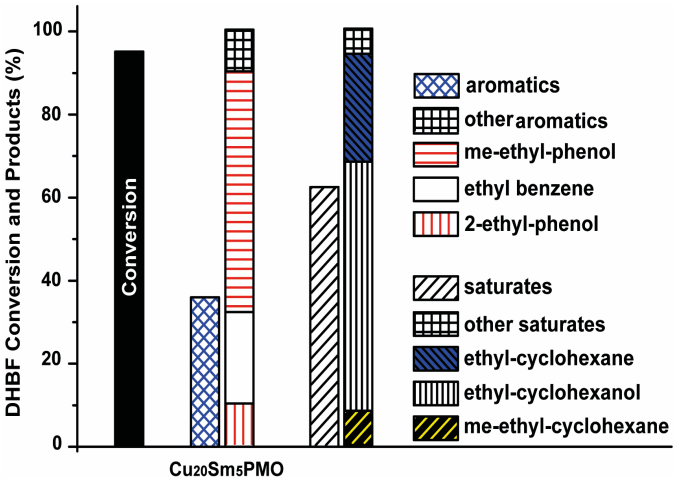

Unidentified products are not included but the estimated yields were small (<2%). The left bar indicates the substrate conversion, the center bars indicate the aromatics yield and distribution, and the right bars indicate the saturated products yield and distribution (see Appendix Table B10). Conditions as in Fig. 14. The mass balance (total products divided by the DHBF consumed) was 92%. These data represent an average of two catalysis experiments under identical conditions.

Notably, neither pathway would separate the lignin subunits coupled by the much stronger β-5 bond shown in Fig. 1. Hydrogenolysis of the stronger phenyl-CH_2 bond in DHBF (effectively the β-5 analog) would give ethoxybenzene, but only traces (<0.5%) of this were observed. Other products (e.g., benzene, cyclohexanol or cyclohexane derivatives,

etc.) that possibly can be attributed to secondary reactions of ethoxybenzene total ~5%. Thus, this pathway, which involves cleaving a strong C-C bond, is at most a minor contribution to the overall reactivity pattern for DHBF hydrogenolysis, which is summarized in Scheme 2.

Control reactions with DHBF in sc-MeOH and sc-MeOH/FA at 300 °for 6 hours without catalyst gave intractable polymeric materials and were not analyzed further.

Scheme 2. Proposed pathway for DHBF conversion as catalyzed by $Cu_{20}Sm_5$PMO in sc-MeOH to give the major products. Possible minor hydrogenolysis pathways via the undetected intermediates 2-phenylethanol and ethoxybenzene are shown using dashed arrows.

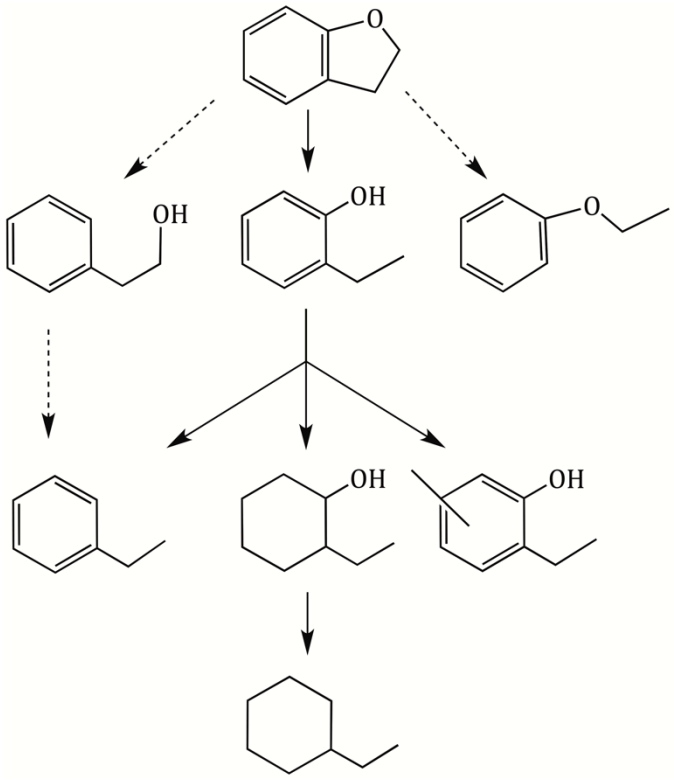

Biphenyl (BP)

Biphenyl was employed as model for the 5-5 lignin bond in reactions with the Cu_{20}PMO catalysts. Simple hydrogenolysis of this linkage would give benzene (eq. 7); however, among key linkages between lignin subunits, the 5-5 bond is likely to be the strongest with calculated bond dissociation energies ranging from 112-118 kcal mol^{-1}.[13] In this context, it is not surprising that less than 4% conversion was observed for the reaction of BP with Cu_{20}PMO in sc-MeOH at 300 °C. Although greater reactivity was observed with the more active $Cu_{20}Sm_5$PMO catalyst at 330 °C, the products were phenylcyclohexane (~82%) and bicyclohexane (~13%), which result from hydrogenating intact biphenyl (Appemdix Table B11). The primary 5-5 bond cleavage products were cyclohexane (3.7%) and methylcyclohexane (~1%) while only traces of benzene (<1% yield based on the stoichiometry of eq. 7) were found.

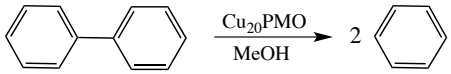

(7)

Increasing the temperature to 330 °C did not show significant difference in the reactivity pattern only an increase in the bicyclohexane/phenylcyclohexane ratio. This suggests that the small amount of 5-5 bond cleavage occurred from biphenyl, rather than from the phenylcyclohexane or bicyclohexane products. Similarly, when control reactions with BP were run in sc-MeOH and sc-MeOH/FA at 330 °C for 6 hours without catalyst, recovery of unreacted biphenyl was (within experimental uncertainty) quantitative.

At the suggestion of a referee, we also briefly examined the reactivity of the biphenyl derivative 2-phenylphenol (BP-OH) with Cu_{20}PMO and $Cu_{20}Sm_5$PMO. As expected for a substituted phenol, BP-OH was several orders of magnitude more reactive than BP and in

both cases was fully consumed after 6 hours in 300 °C sc-MeOH. However, there was no evidence for the cleavage of the 5-5 bond linking the two rings. The products were all dicyclic, the major ones being 2-phenylcyclohexanol and phenylcyclohexane as identified by GC-MS of the product solution (eq. 8).

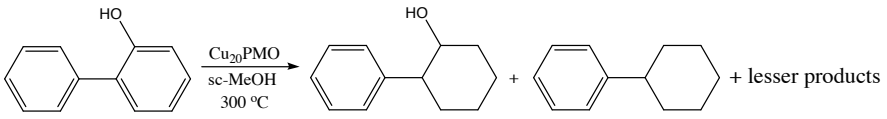

(8)

Organosolv Poplar Lignin (OPL). Reactions of OPL were carried out at 300 °C with the set of catalysts described above. Studies with the model compounds indicate that, while most ethers will undergo hydrogenolysis under these conditions, C-C bonds such as the 5-5 and β-5 linkages between lignin subunits will be resistant to cleavage. Consequently, one would expect under such conditions, that OPL will be disassembled substantially by the CuPMO catalysts, but that the products will be a mixture of monomeric and oligomeric species, modified by aromatic hydrogenation and ring methylation processes. This expectation was confirmed by gel permeation chromatography (GPC). Before reaction the average molecular weight (M_w) of the OPL substrate was determined by GPC to be ~2800 g mol^{-1}. With each catalyst, there was considerable (8-10 fold) decrease in M_w (Table 2, Appendix Fig. B3), but, given imprecision in this technique, especially at the lower molecular weights, the differences between individual catalysts may be within experimental uncertainties. GPC data for samples run for different time intervals (1 to 6 hours) showed a progression from the initial higher values of M_w to those seen at 6 hours, but significant differences between the outcomes for the different catalysts were not obvious (Appendix Table B12).

Table 2. Average molecular weight (M_w) determined by GPC for OPL before and after 6 hour reactions with Cu_{20}PMO catalysts at 300 °C.

Catalyst[a]	M_w (g mol^{-1})
Cu_{20}PMO	340
Cu_{20}PMO+FA	270
Cu_{20}PMOSm_5	300
Cu_{20}PMO+Sm^{3+}	280
OPL[b]	2800

[a]Conditions: 100 mg catalyst, 3 mL of MeOH and 100 mg of OPL. For FA, 100 μL of 88% aq. formic acid (1.17 mols) was added. For Sm^{3+} was added 5% of $Sm(OTf)_3$ regarding to catalyst weighted mass. [b] M_w value for OPL before the reaction. In absence of catalyst, the reaction of OPL in sc-MeOH give considerable insoluble char.

This laboratory has employed a holistic analysis method using proton NMR to examine catalytic transformations of similar substrates as described in Chapter II.[3] For unreacted OPL, the H_E, O_E, and A_E values are 20%, 41%, and 38%, respectively. After 6 hour reaction, there is a 3-fold increase in H_E and marked decreases in O_E and A_E for each catalyst. Decreases in O_E are very likely largely due to HDO of aliphatic carbons, while decreases in A_E can be attributed to ring hydrogenation and methylation. These pathways would correspondingly increase H_E. Appendix Table B13 summarizes the temporal NMR data for OPL reactions with the different catalysts.

Figure 16. Comparison of ^{1}H NMR spectra in $CDCl_3$ (δ= 7.24 ppm) of OPL (A) and of the product solutions after 6 hour reaction in sc-MeOH at 300°C with the following catalyst systems: $Cu_{20}PMO$ (B); $Cu_{20}PMO$+FA (C); $Cu_{20}Sm_5PMO$ (D); and $Cu_{20}PMO+Sm^3$ (E).

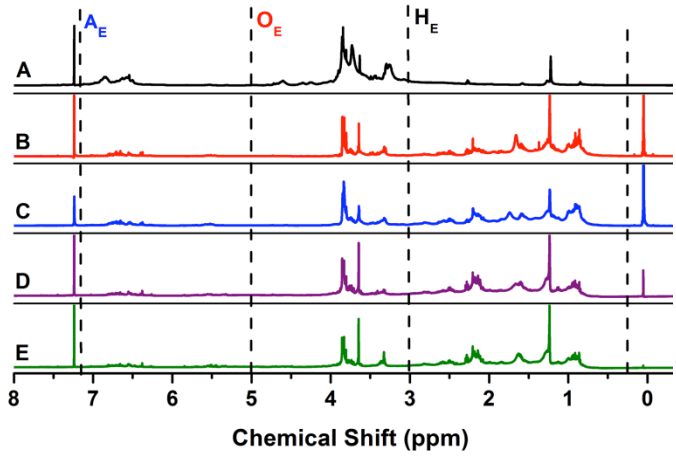

$A_{E:}$ aromatic region (5.0-7.0 ppm), O_E: near oxygen region (3.0 -5.0 ppm), H_E: aliphatic region (0.3 – 3.0 ppm). Conditions: 3.0 mL of MeOH, 100 mg OPL, 100 mg PMO catalyst, 6 hour reaction time.

While the GPC data show that the four catalysts each disassemble OPL over a 6 hour period, the holistic HNMR data indicates that this is accompanied by considerable HDO of aliphatic carbons. However, the percentage of aromatic protons also decreased considerably indicating that, during OPL disassembly, a significant amount of the aromatic content is converted in aliphatic compounds. These results corroborate data obtained with models where hydrogenolysis of α-O-4 and β-O-4 linkages leads to phenolic intermediates that are readily hydrogenated and methylated, thereby reducing the aromatic products.

Table 3. Holistic ^{1}H NMR data in $CDCl_3$ for OPL and for OPL products after 6 hour reaction with Cu_{20}PMO catalysts at 300 °C**.**

Catalyst[a]	H_E[b]	O_E[b]	A_E[b]
Cu_{20}PMO	68	20	12
Cu_{20}PMO+FA	64	22	14
$Cu_{20}PMOSm_5$	60	25	15
$Cu_{20}PMO+Sm^{3+}$	60	25	15
Org. Lignin	20	41	38

[a]Conditions: 100 mg catalyst, 3 mL of MeOH and 100 mg of OPL. For FA, 100 mL of 88% aq. formic acid was added. For Sm^{3+} 5 mg of $Sm(OTf)_3$ was added. [b] Values in the Table correspond to percent of protons in the integrated frequency regions 0.3–3.0 ppm (H_E), 3.0–5.0 ppm (O_E) and 5.0- 7.2 ppm (A_E).

The reaction of OPL with $Cu_{20}Sm_5$PMO with recycled catalyst were probed under standard conditions, 6 hour reaction time at 300 °C, for 4 consecutive runs. The solution was removed and analyzed by holistic ^{1}HNMR and GPC, and the solid catalyst was simply washed with methanol and reused. The NMR and GPC data showed modest differences between the first and second runs (Appendix Table B14), the net result using these analytical methods was that $Cu_{20}Sm_5$PMO was effective for depolymerizing OPL over multiple uses, as earlier studies from this laboratory have demonstrated with Cu_{20}PMO.[4,11]

Leaching Experiments.

These were done with $Cu_{20}Sm_5$PMO at 300 °C using BPE as the substrate. After sequential reactions with this catalyst, the methanolic solutions were separated from the solids and the metal content in the liquid fraction was examined by ICP-OES to determine the extent that Cu^{2+}, Al^{3+}, Mg^{2+} and Sm^{3+} had leached into the solution. This was done for

four consecutive runs to establish the compositional stability of the catalyst upon repetitive use. The net result was that leaching proved to be relatively insignificant; Mg^{2+} leached the most (0.81% total over the four runs), while there was much less leaching of Cu^{2+}, Al^{3+} and Sm^{3+} (0.19, 0.03 and 0.01%, respectively) (Appendix Table B15).

Leaching in the presence of added FA was also probed. ICP measurements examining the catalyst after heating Cu_{20}PMO (100 mg) at 300 °C for 6 hours in sc-MeOH (3.0 mL) containing 1.17 mmol of FA (50 μL of 88% aq. FA) showed no change in the Al: Cu: Mg: ratio 1.0: 0.60: 2:42 from that of the fresh catalyst (1.0: 0.63: 2.40). However, magnesium leaching (giving the ratio 1.0: 0.64: 2.15) was observed for an analogous experiment with a 10-fold higher amount of FA (11.7 mmol).

D. Conclusion

The Cu_{20}PMO and the various modifications examined here are all active catalysts in sc-MeOH (300 °C) for the hydrogenolysis of aryl ethers with hydrogen equivalents drawn from the methanol by reforming. This hydrogenolysis was particularly effective for α-O-4 and β-O-4 aryl ether linkages with the former being the more reactive. The catalysis was slower with the 4-O-5 diaryl ether linkages, necessitating higher temperatures (330 °C) to give high yields (>90%) within a comparable time frame. Not surprisingly, the reactivity order, α-O-4 > β-O-4 > 4-O-5, follows a sequence inverse to the bond strengths of these linkages. The incorporation of Sm^{3+} into the solid matrix to give $Cu_{20}Sm_5$PMO appears to accelerate the hydrogenolysis somewhat, but this may be attributed to an increase in the number of surface base sites. This view is supported by experiments with added formic or acetic acid. When the added acid was equivalent to the number of surface base sites, the reactivity decreased very significantly. A surprising suppression of hydrogenolysis was seen for a few

experiments where the Sm^{3+} was added to the medium as the triflate salt $Sm(OTf)_3$; however, we do not have a ready explanation of this observation. Even the most reactive modification $Cu_{20}Sm_5$PMO proved to be ineffective under these conditions for the cleavage of the 5-5 (diphenyl-like) and β-β carbon-carbon bonds that represent cross-links between monolignin units. While these are much less plentiful than the standard aryl ether linkages, the failure to cleave these much more refractory connections ensures that a certain fraction of the products from lignin reactions will be oligomers that will likely need additional processing.

For each of the models, one major product of the hydrogenolysis is a phenol derivative, and earlier studies[8,11] have identified such phenolics as major sources for product proliferation and the loss of aromaticity. We have speculated that this proliferation may result from reaction of the relatively acidic phenol at the surface base sites, where further hydrogenation to cyclohexanol derivatives and/or aromatic ring methylation occurs. This view was substantiated by the experiments where formic or acetic acid was added to the reaction medium in concentrations roughly equivalent to the surface base sites. In addition to substantially slowing hydrogenolysis of the aryl ether linkages, the aromatic phenolics proved to be substantially less reactive under these conditions toward secondary processes. Thus, while the hydrogenolysis reactivity of such acid modified systems was considerably slower, the selectivity toward aromatic products was much improved. This effect did not carry over in an obvious manner to OPL, which underwent considerable fragmentation to lower molecular weight monomers and oligomers, but none of the modified catalysts showed marked preference for aromatic products according to the holistic NMR analysis.

E. References

1. Springer, S. D.; He, J.; Chui, M.; Little, R. D.; Foston, M. B.; Butler, A. Peroxidative Oxidation of Lignin and a Lignin Model Compound by a Manganese SALEN Derivative. *ACS Sus. Chem. & Eng.*, **2016**, 4 (6), 3212-3219.
2. Macala, G. S.; Matson, T. D.; Johnson, C. L.; Lewis, R. S.; Iretskii, A. V.; Ford, P. C. Hydrogen transfer from supercritical methanol over a solid base catalyst: a model for lignin depolymerization. ChemSusChem, **2009**, 2, 215-217.
3. Barta, K.; Matson, T. D.; Fettig, M. L.; Scott, S. L.; Iretskii, A. V.; Ford, P. C. Catalytic disassembly of an organosolv lignin via hydrogen transfer from supercritical methanol. Green Chem. **2010**, 12, 1640-1647.
4. Matson, T. D.; Barta, K.; Iretskii, A. V.; Ford, P. C. One-pot catalytic conversion of cellulose and of woody biomass solids to liquid fuels. J. Am. Chem. Soc. **2011**, 133, 14090-14097.
5. Parida, K.; Das, J. J. Mg/Al hydrotalcites: preparation, characterization and ketonisation of acetic acid. Mol. Catal. A: Chem. **2000**, 151, 185−192.
6. Kruger, J. S.; Cleveland, N. S.; Shuting, Z.; Katahira, R.; Black, B. A.; Chupka, G. M.; Lammens, T.; Hamilton, P. G.; Biddy, M. J.; Beckman, G. T. Lignin Depolymerization with Nitrate-Intercalated Hydrotalcite Catalysts. ACS Catal. 2016, 6, 1316-1328.
7. Barta, K.; Ford, P. C. Catalytic conversion of nonfood woody biomass solids to organic liquids. Acc. Chem. Res. **2014**, 47, 1503-1512.
8. Bernt, C. M.; Bottari, G.; Barrett, J. A.; Scott, S. L.; Barta, K.; Ford, P. C. Mapping reactivities of aromatic models with a lignin disassembly catalyst. Steps toward controlling product selectivity. Catal. Sci. Technol. **2016**, 6, 2984 - 2994.

9. Scanlon, J. T.; Willis, D. E. Calculation of flame ionization detector relative response factors using the effective carbon number concept. J. Chromatogr. Sci. **1985**, 23, 333-340.
10. Macala, G. S.; Robertson A. W.; Johnson, C. L.; Day, Z. B.; Lewis, R. S.; White, M. G.; Iretskii, A. V.; Ford, P. C. Transesterification catalysts from iron doped hydrotalcite-like precursors: solid bases for biodiesel production. Catal. Lett. **2008**, 122, 205-209.
11. Barrett, J. A.; Gao, Y.; Bernt, C. M.; Chui, M.; Tran, A. T., Foston, M. B.; Ford, P. C. Enhancing Aromatic Production from Reductive Lignin Disassembly: in Situ O-Methylation of Phenolic Intermediates. ACS Sustainable Chem. Eng. **2016**, 4, 6877-6886.
12. Kim, S.; Chmely, S. C.; Nimlos, M. R.; Bomble, Y. J.; Foust, T. D.; Paton, R. S.; Beckham, G. T. Computational study of bond dissociation enthalpies for a large range of native and modified lignins.J. Phys. Chem. Lett., 2011, 2, 2846-2852.
13. van Scheppingen, W; Dorrestijn, E; Arends, I.; Mulder, P.; Korth, H .G. Carbon-oxygen bond strength in diphenyl ether and phenyl vinyl ether: An experimental and computational study. J. Phys. Chem. A. **1997**, 101, 5404-541.

IV. Selective Methylation with Niobium Doped CuPMOs

A. Introduction

This project was in collaboration with Professor Mauricio Boscolo of the Universidade Estadual Paulista, São José do Rio Preto, who was also interested in probing the reactivity and selectivity of the CuPMO by modifying the acidity of the catalyst. Catalysts with specific acidic sites on the solid surface have the ability to change the hydroxyl mobility on its surface, and modulate the selectivity of the alcohol reforming process. Niobium is known to increases the acidity, selectivity, and thermal stability of Al_2O_3, while the incorporation of niobium into alumina also provides increased Brønsted acid sites.[1,2] Fortuitously, Brazil is the leading global producer of niobium, as well as sugar cane.[3] Rich in abundant and underutilizes resources, a niobium and copper doped PMO capable of selectively disassembling waste sugarcane bagasse could greatly benefit the Brazilian economy.

Niobium pentoxide is a reducible material and presents strong metal support interactions, depending of the reduction temperature which is important characteristic for oxidation and hydrogenation reactions.[4] Sun et al.[5] found that the addition of Nb_2O_5 to $CuZnO/Al_2O_3$ does not change the methanol-reforming rate, but significantly influences the reformation of dimethoxymethane. The incorporation of Nb^{5+} in the lattice cannot be made with the dissolution of $NbCl_5$ in aqueous medium because it is highly reactive with water to form Nb_2O_5 (eq. 9). This prevents the process of co-precipitation with other metals from aqueous media but instead gives a two-phase solid.

$$2Nb^{5+} + 5H_2O \rightarrow Nb_2O_{5(s)} \qquad \text{(eq. 9)}$$

An exceptionally complex method developed by Krasnobaeva et al.[6] describes the incorporation of niobium into the lattice of the precipitated hydrotalcite. First a Mg/Al hydrotalcite was synthesized by co-precipitation of aluminum and magnesium nitrate in a basic solution of potassium hydroxide and potassium carbonate. The solid was then filtered and re-suspended in water. Next, carbonate was partially replaced with decavanadate $(V_{10}O_{28})^{6-}$, paramolybdate $(Mo_7O_{24})^{6-}$, or metatungstate $(H_2W_{12}O_{40})^{6}$ by the addition of potassium decavanadate, ammonium paramolybdate, or sodium tungstate respectively. Nitric acid was then added dropwise to the slurry until an optimum pH was achieved, and left to stir to exchange the carbonate ion. After washing and filtering, niobium oxide Nb_2O_5 was alloyed with potassium carbonate at 900 °C for 30 mins and then at 1050 °C for 40 minutes. The glassy cake was dissolved in minimal boiling water and then placed under vacuum over concentrated sulfuric acid until $K_8[Nb_6O_{19}]$ crystals precipitated. These crystals are then added to the hydrotalcite-like slurry as made above and the maximum loading capacity was found to be when the pH of the solution was 13. This group claimed to pioneer the synthesis of hydrotalcite like structures with polyoxoniobate $([Nb_6O_{19}]^{8-}$ ions.

Compared to this exceptionally complicated ion exchange method, Mauricio developed a new, quick and easy synthesis method. All of the metal salts were dissolved in methanol in order to keep $NbCl_5$ soluble in solution, and then precipitated in a basic solution containing sodium carbonate under sonication. This slurry is heated and slurried overnight at 65 °C, filtered, and washed with water, and easily and reliably become a niobium and copper doped HTC.

Takagaki et al. [7] have investigated niobia in biorefinery processes as catalysts for production of furan compounds from carbohydrates, and Ansanay et al. [8] have found

niobium oxide can be used in the delignification of lignocellulosic biomass in an aqueous medium. Thus, the aim of the present study is to evaluate the influence of the niobium in PMO derived from hydrotalcites $M^{2+}/M^{3+} = 3$ containing 10% copper. Decreasing the copper concentration in the PMO will result in a decreased amount of H_2 equivalents, a result that should influence hydrogenation and hydrogenolysis rates. Our premise is that addition of niobium will favor ring methylation preferentially over hydrogenation. The aromatic compounds investigated were: phenol, *o*-cresol, *m*-cresol, dimethylanisole, dimethylphenol, and BPE. The reactions were carried out in methanol under supercritical conditions.

B. Experimental

Materials

Benzyl phenyl ether (BPE) was obtained from Acros Organics while phenol, *o*-cresol, *m*-cresol, dimethylphenol and dimethylanisole were obtained from Sigma-Aldrich. All were used as received. Methanol (99.5%, Aldrich) was dried over activated molecular sieves before use. The salts for the hydrotalcite synthesis, $Cu(NO_3)_2 \cdot 3H_2O$, $Al(NO_3)_3 \cdot 9H_2O$ and $Mg(NO_3)_2 \cdot 6H_2O$, and $NbCl_5$ were purchased from Fisher Scientific and used without further purification.

Figure 17. Model compounds phenol, o-cresol, m-cresol, 2,6-dimethylanisole, 2,6-dimethylphenol, and benzyl phenyl ether (BPE)

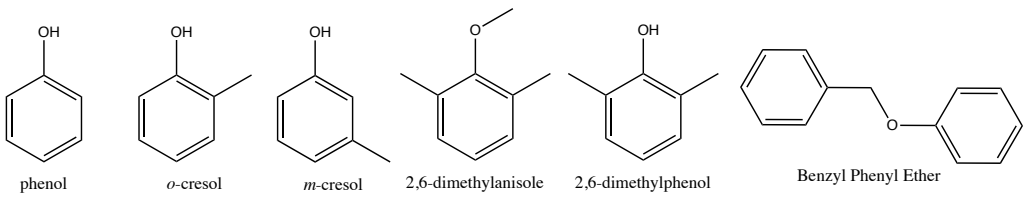

Catalyst Preparation and Characterization

The Cu-doped porous metal oxide Cu_{20}PMO was prepared from Cu-doped HTC by calcining as described previously.[9-11] For $Cu_{10}Nb_x$PMO, synthesis of the HTC precursor involved adding 5 mol percent Nb^{5+} of the overall PMO in the HTC preparation in the form of $NbCl_5$. The coprecipitation was done under sonication in methanol. The procedure was otherwise the same as that employed for the synthesis of Cu_{20}PMOs. Modified methods for the preparation of niobium and copper doped catalysts can be found in Appendix C. Both types of HTC precursors were calcined for 15 hours at 460 °C in air 24 hours prior to using the resulting PMOs in catalysis experiments. There was no difference in the reactivities of the PMO catalysts prepared by calcining freshly prepared HTCs and those that had been stored for up to 6 months before calcination.

X-Ray diffraction patterns were obtained using a Rigaku Miniflex diffractometer 300 with Cu Kα radiation (λ = 1.5418 Å) at tube voltage 30 kV and tube current 10 mA in the 2θ range of 10–70° with a scanning rate of 1.0 °/min. Thermogravimetric studies were performed with a Perkin-Elmer TG4000 thermobalance using a ~5 mg of sample under a N_2 flow (20 mL/min) in the temperature range 100-650 °C. Surface areas were calculated from the N_2 adsorption isotherms at -196 °C (BET) using 1.0 g of PMO's in a Micromeritics TriStar II instrument. The acidity and basicity of the PMO's was calculated from thermogravitric CO_2 and n-butylamine absorption as performed in a Perkin-Elmer TG4000 thermobalance. The HTC solids were calcined at 460 °C under N_2 atmosphere at 100 ^{o}C/min and then cooled to 50 °C at which time N_2 was substituted by CO_2 or by n-butylamine automatically. From the gain in mass. the number of moles of CO_2 or of n-butylamine adsorbed per gram of PMO were calculated.

Catalytic Reactions

The reactions in sc-MeOH were conducted in stainless steel mini-reactors as described before.[12] (*Caution! Under the reaction conditions, these vessels develop high internal pressures. Handle with care.)* For typical reactions with model compounds, the mini-reactors (total volume 10 mL) were loaded with 3 mL of methanol, 100 mg of catalyst, the substrate plus 0.10 mmol of decane as an internal standard. The temporal evolution of the substrate and of each product was determined by preparing a series of 6 mini-reactors that were loaded identically and placed in an oven that was thermostatted at 300 °C for all substrates. After specific reaction intervals (1 to 4 hours), one of these mini-reactors was removed and cooled rapidly by immersing in a water bath to quench the reaction. The reactor was then opened to release the gases, and the volume released was measured by a water displacement method.[13,14] (*Warning: this step requires special care owing to the large volume of gas sometimes released. In addition, both H_2 and CO are released, so proper ventilation is required.*) The methanolic product solutions were separated from the solid catalysts by passing through a 0.2 μm filter to remove any suspended particles. Product analysis of the solution was conducted by GC-FID by comparing the retention times to those of known standards. Product quantification utilized the effective carbon number (ECN) as a weighting factor for identified species to evaluate the area of GC-FID peaks corrected by the area of the internal standard (decane).[15,16] GC-FID analysis parameters, effective carbon numbers (ECN) and response factors (Appendix Tables B1 and B2) for all compounds identified are summarized in the Appendix. Temporal reactivity studies were carried out for each substrate with two different catalyst systems: (a) Cu_{10}PMO alone as the baseline; (b) $Cu_{10}Nb_{1.25}$PMO.

C. Results and Discussion

Catalyst Characterization

Prior to calcining, the precursor Cu_{10}, $Cu_{10}Nb_{1.25}$, $Cu_{10}Nb_{2.5}$, and $Cu_{10}Nb_5$ HTCs were analyzed by XRD to check the hydrotalcite structure. The XRD patterns found for the Cu_{10} and $Cu_{10}Nb_x$ hydrotalcites can be found in Appendix C. The replacement of Mg^{2+} by Cu^{2+} did not affect the HDL structure, but introduction of Nb^{+5} up to 5% resulted in decreased crystallinity according to the patterns observed in diffractograms, but with no characteristics indicating the formation of a bi-phasic solid.

Figure 18. Powder XRD chromatograms $Cu_{10}Nb_5$ HTC, $Cu_{10}Nb_{2.5}$ HTC, $Cu_{10}Nb_{1.25}$ HTC, Cu_{10} HTC, HTC from top to bottom.

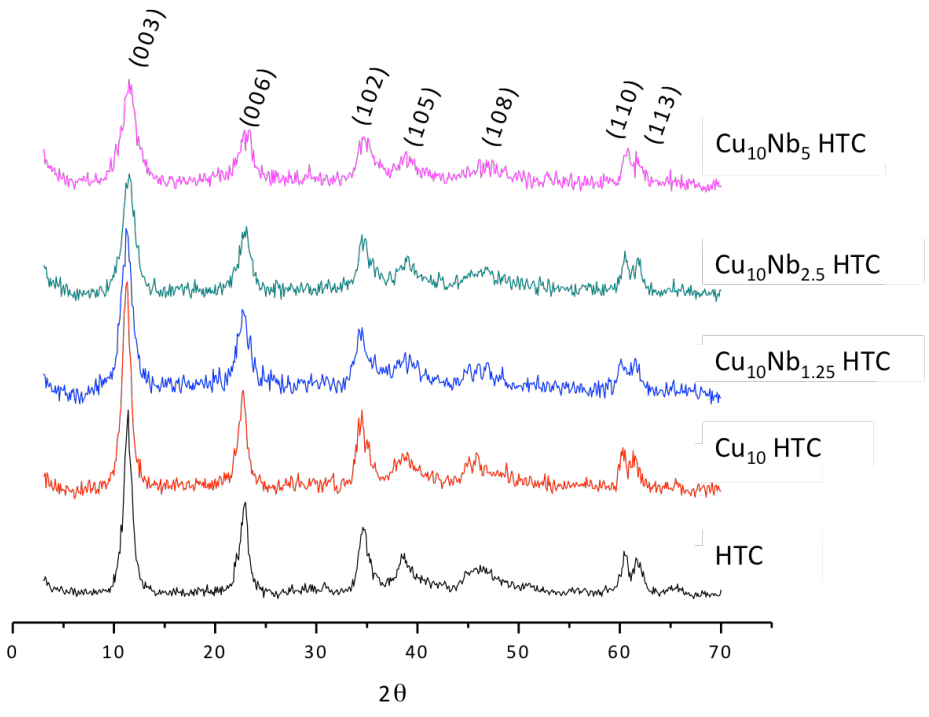

The lattice parameters are displayed on Table 4. The planes (003) and (006) are related to the basal spacing of hydrotalcites and the plane (110) is related to the diffraction plane on the hexagonal axis, regardless to the type of the interlayer anion. Such indexes are used in the calculation of network parameters, and the parameter defined as $\boldsymbol{a} = 2d_{110}$ e $\boldsymbol{c} = 3/2(d_{003} + 2d_{006})$.

Table 4. Crystallographic parameters

Catalyst	d (003)	d (006)	d (110)	*a* (Å)	*c* (Å)	*D* (Å)
HTC	7.58	3.849	1.514	3.028	22.92	75
Cu_{10} HTC	7.83	3.911	1.533	3.065	23.48	79.5
$Cu_{10}Nb_{1.25}$ HTC	7.65	3.86	1.526	3.051	23.06	67.5
$Cu_{10}Nb_{2.5}$ HTC	7.66	3.86	1.532	3.064	23.07	54.0
$Cu_{10}Nb_5$ HTC	7.66	3.80	1.521	3.043	22.88	51.4

The small increase of d_{003} and d_{006}, and the decrease of ***c*** are related to presence of Cu and Nb in the HTC lattice. This can be attributed to an increase in electrostatic attraction between the hydroxyl layer and the interlayer space. The carbonate ions also interact with the lamellar hydroxyl and the greater the shortening of the hydrogen bonds that hold them together, the lower interlayer distance. Regarding parameter ***a,*** the insertion of metals with different ionic radii showed an increase with respect to the value found in the reference material. However, the percentage variations of doping did not cause significant changes, indicating that the presence of Nb^{5+} did not change the typical hydrotalcite structure, corroborating other results that demonstrate the successful synthesis of the HTC with niobium.

The parameter D, *i.e.*, the particle size was calculated according to the Debye-Scherrer equation from the width at half maximum (FWHM) of the planes (003) and (006) values indicate that with increasing of Nb^{5+} content, the particle size decreased.[17]

Figure 19 shows the normalized thermogravimetry curves from the precipitated HTC. Two well-defined thermal mass loss events are evident in each case. The first event (at 100 ~ 250 °C) refers to loss of water, while the second event (250~430 °C) refers to the loss of OH and CO_2 .

Figure. 19. Normalized thermograms from 100-600 °C of HTC, Cu_{10}HTC, $Cu_{10}Nb_{1.25}$HTC, $Cu_{10}Nb_{2.5}$HTC, $Cu_{10}Nb_5$HTC from top to bottom.

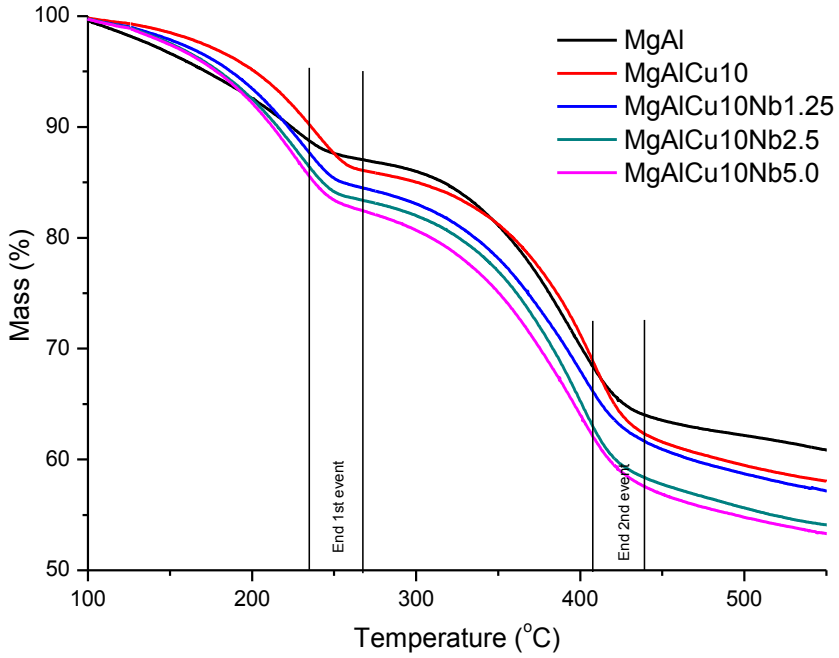

BET analysis was also performed on the catalysts to determine the surface area of the Cu_{10}PMO and $Cu_{10}Nb_x$PMOs.The surface areas determined for the Nb-doped PMOs fell

within a comparable range of approximately 200 m^2g^{-1} (Table 5), indicating that the pore-size of the catalysts was not significantly altered after Nb-surface deposition.

Table 5. Acidity, Bacisity, and Surface area of Cu_{10}HTC, $Cu_{10}Nb_{1.25}$HTC, $Cu_{10}Nb_{2.5}$HTC, $Cu_{10}Nb_5$HTC

	Acidity (mmol g^{-1})	Bacisity (mmol g^{-1})	Surface Area (m^2 g^{-1})
Cu_{10}	0.69	0.82	125
$Cu_{10}Nb_{1.25}$	0.76	0.66	205
$Cu_{10}Nb_{2.5}$	0.86	0.85	192
$Cu_{10}Nb_5$	0.75	0.61	177

To get a better understanding of the surface topography of the catalyst, we used scanning electron microscopy (SEM) imaging (Fig 20). After calcination, the catalyst loses its long-range order and breaks down into smaller sheets. These sheets can be observed in the bottom figures, where the brighter angular edges of the catalyst look almost tiered. Due to the lack of conductivity of these solids, the details of the PMO are not easily observed and would need to be coated with conductive gold to obtain better images.

Figure 20. SEM images of $Cu_{10}Nb_5$ in varying magnifications: 500X(top left), 1,000X (top right), 5,000X (bottom left) 10,000X (bottom right).

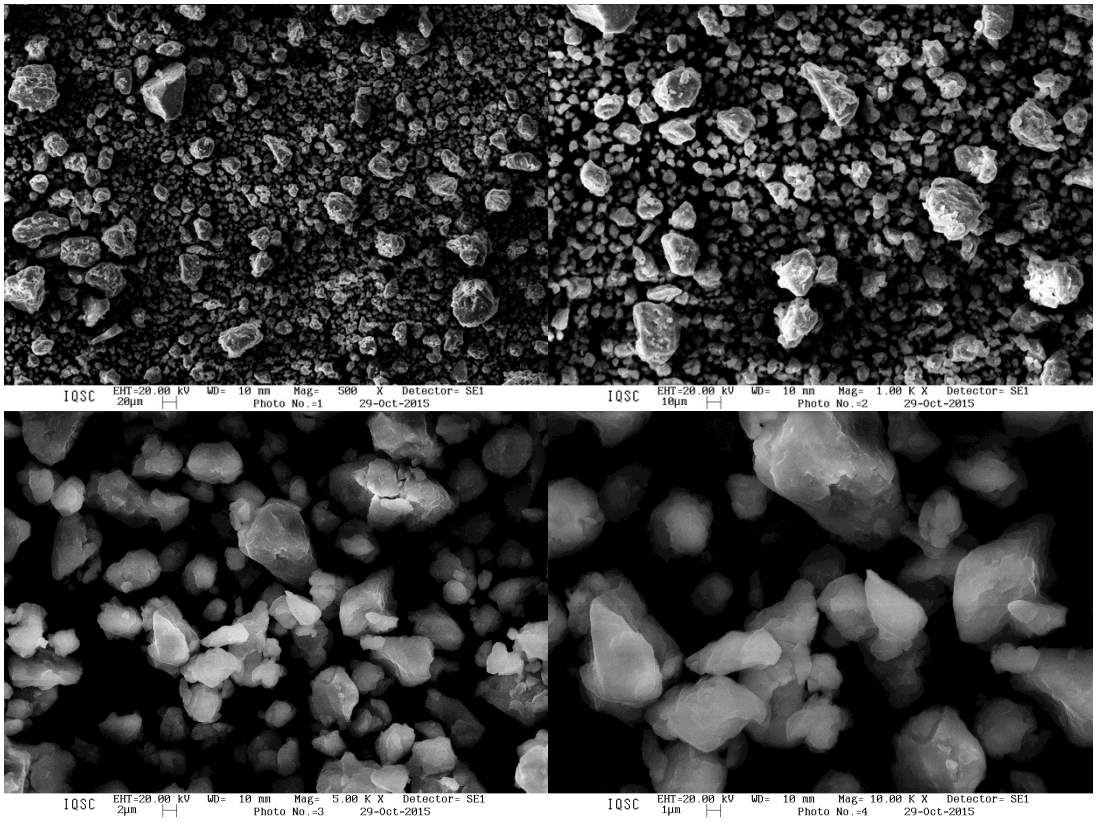

Reactivity with Model Compounds

Preliminary data collected by visiting Professor Mauricio Boscolo suggested that niobium doped catalysts selectively methylated the aromatic rings of small molecule substrates and catalyze the subsequent hydrogenation reactions of those rings.

Figure 21. GC-FID chromatograms and products identified by GC-MS after the reactions of phenol (left) and o-cresol (right) with Cu_{10}PMO (black) and $Cu_{10}Nb_{10}$ PMO (red) catalysts after 4 hours at 300 °C.

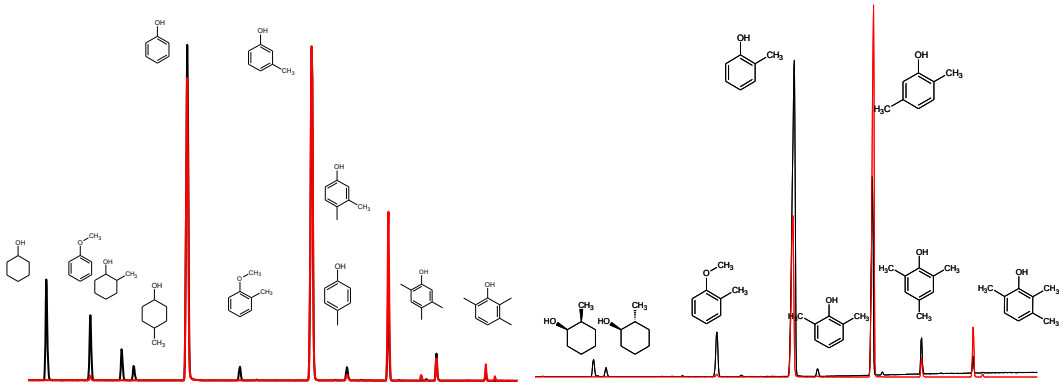

Figure 21 illustrates the different product distributions when reacting phenol and o-cresol with Cu_{10}PMO and $Cu_{10}Nb_{1.25}$PMO. As shown in Figure 21, the products produced in the presence of the niobium-doped catalyst are largely aromatic and undergo further aromatic c-methylation and o-methylation. In the presence of just Cu_{10}, both phenol and o-cresol undergo aromatic hydrogenation, as described by Bernt et. al.[15] Further studies by Barrett et. al.[18] demonstrated an ability to introduce a methylating co-solvent dimethyl carbonate to enhance the yields of aromatic products. However, a reactive stoichiometric co-solvent is far from ideal. A niobium and copper doped catalyst marries the two ideas of decreasing the copper content to decrease the amount of H_2 equivalents produced, and introducing a metal proven to be a methylation catalyst.

Data summarizing the overall reactivity of such catalysts are summarized in Table 6. Decreasing the copper concentration to 10 % resulted in an anticipated decrease in conversion of phenol; with the Cu_{20} catalyst, the phenol would have been converted to

saturated products in 4 hours.

Table 6. Overall reactivity and mass balance of phenol, o- & m-cresol, 2,6-dimethylanisole, 2,6-dimethylphenol, and BPE after 4 hours at 300 °C.

	Phenol		o-cresol		m-cresol	
	Cu_{10}	$Cu_{10}Nb_{1.25}$	Cu_{10}	$Cu_{10}Nb_{1.25}$	Cu_{10}	$Cu_{10}Nb_{1.25}$
Saturates (μmol)	56	18	39	10	0	0
Aromatics (μmol)	501	352	387	440	349	457
Conversion (%)	79	81	81	81	100	98
Mass balance (%)	54	36	42	45	44	58

	Dimethylanisole		Dimethylphenol		BPE	
	Cu_{10}	$Cu_{10}Nb_{1.25}$	Cu_{10}	$Cu_{10}Nb_{1.25}$	Cu_{10}	$Cu_{10}Nb_{1.25}$
Saturates (μmol)	0	0	19	11	65	24
Aromatics (μmol)	1033	1039	1085	1115	1194	1168
Conversion (%)	18	16	25	33	99	100
Mass balance (%)	88	88	81	103	77	72

Surprisingly, m-cresol was observed to be more reactive than o-cresol. Further experiments with 3,5- dimethylanisole and 3,5-dimethylphenol with Cu_{10} PMO and $Cu_{10}Nb_{1.25}$ would be helpful to investigate the selectivity of methylation. However, as shown in Table 6, the poor mass balances seen for the six model compounds do not provide much confidence in the quantitative product distributions.

D. Conclusion

In an effort to prepare a catalyst capable of performing more selective disassembly of lignocellulosic biomass, four Cu_{10}PMO catalysts with varying amounts of niobium (1.25, 2.5, 5.0, 10.0%) were synthesized and investigated. Decreasing the overall copper content in the Cu_{10}PMO and $Cu_{10}Nb_{1.25}$PMO examined lowered the reactivity of the catalysts in sc-MeOH (300 °C) while improving the selectivity towards aromatic products. Although changes in the niobium concentration did not greatly alter the reactivity, the niobium-doped catalysts did display greater selectivity toward the formation of aromatic products in their reactions with several model compounds. The source of this selectivity was apparently the greater reactivity toward both O- and ring methylation of phenolic intermediates. The much lower reactivities of the resulting compounds toward ring methylation preserves the overall aromaticity of the products. The niobium-doped catalysts exhibited the ability to perform hydrogenolysis, hydro-deoxygenation, methylation, and hydrogenation. The selectivity of these catalysts suggests their future possible applications in producing commodity aromatic chemicals from lignocellulosic biomass.

E. References

1. Tanabe, K. Catalytic Applications of Niobium Compounds. *Catalysis Today* **2003**, 78, 65
2. Dakta, J. ; Turek, A.M. ; Jehng, J.M. ; Wachs, I.E. Acidic Properties of Supported Niobium Oxide Catalysts : An Infrared Spectroscopy Investigation. *Journal of Catalysis*. **1992**, 135, 186-199.
3. United States Geological Survey Mineral Resources Program. "Niobium and Tantalum-Indispensable Twins". Fact Sheet. Reston, VA. June 2014. Web.
4. Guarido, C.E.M.; Cesar, D.V.; Souza, M.M.V.M.; Schmal, M. Ethanol Reforming and Partial Oxidation with Cu/Nb_2O_5 catalyst. *Catalysis Today*. **2009**, 142, 252
5. Qing, S.; Auroux, A.; Shen, J. Surface acidity of niobium phosphate and steam reforming of dimethoxymethane over CuZnO/Al 2O 3–NbP complex catalysts. *Journal of Catalysis*. **2006**, 244, 1-7.
6. Krasnobaeva O.N.; Belomestnykh, I.P.; Nosova, T.A.; Elizarova, T.A.; Isagulyants, G.V.; Kolesnikov, S.P.; Danilov, V.P. Niobium-Containing Catalysts fir Oxydehydrogenation of Hydrocarbons and Alcohols. *Russian Journal of Inorganic Chemistry*. **2011**, 56, 168-172.
7. Takagaki, A.; Ohara, M.; Nishimura, S.; Ebitani, K. A One-Pot Reaction for Biorefinery: Combination of Solid Acid and Base Catalysts for Direct Production of 5-hydroxymethylfurfural from saccharides. *Chemical Communications* **2009,** 41, 6276.
8. Ansanay, Y; Kolar, P.; Sharma-Shivappa, R.R.; Cheng, J.J. Niobium oxide catalyst for delignification of switchgrass for fermentable sugar production. Industr. Crops Prod. **2014,** 52, 790-5.

9. Macala, G. S.; Matson, T. D.; Johnson, C. L.; Lewis, R. S.; Iretskii, A. V.; Ford, P. C. Hydrogen transfer from supercritical methanol over a solid base catalyst: a model for lignin depolymerization. *ChemSusChem*, **2009**, *2*, 215-217.
10. Barta, K.; Matson, T. D.; Fettig, M. L.; Scott, S. L.; Iretskii, A. V.; Ford, P. C. Catalytic disassembly of an organosolv lignin via hydrogen transfer from supercritical methanol. *Green Chem.* **2010**, *12*, 1640-1647.
11. Matson, T. D.; Barta, K.; Iretskii, A. V.; Ford, P. C. One-pot catalytic conversion of cellulose and of woody biomass solids to liquid fuels. *J. Am. Chem. Soc.* **2011**, *133*, 14090-14097.
12. Barta, K.; Ford, P. C. Catalytic conversion of nonfood woody biomass solids to organic liquids. *Acc. Chem. Res.* **2014**, *47*, 1503-1512.
13. Barta, K.; Matson, T. D.; Fettig, M. L.; Scott, S. L.; Iretskii, A. V.; Ford, P. C. Catalytic disassembly of an organosolv lignin via hydrogen transfer from supercritical methanol. *Green Chem.* **2010**, *12*, 1640-1647.
14. Matson, T. D.; Barta, K.; Iretskii, A. V.; Ford, P. C. One-pot catalytic conversion of cellulose and of woody biomass solids to liquid fuels. *J. Am. Chem. Soc.* **2011**, *133*, 14090-14097.
15. Bernt, C. M.; Bottari, G.; Barrett, J. A.; Scott, S. L.; Barta, K.; Ford, P. C. Mapping reactivities of aromatic models with a lignin disassembly catalyst. Steps toward controlling product selectivity. *Catal. Sci. Technol.* **2016,** *6*, 2984 - 2994.
16. Scanlon, J. T.; Willis, D. E. Calculation of flame ionization detector relative response factors using the effective carbon number concept. *J. Chromatogr. Sci*. **1985**, *23*, 333-340.

17. Benito, J.M.; de Jesus, E.; de la Mata, F.J.; Flores, J.C. Carbosilane Dendrimers Containing Peripheral Cyclopentadienyl Niobium and Tantalum-imido Complexes. *Journal of Organometallic Chemistry*. **2006**, 691, 3602.
18. Barrett, J. A.; Gao, Y.; Bernt, C. M.; Chui, M.; Tran, A. T., Foston, M. B.; Ford, P. C. Enhancing Aromatic Production from Reductive Lignin Disassembly: in Situ O-Methylation of Phenolic Intermediates. ACS Sustainable Chem. Eng. 2016, 4, 6877-6886.

V. Sulfur Resistant Molybdenum Doped CuPMOs

A. Introduction

In the paper industry, excess pulp and biomass wastes are often treated with sulfuric acid, resulting in the production of lignosulfonate. The Cu_{20}PMO catalyst has been shown to perform poorly in the presence of sulfur,[1] and this limits potential applications in the disassembly of lignin derivatives from certain processes. In Chapter III, we discussed the effects of adding mineral acids to the reaction mixture. The addition of both hydrochloric acid and sulfuric acid poisoned the catalyst. When opening the reactor with sulfuric acid, we immediately smelled the sulfur dioxide, and the reactor(s) were placed into the fume hood for ventilation. After the vessel was thoroughly purged with air, the catalyst was filtered and the filtrate was a pale blue color, indicating that a significant amount of copper had leached into the methanol solution. MoS_2 is an industrially used catalyst to enhance desulfurization and deoxygenation, thus molybdenum has been suggested as a potential additional dopant to the current Cu_{20}PMO catalyst to combat sulfur poisoning.[2] The models investigated were the α-O-4 linkage model BPE, the β-5 linkage model DHBF, the sulfur aromatic compound benzyl mercaptan, and the sulfonate aromatic compound methyl p-toluene sulfonate (Figure 22). The catalyst was synthesized to have varying amounts (1.25, 2.5, 5, 10 %) weight percent of molybdenum in the overall calcined PMO. The various doping levels of molybdenum did not display differences in reactivity, however the mere presence of molybdenum greatly altered the reactivity and selectivity. Reactions with BPE and DHBF produced nearly all aromatic products when reacted with a molybdenum doped catalyst. Unfortunately, the products from the reactions with benzyl mercaptan and methyl p-toluene sulfonate did not yield reliable and quantifiable data.

B. Experimental

Materials

Benzyl phenyl ether (BPE), methyl p-toluene sulfonate (MPTS) and benzyl mercaptan (BM) were obtained from Acros Organics while 2,3 dihydrobenzofuran (DHBF) was obtained from Oakwood Chemical. All were used as received. Methanol (99.5%, Aldrich) was dried over activated molecular sieves before use. The salts for the hydrotalcite synthesis, $Cu(NO_3)_2 \cdot 3H_2O$, $Al(NO_3)_3 \cdot 9H_2O$ and $Mg(NO_3)_2 \cdot 6H_2O$, were purchased from Fisher Scientific and used without further purification.

Figure 22. Model compounds benzyl phenyl ether (BPE) 2,3-dihydrobenzofuran (DHBF), methyl p-toluene sulfonate (MPTS), and benzyl mercaptan (BM)

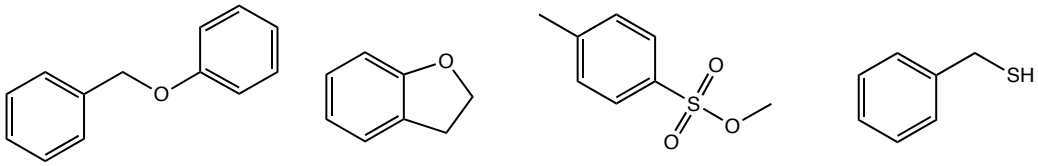

benzyl phenyl ether (BPE) dihydrobenzofuran methyl-p-toluene sulfonate benzyl mercaptan

Catalyst Preparation and Characterization

The Cu-doped porous metal oxide Cu_{20}PMO was prepared from Cu-doped HTC by calcining as described previously.[3-5] For $Cu_{20}Mo_x$PMO, synthesis of the HTC precursor involved adding 5 mol percent Mo^{6+} of the overall in the HTC preparation in the form of ammonium molybdate tetrahydrate ($(NH_4)_4Mo_7O_{24} \cdot 4H_2O$). The procedure was otherwise the same as that employed for the synthesis of Cu_{20}PMOs. A modified method of molybdenum surface deposition onto the hydrotalcite via equilibrium deposition filtration can be found in Appendix D.[6] Both types of HTC precursors were calcined for 15 hours at

460 °C in air to give the PMO within 24 hours prior to use in catalysis experiments. There was no difference in the reactivities of the PMO catalysts prepared by calcining freshly prepared HTCs and those that had been stored for up to 6 months before calcination.

Surface areas of the Cu_{20}PMO and $Cu_{20}Mo_x$PMO catalysts, freshly calcined overnight at 460 °C, were measured using a Tristar 3000 porosimeter. A weighed sample (~150 mg) of each catalyst was loaded into an analysis tube and then degassed at 225 °C under a stream of N_2(g) overnight. A full isotherm was collected to determine surface area, pore volume, and pore size. The HTC catalyst was also analyzed by powder X-ray diffraction (XRD) using a Bruker D8 Advance High Temperature Powder Diffractometer.

Catalytic Reactions

The reactions in sc-MeOH were conducted in stainless steel mini-reactors as described before.[7] (*Caution! Under the reaction conditions, these vessels develop high internal pressures. Handle with care.)* For typical reactions with model compounds, the mini-reactors (total volume 10 mL) were loaded with 3 mL of methanol, 100 mg of catalyst, the substrate plus 0.10 mmol of decane as an internal standard. The temporal evolution of the substrate and of each product was determined by preparing a series of 6 mini-reactors that were loaded identically and placed an oven thermostatted at 300 °C for BPE, DHBF, MPTS, and BM. After specific reaction intervals (1 to 6 hours), one of these mini-reactors was removed and cooled rapidly by immersing in a water bath to quench the reaction. The reactor was then opened to release the gases, and the volume released was measured by a water displacement method.[4,8] (*Warning: this step requires special care owing to the large volume of gas sometimes released. In addition, both H_2 and CO are released, so proper ventilation is required.*) The methanolic product solutions were separated from the solid

catalysts by passing through a 0.2 μm filter to remove any suspended particles. Product analysis of the solution was conducted by GC-FID by comparing the retention times to those of known standards. Product quantification utilized the effective carbon number (ECN) as a weighting factor for identified species to evaluate the area of GC-FID peaks corrected by the area of the internal standard (decane).[9,11] GC-FID analysis parameters, effective carbon numbers (ECN) and response factors (Appendix Tables B1 and B2) for all compounds identified are summarized in the Appendix.

Temporal reactivity studies were carried out for each substrate with five different catalyst systems: (a) Cu_{20}PMO alone as the baseline; (b) $Cu_{20}Mo_{1.25}$PMO with ~1.25 weight % molybdenum of the calcined PMO; (c) $Cu_{20}Mo_{2.5}$PMO with ~2.5 weight % molybdenum of the calcined PMO; (d) $Cu_{20}Mo_5$PMO with ~5 weight % molybdenum of the calcined PMO; (e) $Cu_{20}Mo_{10}$PMO with ~10 weight % molybdenum of the calcined PMO.

C. Results and Discussion

Catalyst Characterization

Prior to calcining, the Cu_{20}, $Cu_{20}Mo_{1.25}$, $Cu_{20}Mo_{2.5}$, $Cu_{20}Mo_5$, and $Cu_{20}Mo_{10}$ HTC's were analyzed by XRD to verify the hydrotalcite structure. The XRD patterns found for the Cu_{20} and $Cu_{20}Mo_{1.25}$, $Cu_{20}Mo_{2.5}$, $Cu_{20}Mo_5$, and $Cu_{20}Mo_{10}$ hydrotalcites (Appendix Fig. B1) are consistent with the literature data for HTCs. The catalysts will be analyzed by ICP to ensure the metal ratios are in agreement with the calculated concentrations.[10] In addition, the surface areas and porosities of the calcined PMOs were determined using porosimetry, summarized in Table 7. The addition of molybdenum does little to the measured surface area, pore size, and pore volume. These values are also similar to those collected in Chapter

III for Cu_{20}PMO and $Cu_{20}Sm_5$PMO, indicating these hydrotalcite structures display very similar characteristics, regardless of dopant.

Table 7. Surface area, pore volume, and pore size of Cu_{20}PMO, $Cu_{20}Mo_{1.25}$PMO, $Cu_{20}Mo_{2.5}$PMO, $Cu_{20}Mo_5$PMO, $Cu_{20}Mo_{10}$PMO,

Catalyst	Surface Area ($m^2\ g^{-1}$)	Pore Volume ($cm^3 g^{-1}$)	Pore Size (nm)
Cu_{20}	200	1.11	22.3
$Cu_{20}Mo_{1.25}$	214	1.02	19.1
$Cu_{20}Mo_{2.5}$	219	1.2	21.9
$Cu_{20}Mo_5$	170	1.05	24.7
$Cu_{20}Mo_{10}$	168	1.1	26

Benzyl Phenyl Ether (BPE)

Extensive studies with BPE and Cu_{20}PMO have been shown by Bernt, et, al.[9] and Barrett, et. al.[12] where BPE undergoes rapid ether hydrogenolysis followed by subsequent aromatic hydrogenation. This reaction was repeated to ensure the catalytic activity of the original Cu_{20} catalyst synthesized displayed similar reactivity as shown in Chapter III.

Molybdenum-doped PMOs displayed reactivity towards the model compound BPE, exhibiting on average 80% conversion of this model over a six hour-period. The major products in the reactions of benzyl phenyl ether with the above catalysts were toluene and phenol. When compared to the Cu_{20}PMO catalyst, Mo-doped catalysts exhibited lower reactivity. This is evidenced by the fact that after three hours, Cu_{20}PMO converted 100% of BPE to other products, while only 80% of BPE was converted by Mo-doped catalysts.

Figure 23. Temporal BPE consumption and major products from the reaction with Cu_{20}PMO at 300 °C.

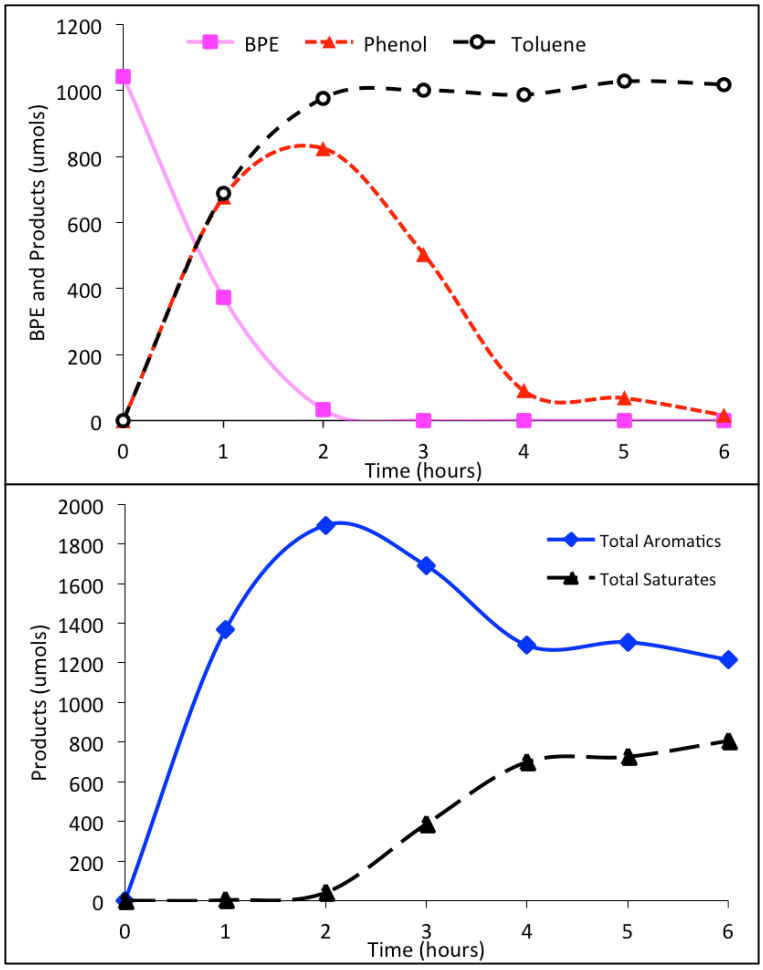

While reactivity of Mo-doped catalysts is lower than the Cu_{20}PMO, these catalysts exhibited a different selectivity in their reactions with BPE. Figure 23 compares catalytic selectivity in BPE conversion, displaying the production of total aromatic compounds and total saturated compounds over a six-hour time period. Cu_{20}PMO converts BPE to a mixture of aromatic compounds and saturated compounds. As anticipated from Chapter III, after six hours we achieved 100% conversion with toluene in nearly stoichiometric amounts, and

phenol derived cyclohexanol and methylcyclohexanols as the main products with 97 % mass balance.

Figure 24. Temporal BPE consumption and major products from the reaction with $Cu_{20}Nb_{1.25}$ PMO at 300 °C.

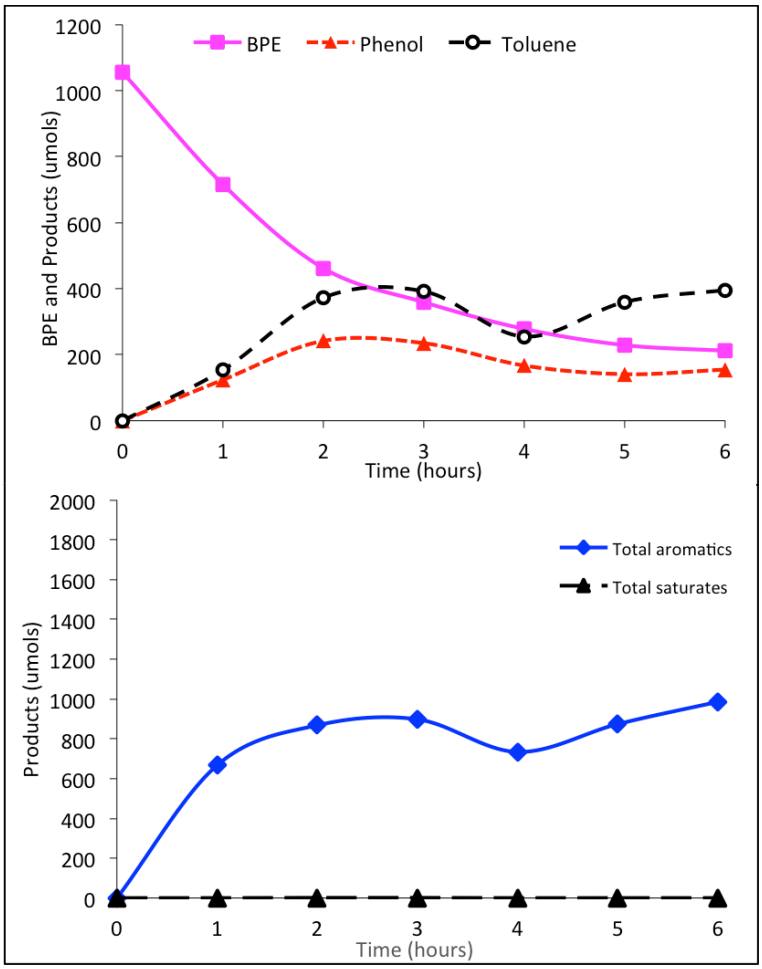

In contrast, aromatic ring hydrogenation appeared to be suppressed with the molybdenum doped catalysts so that aromatic products were exclusively observed from their reaction with BPE. However, after reacting for 4 hours at 300 °C with $Cu_{20}Mo_{1.25}$, we only achieved 80 % conversion and 67 % mass balance. Surprisingly, only 47 % of the normally

very stable toluene was recovered after six hours, while unidentified monomers and dimers were observed. See Appendix D Table D2 for full product list.

One possible reason for this alteration in selectivity may be due to the blocking of active sites within the porous metal oxide by molybdenum on the catalyst surface. As mentioned previously, Cu_{20}PMO is responsible for the production of hydrogen gas through its reactions with methanol, carbon monoxide, and water (eqs 1,2). The hydrogen gas produced provides the necessary reducing equivalents in reactions carried out by the catalyst on the substrate. A lower amount of hydrogen gas production would result in less available reducing equivalents for reactions such as aromatic hydrogenation.

2,3- Dihydrobenzofuran (DHBF)

Mo-doped catalysts exhibited low reactivity towards the model compound DHBF. Reactivity of the Cu_{20}PMO catalyst towards the conversion of DHBF is also lower than its reactivity towards BPE, demonstrating only 36% conversion over a six-hour period. While reactivity of the Mo-doped catalysts towards DHBF is significantly lower than that of the original catalyst (9.2% by $Cu_{20}Mo_{10}$PMO after 6 hours), different selectivity was again observed. As observed with BPE conversion, Mo-doped catalyst activity produced exclusively aromatic compounds in reactions with DHBF(Figure 25). The major products were methylanisole, cresols, and xylenols.

Figure 25. Temporal DHBF consumption and major products from the reaction with Cu_{20}PMO (top) and $Cu_{20}Mo_{1.25}$PMO (bottom) at 300 °C.

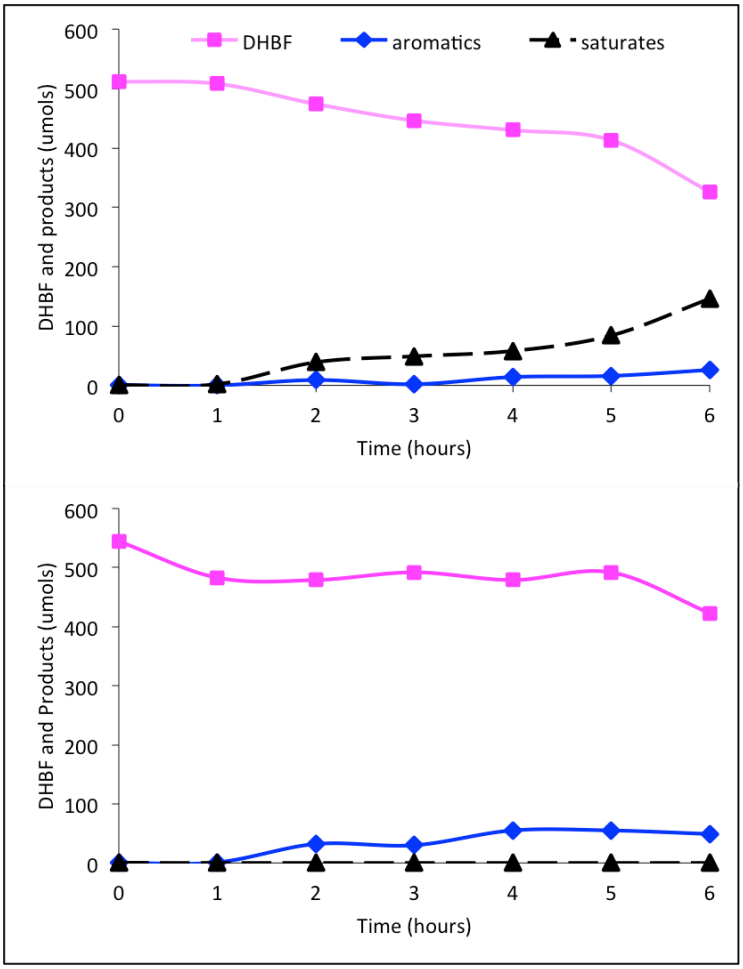

This activity differs from that of the Cu_{20}PMO in that the major product of the catalysis of DHBF by Cu_{20}PMO under analogous conditions is 2-ethylcylohexanol, a saturated molecule. 2-ethylcyclohexanol is produced as a result of aromatic hydrogenation of 2-ethylphenol, another major product in the reaction between Cu_{20}PMO and DHBF

Methyl P-Touene Sulfonate (MTPS)

The next model compound subjected to reactions with the synthesized catalyst was methyl-p-toluene sulfonate. After two hours, this substrate was no longer observed in GC-FID analysis, the major product observed from this reaction was toluene. However, results from reactions of all catalysts towards methyl-p-toluene indicate the production of a large amount of unknown monomers. See Appendix Tables D12-13 for data tables containing detailed product distributions. Furthermore, while all catalysts appear to be reactive towards the substrate, the mass balance was poor. At this point in time, it is thought that this reaction results in the production of insoluble organic products, which would result in the shortage of products within the liquid sample. Further analysis of the solids recovered after catalysis would be required to investigate this hypothesis.

Benzyl Mercaptan (BM)

The final model compound that was investigated is benzyl mercaptan. This compound was chosen as a simple model to examine the reactivity of our catalyst in the presence of sulfur impurities. All catalysts were subjected to reaction with this substrate at 300°C for 6 hours. The conversion efficiency of the all catalysts investigated was high, ranging from 93.5-97.7% after 6 hours. Major identified products for this reaction include toluene and benzyl alcohol. A large amount of unknown monomers was produced in the reaction, and the elucidation of their identities is necessary for subsequent analysis. See Appendix Table D14 for data tables containing detailed product distributions.

D. Conclusion

Efforts to create a robust catalyst capable of performing selective disassembly of lignocellulosic biomass, four Cu_{20}PMO catalysts with varying amounts of molybdenum (1.25, 2.5, 5.0, 10.0%) were prepared and investigated. The Mo-doped catalysts exhibited the ability to perform hydrogenolysis, hydro-deoxygenation, methylation, hydrogenation, and condensation. These catalysts displayed a high amount of selectivity in their reactions with model compounds, producing exclusively aromatic products when reacted with benzyl phenyl ether and 2,3-dihydrobenzofuran. Unfortunately, the catalyst did not perform as well with sulfur compounds methyl p-toluene sulfonate and benzyl mercaptan. Previous chapters highlighted the increased activity of the catalyst in the presence of samarium, as well as increased selectivity of a niobium dopant. The addition of molybdenum to the catalyst displayed increased selectivity towards aromatic compounds, but with poor mass balance. It is possible the molybdenum deactivates the active sites of the catalyst and hinders the methanol reforming process, decreasing the H_2 production, thus forming insoluble products. The sulfur compounds likely poison the catalyst during the reaction, and again form insoluble chars. The initial selectivitties of these catalysts towards aromatic products are promising, however more work must be done towards developing sustainable catalysts resistant to sulfur capable of processing waste derived from the paper pulping process.

E. References

1. Baskerville, C. Reduction of Concentrated Sulfuric Acid by Copper. *Journal of the American Chemical Society,* **1896**, 18 (11), 942-947
2. Topsøe, H.; Clausen, B. S.; Massoth F. E. *Hydrotreating Catalysis, Science and Technology*; Andersen, J. R., Boudart, M., Eds.; Springer: Berlin, **1996**; Vol. 11.
3. Macala, G. S.; Matson, T. D.; Johnson, C. L.; Lewis, R. S.; Iretskii, A. V.; Ford, P. C. Hydrogen transfer from supercritical methanol over a solid base catalyst: a model for lignin depolymerization. *ChemSusChem*, **2009**, *2*, 215-217.
4. Barta, K.; Matson, T. D.; Fettig, M. L.; Scott, S. L.; Iretskii, A. V.; Ford, P. C. Catalytic disassembly of an organosolv lignin via hydrogen transfer from supercritical methanol. *Green Chem.* **2010**, *12*, 1640-1647.
5. Barta, K.; Ford, P. C. Catalytic conversion of nonfood woody biomass solids to organic liquids. Acc. Chem. Res. 2014, 47, 1503-1512.
6. Fountzoula, Ch.; Spanos, N.; Matralis, H.K.; Kordulis, Ch. *Applied Catalysis B: Environmental*, **2002**, 35, 295.
7. Barta, K.; Ford, P. C. Catalytic conversion of nonfood woody biomass solids to organic liquids. Acc. Chem. Res. **2014**, 47, 1503-1512.
8. Matson, T. D.; Barta, K.; Iretskii, A. V.; Ford, P. C. One-pot catalytic conversion of cellulose and of woody biomass solids to liquid fuels. *J. Am. Chem. Soc.* **2011**, *133*, 14090-14097.
9. Bernt, C. M.; Bottari, G.; Barrett, J. A.; Scott, S. L.; Barta, K.; Ford, P. C. Mapping reactivities of aromatic models with a lignin disassembly catalyst. Steps toward controlling product selectivity. *Catal. Sci. Technol.* **2016,** *6*, 2984 - 2994.

10. Macala, G. S.; Robertson A. W.; Johnson, C. L.; Day, Z. B.; Lewis, R. S.; White, M. G.; Iretskii, A. V.; Ford, P. C. Transesterification catalysts from iron doped hydrotalcite-like precursors: solid bases for biodiesel production. Catal. Lett. 2008, 122, 205-209.
11. Scanlon, J. T.; Willis, D. E. Calculation of flame ionization detector relative response factors using the effective carbon number concept. *J. Chromatogr. Sci*. **1985**, *23*, 333-340.
12. Barrett, J. A.; Gao, Y.; Bernt, C. M.; Chui, M.; Tran, A. T., Foston, M. B.; Ford, P. C. Enhancing Aromatic Production from Reductive Lignin Disassembly: in Situ O-Methylation of Phenolic Intermediates. ACS Sustainable Chem. Eng. 2016, 4, 6877-6886.

Appendix A

A1. Synthesis and Characterization of $Cu_{20}Pr_5HTC$

Figure A1: Powder X-Ray Diffraction pattern for $Cu_{20}Pr_5HTC$

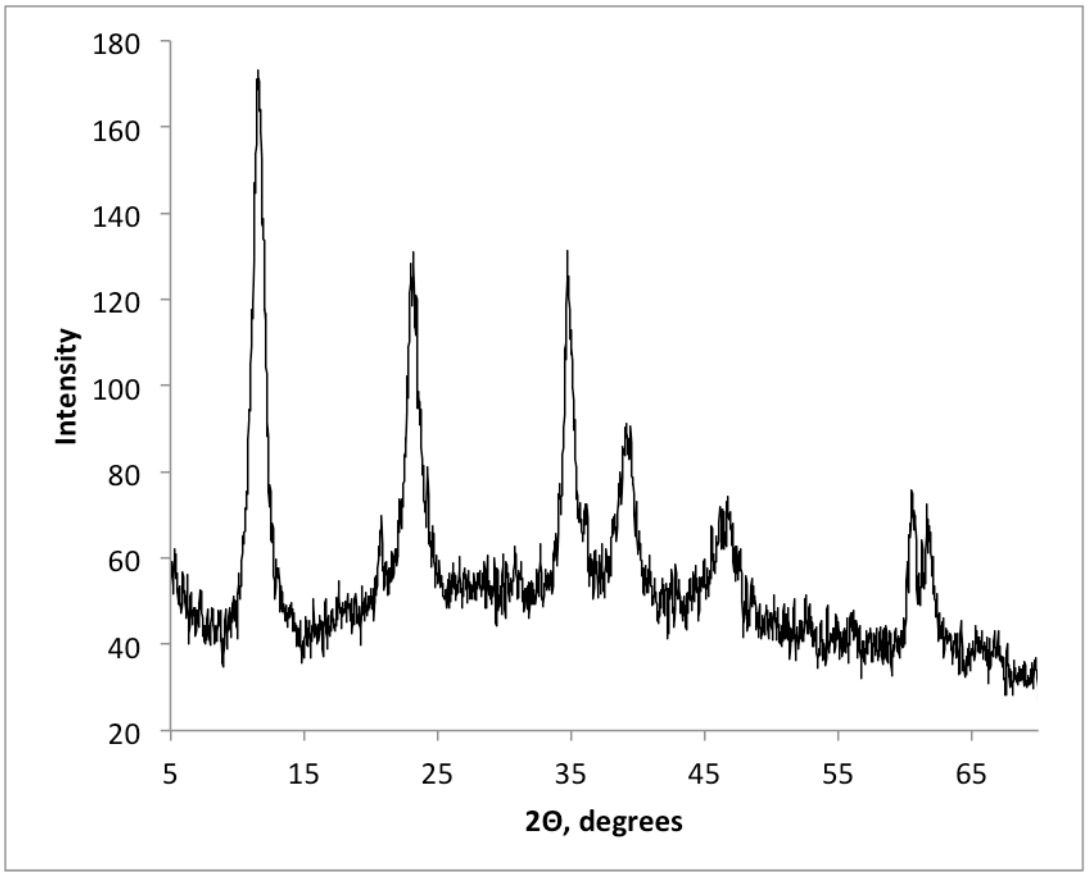

$Cu_{20}Pr_5$ HTC was synthesized by a modified coprecipitation method. 1.06 g Na_2CO_3 was added to 75 mL of DI H_2O in a 600 mL beaker with stirring and heated to 60 °C. In a 50 mL beaker, 6.15 g of $Mg(NO_3)_2 \cdot 6H_2O$ and 1.45 g $Cu(NO_3)_2 \cdot 3H_2O$ was added to 25 mL of DI H_2O. A second solution of 3.56 g $Al(NO_3)_3 \cdot 9H_2O$ and 0.375 g $Pr(CF_3SO_3)_3 \cdot 9H_2O$ was added to 25 mL of DI H_2O. The two metal solutions were combined and added dropwise to the vigorously stirring Na_2CO_3 solution and a light blue precipitate instantly formed. A pH

of ~10 for the solution must be maintained for accurate synthesis. This was achieved by alternating aliquots of 1 M NaOH and the metal solution and checked with pH paper. The final solution was covered and left to age while stirring for 10 days between 60-65 °C. The catalyst was monitored daily often adding small amounts of 1 M NaOH to maintain a pH of ~10 throughout the aging process. After 10 days, the catalyst was filtered in a Buchner funnel and added to a solution of 1 g Na_2CO_3 in 500 mL of DI H_2O. The catalyst was stirred at room temperature for a minimum of 4 hours and then filtered in a Buchner funnel. When only a thin layer of water remained over the catalyst cake during filtration, 300 mL of DI H_2O was gently added to thoroughly wash the catalyst. The light blue catalyst was transferred to an evaporating dish and placed in an oven at 110 °C overnight. After completely dried, the catalyst was ground in a mortar and pestle and stored. The solid was then analyzed though powder XRD resulting in a pattern characteristic of an undoped hydrotalcite.

A2. Synthesis and Characterization of $Cu_{20}Nd_5HTC$

Figure A2: Powder X-Ray Diffraction pattern for $Cu_{20}Nd_5HTC$

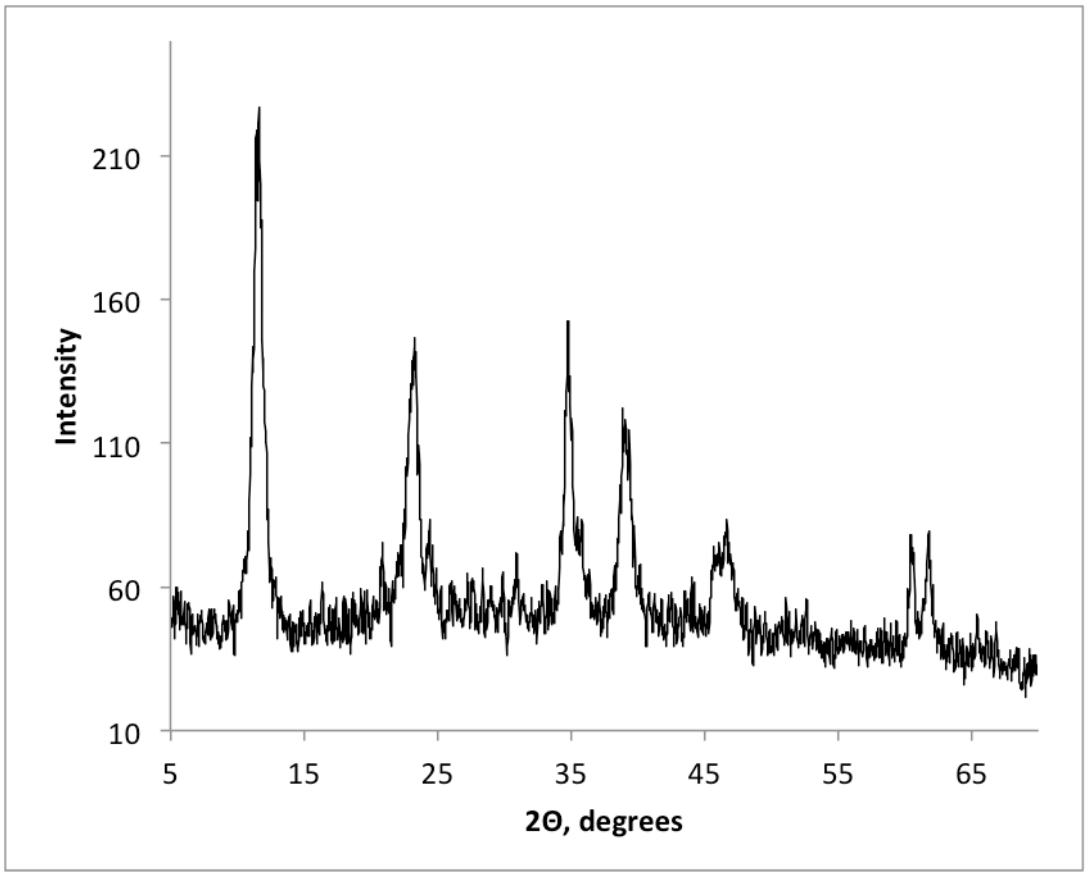

$Cu_{20}Nd_5$ HTC was synthesized by a modified coprecipitation method. 1.06 g Na_2CO_3 was added to 75 mL of DI H_2O in a 600 mL beaker with stirring and heated to 60 °C. In a 50 mL beaker, 6.15 g of $Mg(NO_3)_2 \cdot 6H_2O$ and 1.45 g $Cu(NO_3)_2 \cdot 3H_2O$ was added to 25 mL of DI H_2O. A second solution of 3.56 g $Al(NO_3)_3 \cdot 9H_2O$ and 0.377 g $Nd(CF_3SO_3)_3 \cdot 9H_2O$ was added to 25 mL of DI H_2O. The two metal solutions were combined and added dropwise to the vigorously stirring Na_2CO_3 solution and a light blue precipitate instantly formed. A pH of ~10 for the solution must be maintained for accurate synthesis. This was achieved by alternating aliquots of 1 M NaOH and the metal solution and checked with pH paper. The

final solution was covered and left to age while stirring for 10 days between 60-65 °C. The catalyst was monitored daily often adding small amounts of 1 M NaOH to maintain a pH of ~10 throughout the aging process. After 10 days, the catalyst was filtered in a Buchner funnel and added to a solution of 1 g Na_2CO_3 in 500 mL of DI H_2O. The catalyst was stirred at room temperature for a minimum of 4 hours and then filtered in a Buchner funnel. When only a thin layer of water remained over the catalyst cake during filtration, 300 mL of DI H_2O was gently added to thoroughly wash the catalyst. The light blue catalyst was transferred to an evaporating dish and placed in an oven at 110 °C overnight. After completely dried, the catalyst was ground in a mortar and pestle and stored. The solid was then analyzed though powder XRD resulting in a pattern characteristic of an undoped hydrotalcite.

A3. Synthesis and Characterization of $Cu_{20}Sm_5HTC$

Figure A3: Powder X-Ray Diffraction pattern for $Cu_{20}Sm_5HTC$

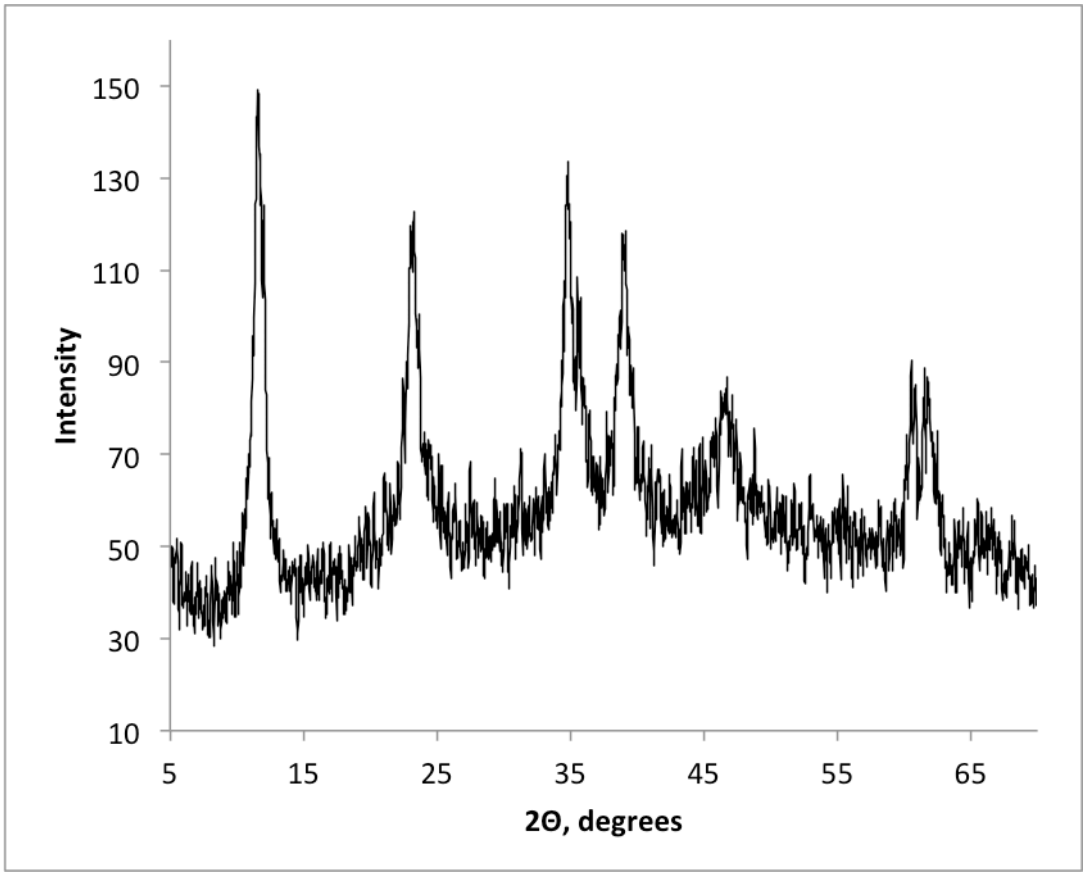

$Cu_{20}Sm_5$ HTC was synthesized by a modified coprecipitation method. 1.06 g Na_2CO_3 was added to 75 mL of DI H_2O in a 600 mL beaker with stirring and heated to 60 °C. In a 50 mL beaker, 6.15 g of $Mg(NO_3)_2 \cdot 6H_2O$ and 1.45 g $Cu(NO_3)_2 \cdot 3H_2O$ was added to 25 mL of DI H_2O. A second solution of 3.56 g $Al(NO_3)_3 \cdot 9H_2O$ and 0.380 g $Sm(CF_3SO_3)_3 \cdot 9H_2O$ was added to 25 mL of DI H_2O. The two metal solutions were combined and added dropwise to the vigorously stirring Na_2CO_3 solution and a light blue precipitate instantly formed. A pH of ~10 for the solution must be maintained for accurate synthesis. This was achieved by alternating aliquots of 1 M NaOH and the metal solution and checked with pH paper. The

final solution was covered and left to age while stirring for 10 days between 60-65 °C. The catalyst was monitored daily often adding small amounts of 1 M NaOH to maintain a pH of ~10 throughout the aging process. After 10 days, the catalyst was filtered in a Buchner funnel and added to a solution of 1 g Na_2CO_3 in 500 mL of DI H_2O. The catalyst was stirred at room temperature for a minimum of 4 hours and then filtered in a Buchner funnel. When only a thin layer of water remained over the catalyst cake during filtration, 300 mL of DI H_2O was gently added to thoroughly wash the catalyst. The light blue catalyst was transferred to an evaporating dish and placed in an oven at 110 °C overnight. After completely dried, the catalyst was ground in a mortar and pestle and stored. The solid was then analyzed though powder XRD resulting in a pattern characteristic of an undoped hydrotalcite.

A4. Synthesis and Characterization of $Cu_{20}Eu_5HTC$

Figure A4: Powder X-Ray Diffraction pattern for $Cu_{20}Eu_5HTC$

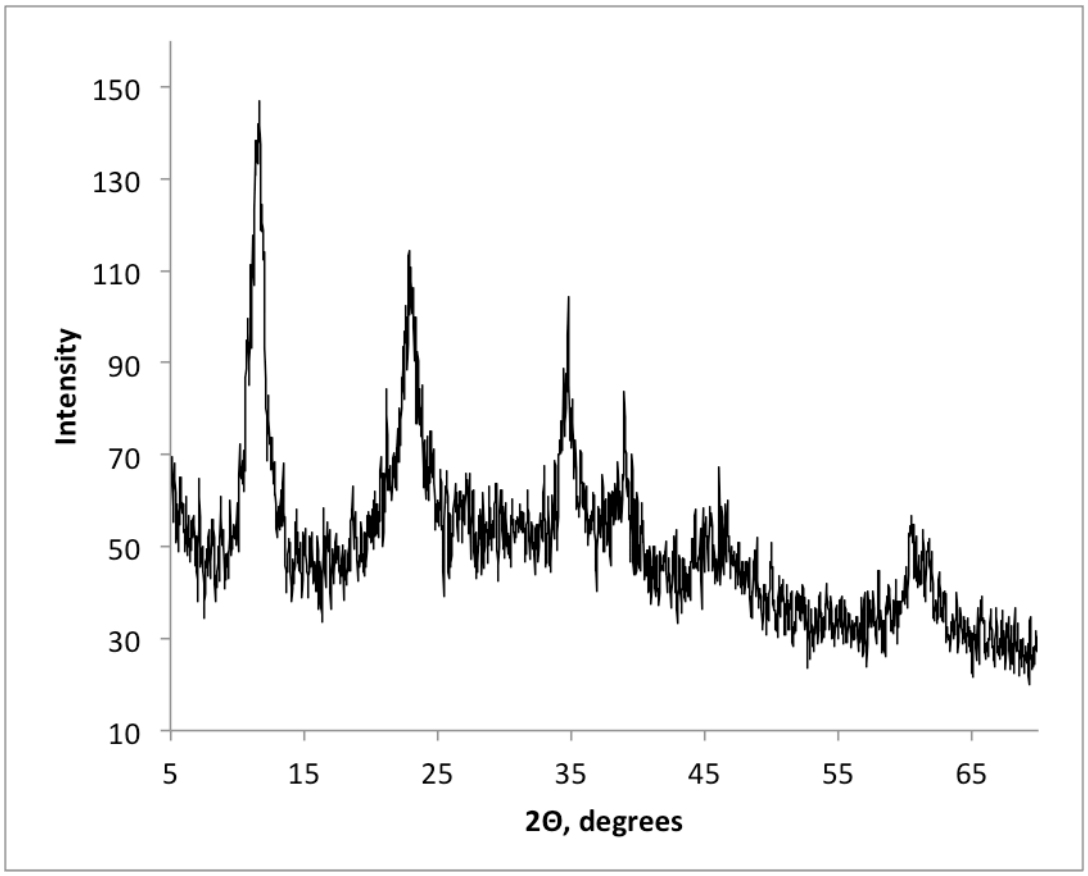

$Cu_{20}Eu_5$ HTC was synthesized by a modified coprecipitation method. 1.06 g Na_2CO_3 was added to 75 mL of DI H_2O in a 600 mL beaker with stirring and heated to 60 °C. In a 50 mL beaker, 6.15 g of $Mg(NO_3)_2 \cdot 6H_2O$ and 1.45 g $Cu(NO_3)_2 \cdot 3H_2O$ was added to 25 mL of DI H_2O. A second solution of 3.56 g $Al(NO_3)_3 \cdot 9H_2O$ and 0.381 g $Eu(CF_3SO_3)_3 \cdot 9H_2O$ was added to 25 mL of DI H_2O. The two metal solutions were combined and added dropwise to the vigorously stirring Na_2CO_3 solution and a light blue precipitate instantly formed. A pH of ~10 for the solution must be maintained for accurate synthesis. This was achieved by alternating aliquots of 1 M NaOH and the metal solution and checked with pH paper. The

final solution was covered and left to age while stirring for 10 days between 60-65 °C. The catalyst was monitored daily often adding small amounts of 1 M NaOH to maintain a pH of ~10 throughout the aging process. After 10 days, the catalyst was filtered in a Buchner funnel and added to a solution of 1 g Na_2CO_3 in 500 mL of DI H_2O. The catalyst was stirred at room temperature for a minimum of 4 hours and then filtered in a Buchner funnel. When only a thin layer of water remained over the catalyst cake during filtration, 300 mL of DI H_2O was gently added to thoroughly wash the catalyst. The light blue catalyst was transferred to an evaporating dish and placed in an oven at 110 °C overnight. After completely dried, the catalyst was ground in a mortar and pestle and stored. The solid was then analyzed though powder XRD resulting in a pattern characteristic of an undoped hydrotalcite.

A5. Synthesis and Characterization of $Cu_{20}Gd_5HTC$

Figure A5: Powder X-Ray Diffraction pattern for $Cu_{20}Gd_5HTC$

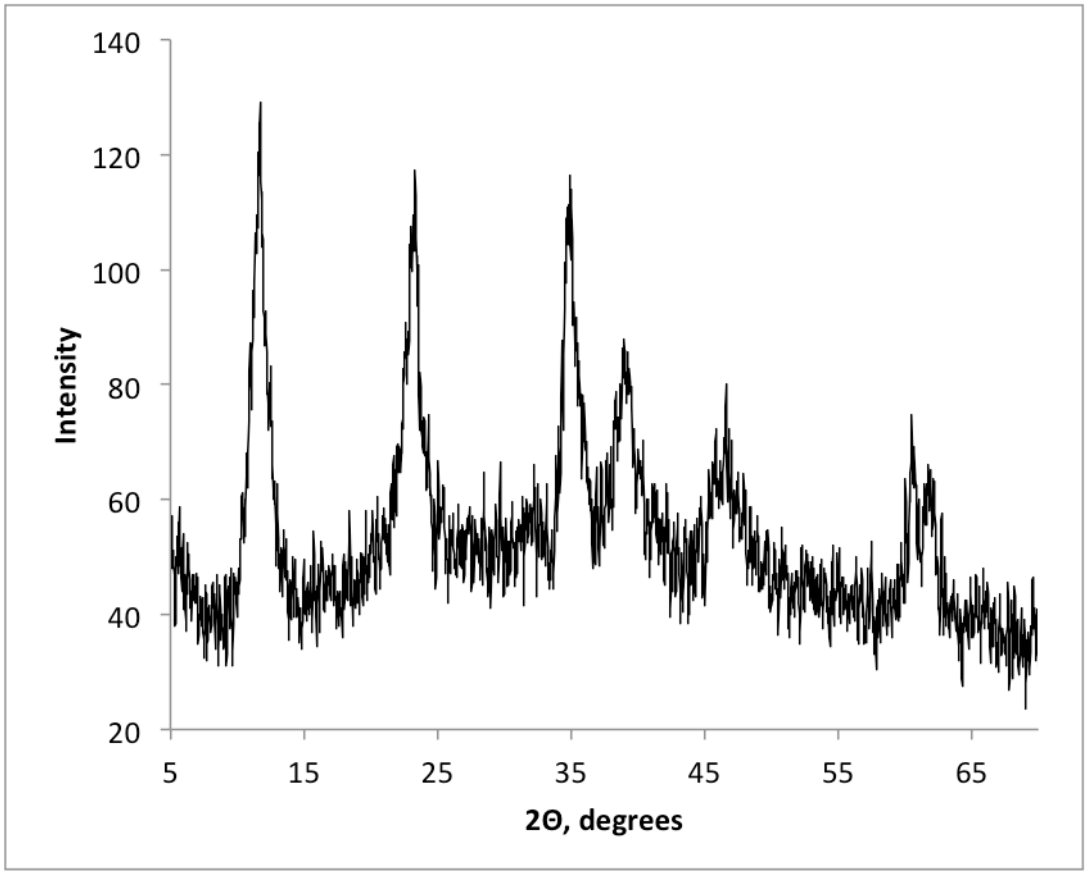

$Cu_{20}Gd_5$ HTC was synthesized by a modified coprecipitation method. 1.06 g Na_2CO_3 was added to 75 mL of DI H_2O in a 600 mL beaker with stirring and heated to 60 °C. In a 50 mL beaker, 6.15 g of $Mg(NO_3)_2 \cdot 6H_2O$ and 1.45 g $Cu(NO_3)_2 \cdot 3H_2O$ was added to 25 mL of DI H_2O. A second solution of 3.56 g $Al(NO_3)_3 \cdot 9H_2O$ and 0.383 g $Gd(CF_3SO_3)_3 \cdot 9H_2O$ was added to 25 mL of DI H_2O. The two metal solutions were combined and added dropwise to the vigorously stirring Na_2CO_3 solution and a light blue precipitate instantly formed. A pH

of ~10 for the solution must be maintained for accurate synthesis. This was achieved by alternating aliquots of 1 M NaOH and the metal solution and checked with pH paper. The final solution was covered and left to age while stirring for 10 days between 60-65 °C. The catalyst was monitored daily often adding small amounts of 1 M NaOH to maintain a pH of ~10 throughout the aging process. After 10 days, the catalyst was filtered in a Buchner funnel and added to a solution of 1 g Na_2CO_3 in 500 mL of DI H_2O. The catalyst was stirred at room temperature for a minimum of 4 hours and then filtered in a Buchner funnel. When only a thin layer of water remained over the catalyst cake during filtration, 300 mL of DI H_2O was gently added to thoroughly wash the catalyst. The light blue catalyst was transferred to an evaporating dish and placed in an oven at 110 °C overnight. After completely dried, the catalyst was ground in a mortar and pestle and stored. The solid was then analyzed though powder XRD resulting in a pattern characteristic of an undoped hydrotalcite.

A6. Synthesis and Characterization of $Cu_{20}Tb_5HTC$

Figure A6: Powder X-Ray Diffraction pattern for $Cu_{20}Tb_5HTC$

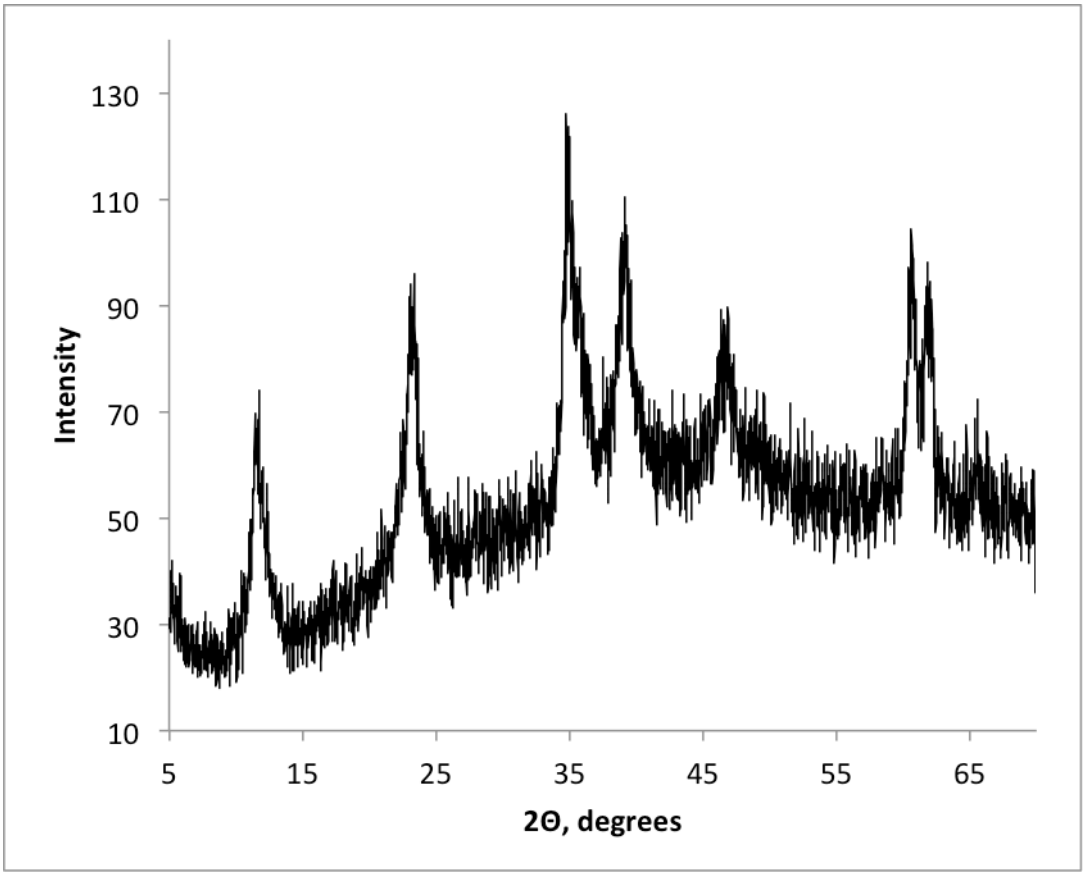

$Cu_{20}Tb_5$ HTC was synthesized by a modified coprecipitation method. 1.06 g Na_2CO_3 was added to 75 mL of DI H_2O in a 600 mL beaker with stirring and heated to 60 °C. In a 50 mL beaker, 6.15 g of $Mg(NO_3)_2 \cdot 6H_2O$ and 1.45 g $Cu(NO_3)_2 \cdot 3H_2O$ was added to 25 mL of DI H_2O. A second solution of 3.56 g $Al(NO_3)_3 \cdot 9H_2O$ and 0.384 g $Tb(CF_3SO_3)_3 \cdot 9H_2O$ was added to 25 mL of DI H_2O. The two metal solutions were combined and added dropwise to the vigorously stirring Na_2CO_3 solution and a light blue precipitate instantly formed. A pH of ~10 for the solution must be maintained for accurate synthesis. This was achieved by alternating aliquots of 1 M NaOH and the metal solution and checked with pH paper. The

final solution was covered and left to age while stirring for 10 days between 60-65 °C. The catalyst was monitored daily often adding small amounts of 1 M NaOH to maintain a pH of ~10 throughout the aging process. After 10 days, the catalyst was filtered in a Buchner funnel and added to a solution of 1 g Na_2CO_3 in 500 mL of DI H_2O. The catalyst was stirred at room temperature for a minimum of 4 hours and then filtered in a Buchner funnel. When only a thin layer of water remained over the catalyst cake during filtration, 300 mL of DI H_2O was gently added to thoroughly wash the catalyst. The light blue catalyst was transferred to an evaporating dish and placed in an oven at 110 °C overnight. After completely dried, the catalyst was ground in a mortar and pestle and stored. The solid was then analyzed though powder XRD resulting in a pattern characteristic of an undoped hydrotalcite.

A7. Synthesis and Characterization of $Cu_{20}Dy_5HTC$

Figure A7: Powder X-Ray Diffraction pattern for $Cu_{20}Dy_5HTC$

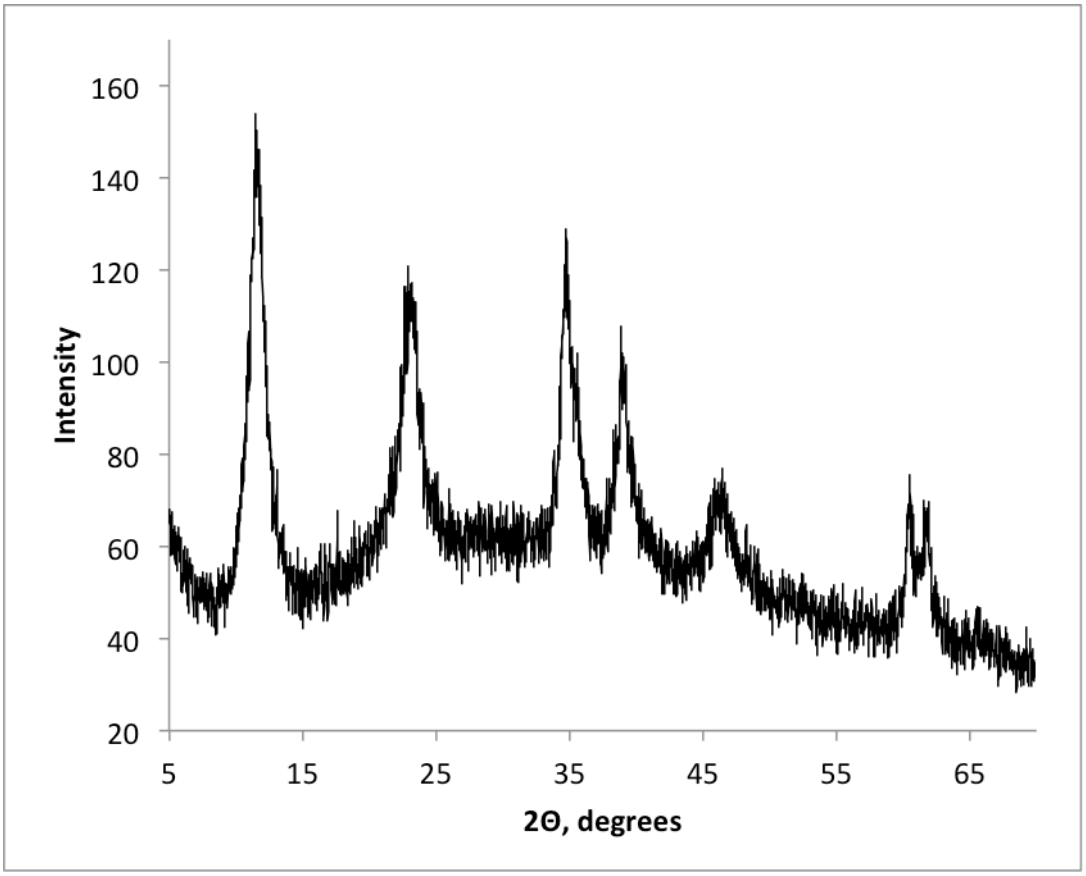

$Cu_{20}Dy_5$ HTC was synthesized by a modified coprecipitation method. 1.06 g Na_2CO_3 was added to 75 mL of DI H_2O in a 600 mL beaker with stirring and heated to 60 °C. In a 50 mL beaker, 6.15 g of $Mg(NO_3)_2 \cdot 6H_2O$ and 1.45 g $Cu(NO_3)_2 \cdot 3H_2O$ was added to 25 mL of DI H_2O. A second solution of 3.56 g $Al(NO_3)_3 \cdot 9H_2O$ and 0.38 g $Dy(CF_3SO_3)_3 \cdot 9H_2O$ was added to 25 mL of DI H_2O. The two metal solutions were combined and added dropwise to the vigorously stirring Na_2CO_3 solution and a light blue precipitate instantly formed. A pH of ~10 for the solution must be maintained for accurate synthesis. This was achieved by alternating aliquots of 1 M NaOH and the metal solution and checked with pH paper. The

final solution was covered and left to age while stirring for 10 days between 60-65 °C. The catalyst was monitored daily often adding small amounts of 1 M NaOH to maintain a pH of ~10 throughout the aging process. After 10 days, the catalyst was filtered in a Buchner funnel and added to a solution of 1 g Na_2CO_3 in 500 mL of DI H_2O. The catalyst was stirred at room temperature for a minimum of 4 hours and then filtered in a Buchner funnel. When only a thin layer of water remained over the catalyst cake during filtration, 300 mL of DI H_2O was gently added to thoroughly wash the catalyst. The light blue catalyst was transferred to an evaporating dish and placed in an oven at 110 °C overnight. After completely dried, the catalyst was ground in a mortar and pestle and stored. The solid was then analyzed though powder XRD resulting in a pattern characteristic of an undoped hydrotalcite.

A8. Synthesis and Characterization of $Cu_{20}Ho_5HTC$

Figure A8: Powder X-Ray Diffraction pattern for $Cu_{20}Ho_5HTC$

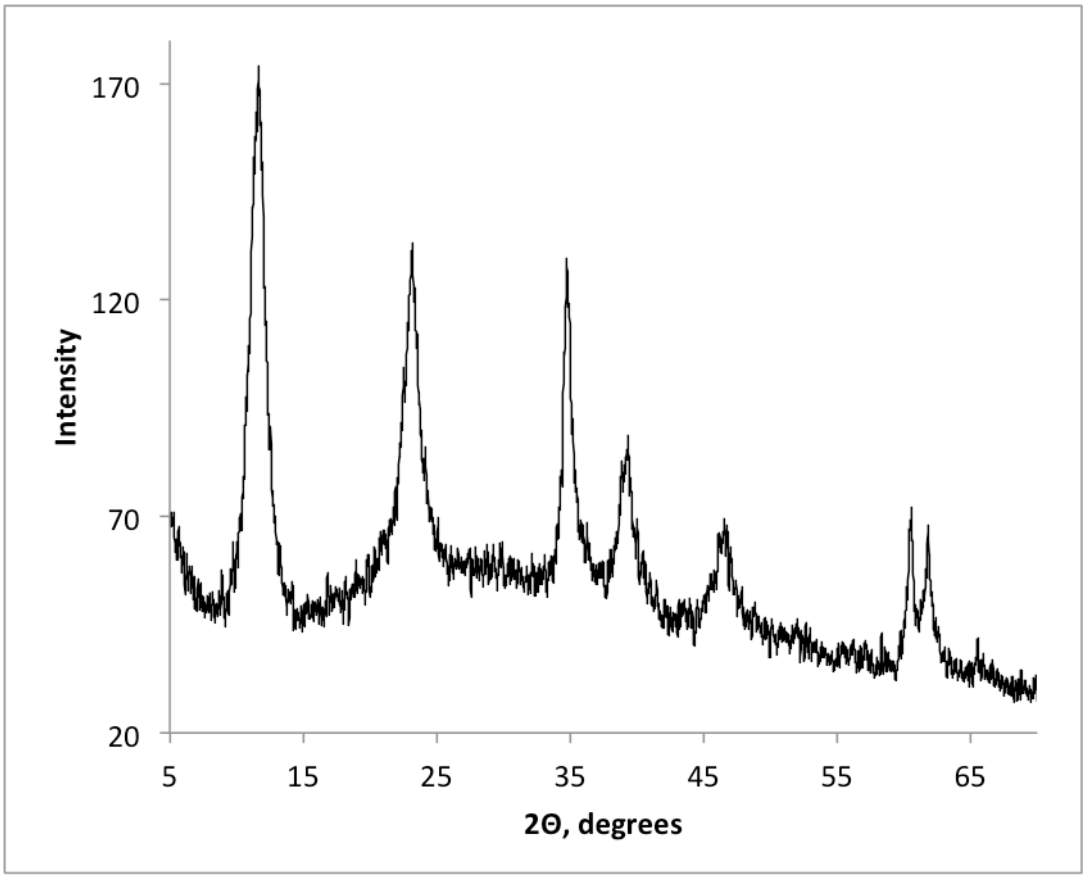

$Cu_{20}Ho_5$ HTC was synthesized by a modified coprecipitation method. 1.06 g Na_2CO_3 was added to 75 mL of DI H_2O in a 600 mL beaker with stirring and heated to 60 °C. In a 50 mL beaker, 6.15 g of $Mg(NO_3)_2 \cdot 6H_2O$ and 1.45 g $Cu(NO_3)_2 \cdot 3H_2O$ was added to 25 mL of DI H_2O. A second solution of 3.56 g $Al(NO_3)_3 \cdot 9H_2O$ and 0.387 g $Ho(CF_3SO_3)_3 \cdot 9H_2O$ was added to 25 mL of DI H_2O. The two metal solutions were combined and added dropwise to the vigorously stirring Na_2CO_3 solution and a light blue precipitate instantly formed. A pH of ~10 for the solution must be maintained for accurate synthesis. This was achieved by alternating aliquots of 1 M NaOH and the metal solution and checked with pH paper. The

final solution was covered and left to age while stirring for 10 days between 60-65 °C. The catalyst was monitored daily often adding small amounts of 1 M NaOH to maintain a pH of ~10 throughout the aging process. After 10 days, the catalyst was filtered in a Buchner funnel and added to a solution of 1 g Na_2CO_3 in 500 mL of DI H_2O. The catalyst was stirred at room temperature for a minimum of 4 hours and then filtered in a Buchner funnel. When only a thin layer of water remained over the catalyst cake during filtration, 300 mL of DI H_2O was gently added to thoroughly wash the catalyst. The light blue catalyst was transferred to an evaporating dish and placed in an oven at 110 °C overnight. After completely dried, the catalyst was ground in a mortar and pestle and stored. The solid was then analyzed though powder XRD resulting in a pattern characteristic of an undoped hydrotalcite.

A9. Synthesis and Characterization of $Cu_{20}Er_5HTC$

Figure A9: Powder X-Ray Diffraction pattern for $Cu_{20}Er_5HTC$

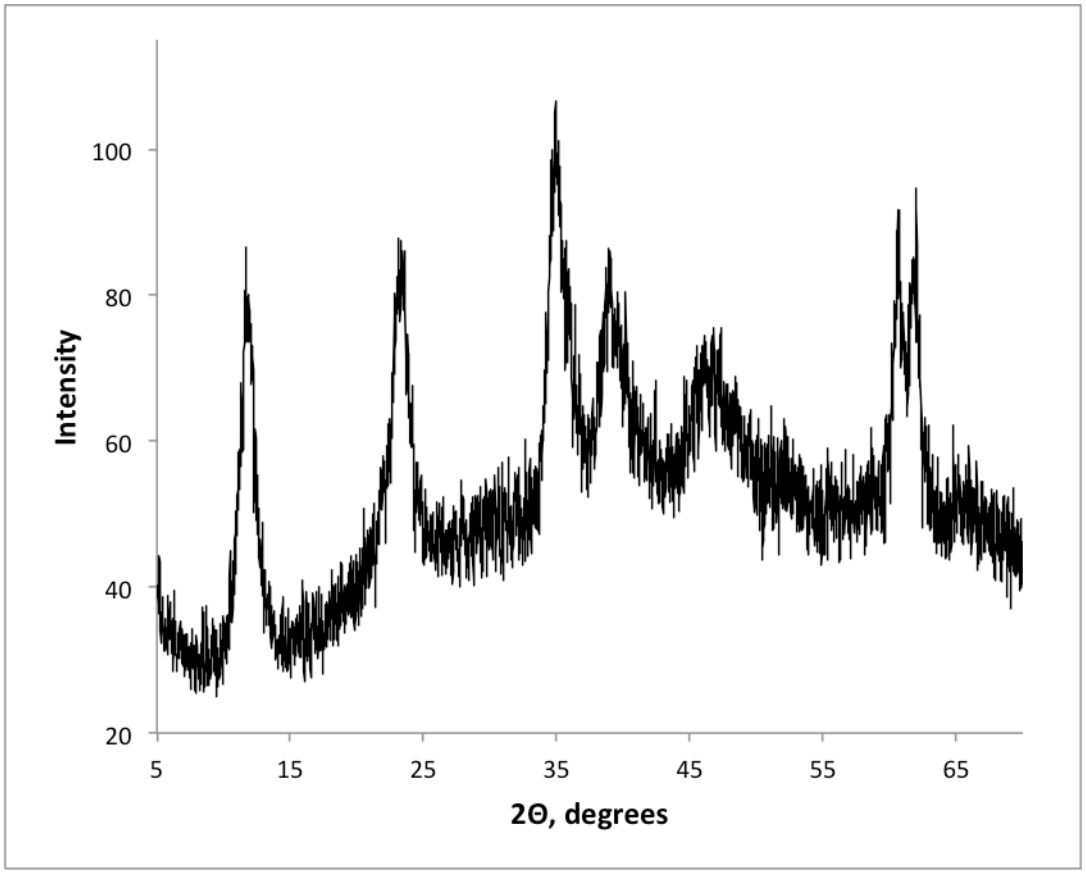

$Cu_{20}Ho_5$ HTC was synthesized by a modified coprecipitation method. 1.06 g Na_2CO_3 was added to 75 mL of DI H_2O in a 600 mL beaker with stirring and heated to 60 °C. In a 50 mL beaker, 6.15 g of $Mg(NO_3)_2 \cdot 6H_2O$ and 1.45 g $Cu(NO_3)_2 \cdot 3H_2O$ was added to 25 mL of DI H_2O. A second solution of 3.56 g $Al(NO_3)_3 \cdot 9H_2O$ and 0.388 g $Er(CF_3SO_3)_3 \cdot 9H_2O$ was added to 25 mL of DI H_2O. The two metal solutions were combined and added dropwise to the vigorously stirring Na_2CO_3 solution and a light blue precipitate instantly formed. A pH of ~10 for the solution must be maintained for accurate synthesis. This was achieved by alternating aliquots of 1 M NaOH and the metal solution and checked with pH paper. The

final solution was covered and left to age while stirring for 10 days between 60-65 °C. The catalyst was monitored daily often adding small amounts of 1 M NaOH to maintain a pH of ~10 throughout the aging process. After 10 days, the catalyst was filtered in a Buchner funnel and added to a solution of 1 g Na_2CO_3 in 500 mL of DI H_2O. The catalyst was stirred at room temperature for a minimum of 4 hours and then filtered in a Buchner funnel. When only a thin layer of water remained over the catalyst cake during filtration, 300 mL of DI H_2O was gently added to thoroughly wash the catalyst. The light blue catalyst was transferred to an evaporating dish and placed in an oven at 110 °C overnight. After completely dried, the catalyst was ground in a mortar and pestle and stored. The solid was then analyzed though powder XRD resulting in a pattern characteristic of an undoped hydrotalcite.

A10. Synthesis and Characterization of $Cu_{20}Tm_5HTC$

Figure A10: Powder X-Ray Diffraction pattern for $Cu_{20}Tm_5HTC$

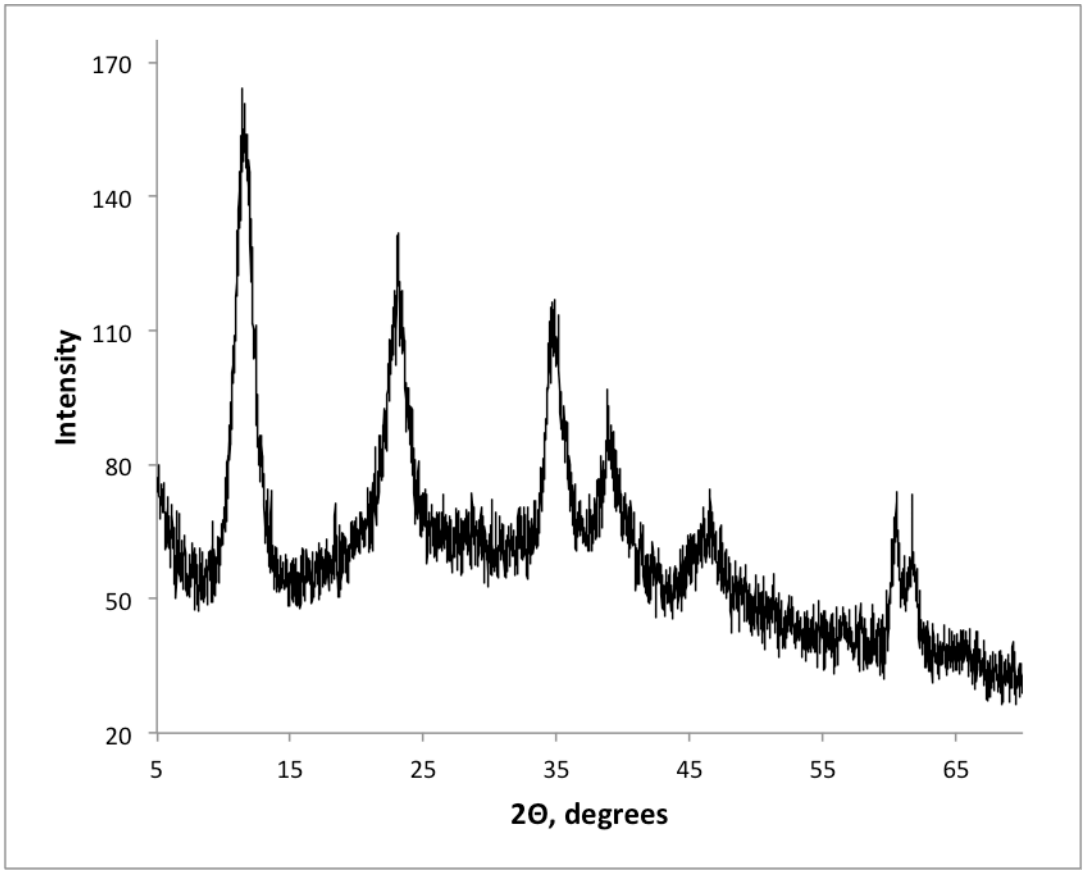

$Cu_{20}Tm_5$ HTC was synthesized by a modified coprecipitation method. 1.06 g Na_2CO_3 was added to 75 mL of DI H_2O in a 600 mL beaker with stirring and heated to 60 °C. In a 50 mL beaker, 6.15 g of $Mg(NO_3)_2 \cdot 6H_2O$ and 1.45 g $Cu(NO_3)_2 \cdot 3H_2O$ was added to 25 mL of DI H_2O. A second solution of 3.56 g $Al(NO_3)_3 \cdot 9H_2O$ and 0.389 g $Tm(CF_3SO_3)_3 \cdot 9H_2O$ was added to 25 mL of DI H_2O. The two metal solutions were combined and added dropwise to the vigorously stirring Na_2CO_3 solution and a light blue precipitate instantly formed. A pH of ~10 for the solution must be maintained for accurate synthesis. This was achieved by alternating aliquots of 1 M NaOH and the metal solution and checked with pH paper. The

final solution was covered and left to age while stirring for 10 days between 60-65 °C. The catalyst was monitored daily often adding small amounts of 1 M NaOH to maintain a pH of ~10 throughout the aging process. After 10 days, the catalyst was filtered in a Buchner funnel and added to a solution of 1 g Na_2CO_3 in 500 mL of DI H_2O. The catalyst was stirred at room temperature for a minimum of 4 hours and then filtered in a Buchner funnel. When only a thin layer of water remained over the catalyst cake during filtration, 300 mL of DI H_2O was gently added to thoroughly wash the catalyst. The light blue catalyst was transferred to an evaporating dish and placed in an oven at 110 °C overnight. After completely dried, the catalyst was ground in a mortar and pestle and stored. The solid was then analyzed though powder XRD resulting in a pattern characteristic of an undoped hydrotalcite.

A11. Synthesis and Characterization of $Cu_{20}Yb_5HTC$

Figure A11: Powder X-Ray Diffraction pattern for $Cu_{20}Yb_5HTC$

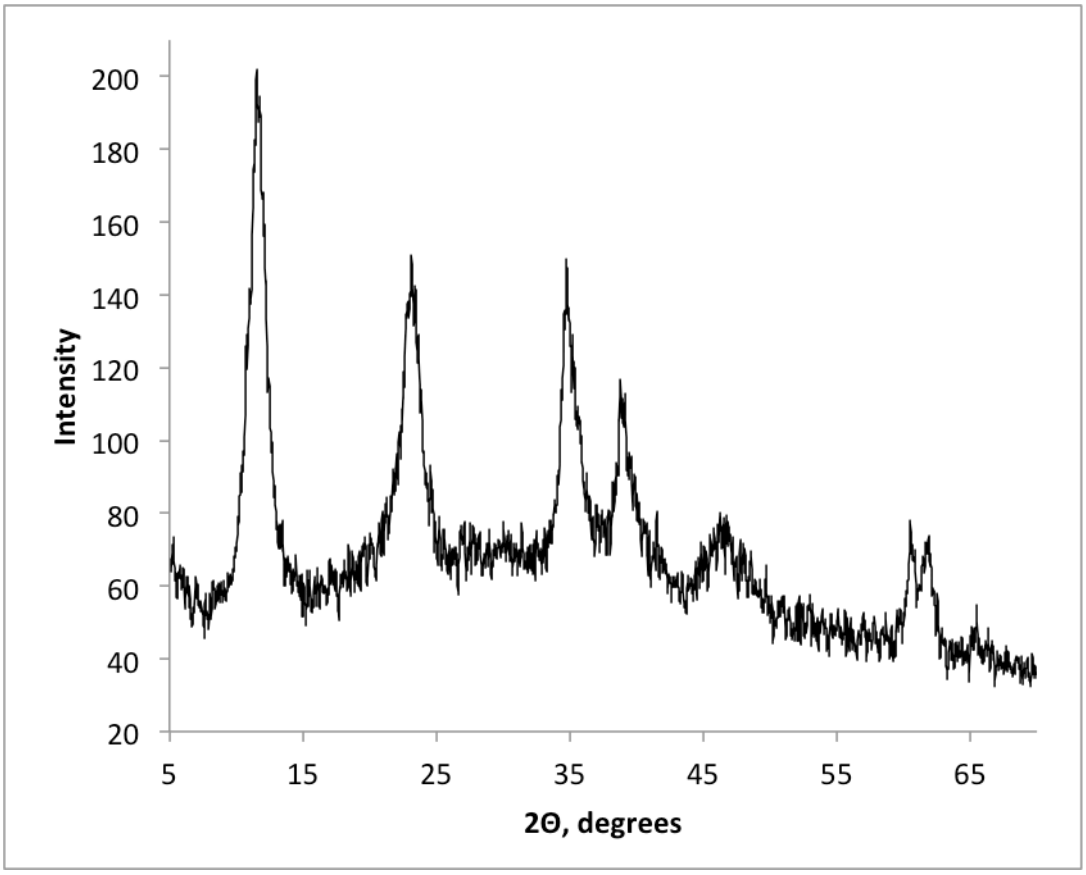

$Cu_{20}Yb_5$ HTC was synthesized by a modified coprecipitation method. 1.06 g Na_2CO_3 was added to 75 mL of DI H_2O in a 600 mL beaker with stirring and heated to 60 °C. In a 50 mL beaker, 6.15 g of $Mg(NO_3)_2 \cdot 6H_2O$ and 1.45 g $Cu(NO_3)_2 \cdot 3H_2O$ was added to 25 mL of DI H_2O. A second solution of 3.56 g $Al(NO_3)_3 \cdot 9H_2O$ and 0.391 g $Yb(CF_3SO_3)_3 \cdot 9H_2O$ was added to 25 mL of DI H_2O. The two metal solutions were combined and added dropwise to the vigorously stirring Na_2CO_3 solution and a light blue precipitate instantly formed. A pH of ~10 for the solution must be maintained for accurate synthesis. This was achieved by alternating aliquots of 1 M NaOH and the metal solution and checked with pH paper. The

final solution was covered and left to age while stirring for 10 days between 60-65 °C. The catalyst was monitored daily often adding small amounts of 1 M NaOH to maintain a pH of ~10 throughout the aging process. After 10 days, the catalyst was filtered in a Buchner funnel and added to a solution of 1 g Na_2CO_3 in 500 mL of DI H_2O. The catalyst was stirred at room temperature for a minimum of 4 hours and then filtered in a Buchner funnel. When only a thin layer of water remained over the catalyst cake during filtration, 300 mL of DI H_2O was gently added to thoroughly wash the catalyst. The light blue catalyst was transferred to an evaporating dish and placed in an oven at 110 °C overnight. After completely dried, the catalyst was ground in a mortar and pestle and stored. The solid was then analyzed though powder XRD resulting in a pattern characteristic of an undoped hydrotalcite.

A12. Synthesis and Characterization of $Cu_{20}Lu_5HTC$

Figure A12: Powder X-Ray Diffraction pattern for $Cu_{20}Lu_5HTC$

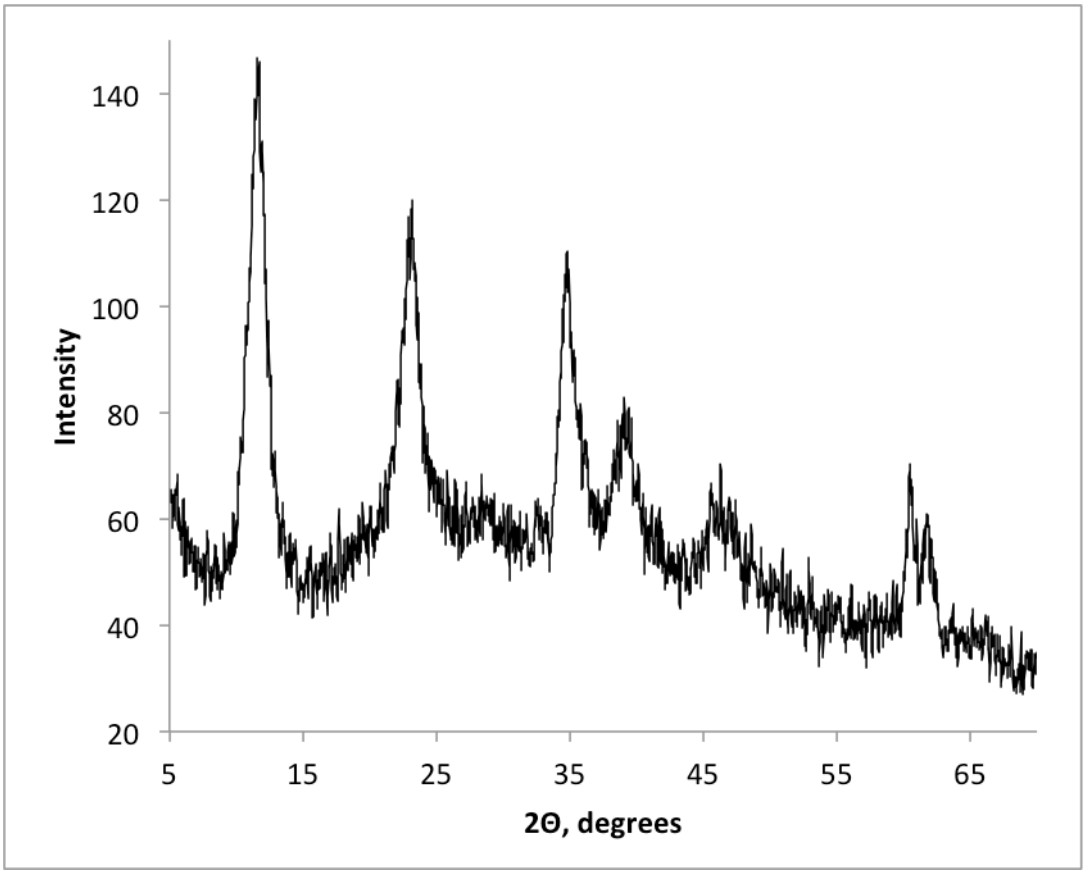

$Cu_{20}oLu_5$ HTC was synthesized by a modified coprecipitation method. 1.06 g Na_2CO_3 was added to 75 mL of DI H_2O in a 600 mL beaker with stirring and heated to 60 °C. In a 50 mL beaker, 6.15 g of $Mg(NO_3)_2 \cdot 6H_2O$ and 1.45 g $Cu(NO_3)_2 \cdot 3H_2O$ was added to 25 mL of DI H_2O. A second solution of 3.56 g $Al(NO_3)_3 \cdot 9H_2O$ and 0.383 g $Lu(CF_3SO_3)_3 \cdot 8H_2O$ was added to 25 mL of DI H_2O. The two metal solutions were combined and added dropwise to the vigorously stirring Na_2CO_3 solution and a light blue precipitate instantly formed. A pH of ~10 for the solution must be maintained for accurate synthesis. This was achieved by alternating aliquots of 1 M NaOH and the metal solution and checked with pH paper. The

final solution was covered and left to age while stirring for 10 days between 60-65 °C. The catalyst was monitored daily often adding small amounts of 1 M NaOH to maintain a pH of ~10 throughout the aging process. After 10 days, the catalyst was filtered in a Buchner funnel and added to a solution of 1 g Na_2CO_3 in 500 mL of DI H_2O. The catalyst was stirred at room temperature for a minimum of 4 hours and then filtered in a Buchner funnel. When only a thin layer of water remained over the catalyst cake during filtration, 300 mL of DI H_2O was gently added to thoroughly wash the catalyst. The light blue catalyst was transferred to an evaporating dish and placed in an oven at 110 °C overnight. After completely dried, the catalyst was ground in a mortar and pestle and stored. The solid was then analyzed though powder XRD resulting in a pattern characteristic of an undoped hydrotalcite.

Table A1. Volume of gas produced and percent of aliphatic (H), aromatic (A), and near oxygen (O) protons after 4 hours of reaction at 300 °C with Cu_{20} and $Cu_{20}Ln_5$ catalysts

Catalyst	Gas evolved (mL)	H	A	O
Cu_{20}	220	54	31	15
$Cu_{20}Pr_5$	320	65	22	13
$Cu_{20}Nd_5$	310	65	21	14
$Cu_{20}Sm_5$	400	77	9	14
$Cu_{20}Eu_5$	250	63	22	15
$Cu_{20}Gd_5$	330	63	20	17
$Cu_{20}Tb_5$	340	72	14	14
$Cu_{20}Dy_5$	300	66	20	14
$Cu_{20}Ho_5$	360	66	19	15
$Cu_{20}Er_5$	350	70	15	15
$Cu_{20}Tm_5$	280	65	22	13
$Cu_{20}Yb_5$	300	65	20	15
$Cu_{20}Lu_5$	190	58	28	14

Appendix B

Figure B1. XRD spectra for non-doped and doped hydrotalcites.

A: commercial (3:1 Mg:Al); **B:** Cu_{20}HTC (20% of Mg^{2+} substituted by Cu^{2+}); **C:** $Cu_{20}Sm_5$HTC (20% of Mg^{2+} replaced by Cu^{2+} and 5% of Al^{3+} by Sm^{3+})

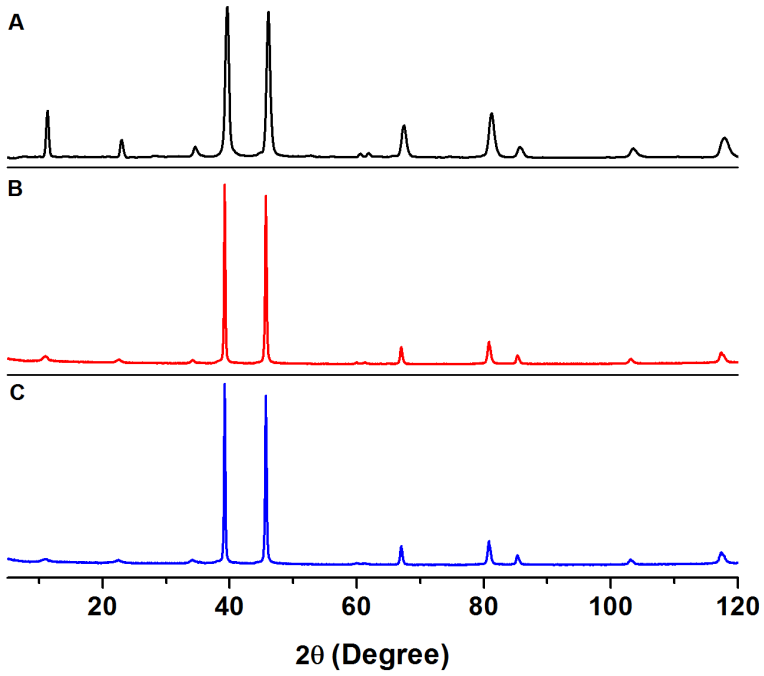

Figure B2. Product Distributions from BPE

Distributions of other aromatics (*top*) and saturates (*bottom*) derived from the secondary reactions of phenol generated by BPE hydrogenolysis (conditions described in Figure 4) after 6 hours. For each, the bar on the left depicts the fraction of the phenol-derived products represented by the other aromatics or saturates, respectively, while the bar on the right depicts the distribution of these products.

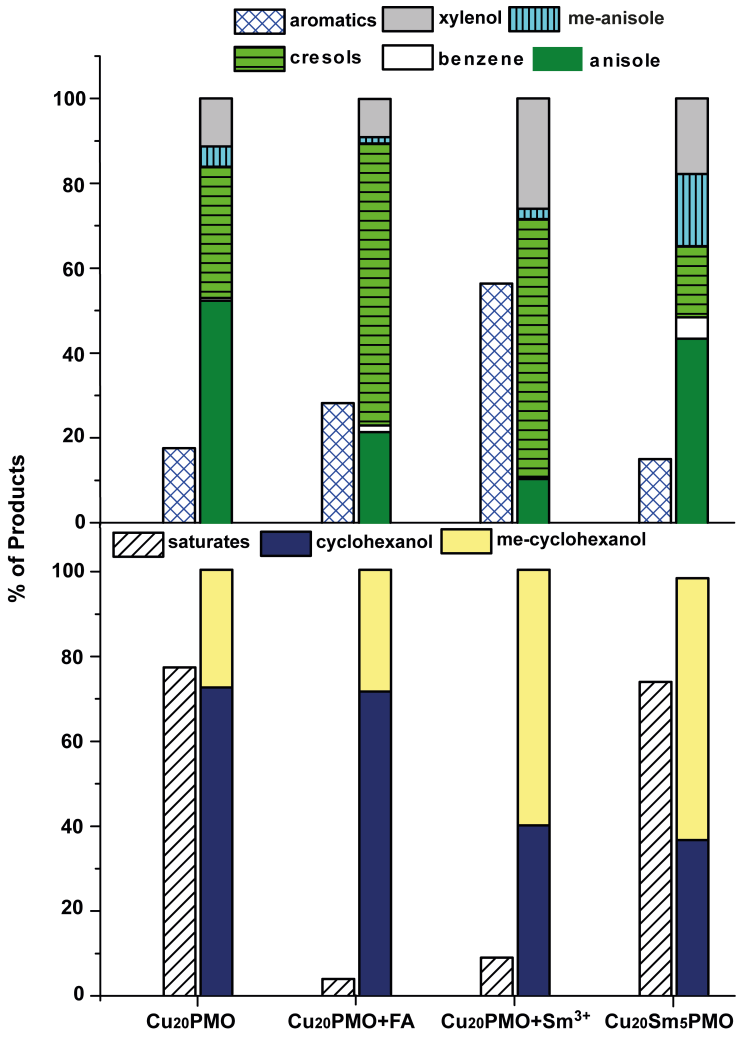

Figure B3. Product Distributions from PPE

Distribution of aromatic (*top*) and saturated (*bottom*) products thought to be derived from subsequent reactions of the primary phenol product from PPE (for conditions see Fig. 6 caption) after 6 hours of reaction. For each case, the left bar depicts the fraction of the phenol-derived products represented by the other aromatics or saturates, respectively, while the bar on the right depicts the distribution of these products.

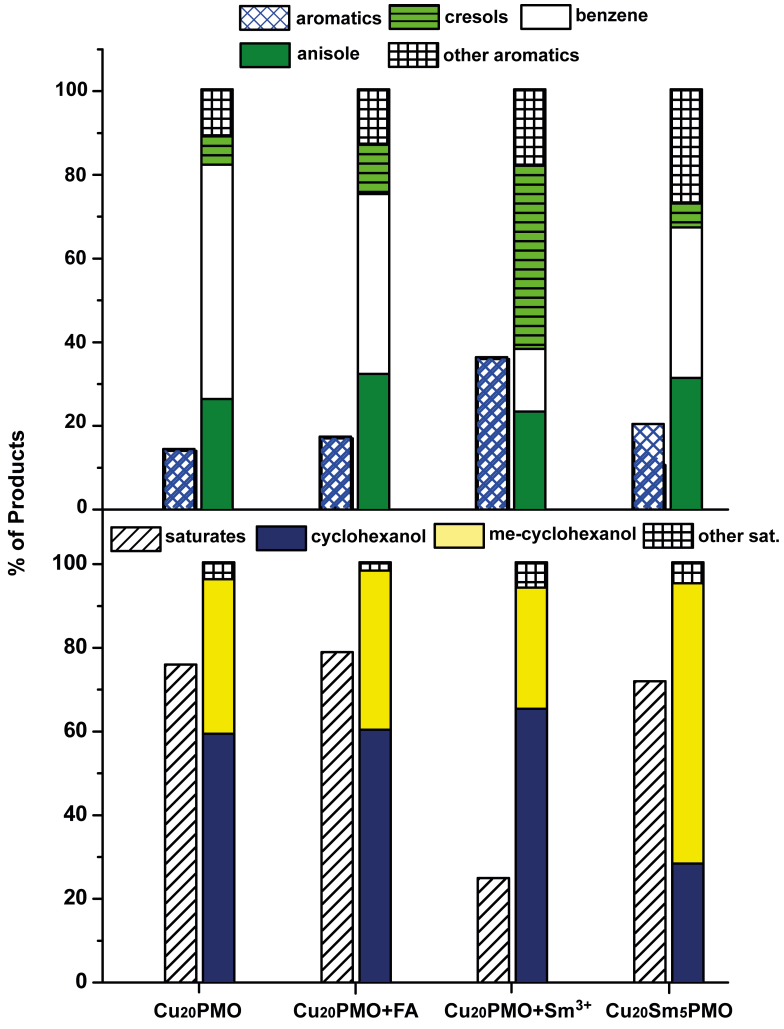

Figure B4. GPC Chromatograms and Molecular Weights from organosolv with doped and doped catalysts

GPC traces for organosolv poplar lignin (A) and OPL after reaction with different catalysts: Cu_{20}PMO (B); Cu_{20}PMO+FA (C); $Cu_{20}Sm_5$PMO (D); Cu_{20}PMO+Sm^{3+} (E). (Reaction time 6 hours at 300 °C in sc-MeOH)

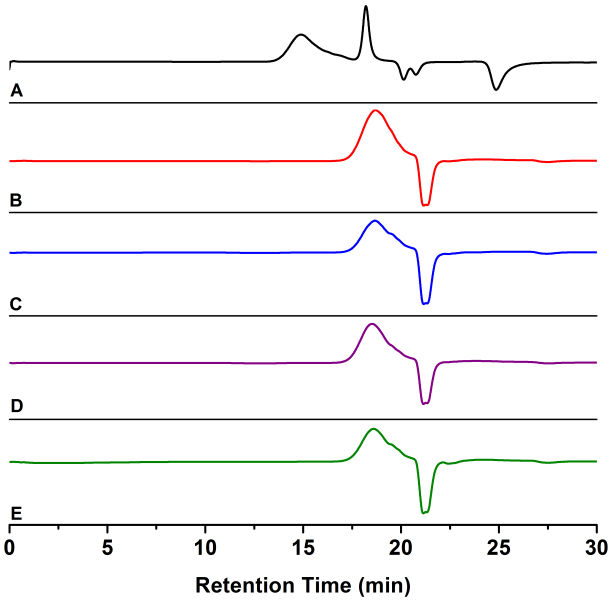

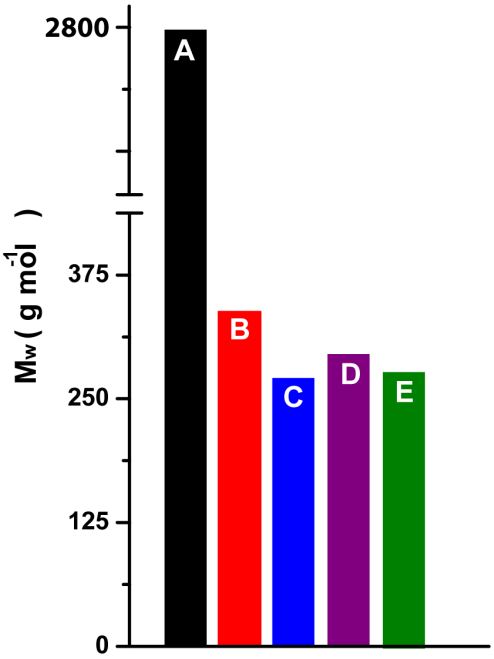

Table B1. GC-FID parameters and conditions

Column	**Agilent DB-1**	**Agilent HP-1**
Carrier Gas	Helium	Helium
Gas Flow	28.6 ml min^{-1}	28.6 ml min^{-1}
Pressure	104.8 kPa	104.8 kPa
Injection Volume	60mL	60mL
Inlet Temp	200 °C	200 °C
Column Start Temp	70 °C	70 °C
Column Final Temp	300 °C	300 °C
Detector Temp	310 °C	310 °C
Split Ratio	20:1	20:1
Temperature Ramp		
0 – 2 min	70 °C	70 °C
2 – 21 min	70 – 300 °C	70 – 300 °C
21 – 23 min	300 °C	300 °C

Table B2. Effective Carbon Number (ECN) and response factors (r.f) used for GC-FID calculations.

Compound	Calc r.f	Rel. r.f	ECN	aliph C	arom C	olef C	carb C	ether O	1° alcoh O	2° alcoh O
decane (standard)	44849	1.00	10.00	10	0	0	0	0	0	0
BPE	53819	0.83	12.00	1	12	0	0	1	0	0
DPE	49334	0.91	11.00	0	12	0	0	1	0	0
DHBF	31394	1.43	7.00	2	6	0	0	1	0	0
PPE	58304	0.77	13.00	2	12	0	0	1	0	0
BP	53819	0.83	12.00	0	12	0	0	0	0	0
anisole	26909	1.67	6.00	1	6	0	0	1	0	0
benzene	26909	1.67	6.00	0	6	0	0	0	0	0
phenylcyclohexane	53819	0.83	12.00	6	6	0	0	0	0	0
bicyclohexane	53819	0.83	12.00	12	0	0	0	0	0	0
2-ethylcyclohexanol	33637	1.33	7.50	2	6	0	0	0	1	0
ethylbenzene	35879	1.25	8.00	2	6	0	0	0	0	0
ethylcyclohexane	35879	1.25	8.00	8	0	0	0	0	0	0
benzyl alcohol	29152	1.54	6.50	1	6	0	0	0	1	0
o-cresol	28031	1.60	6.25	1	6	0	0	0	0	1
p/m-cresol	28031	1.60	6.25	1	6	0	0	0	0	1
cyclohexane	26909	1.67	6.00	6	0	0	0	0	0	0
cyclohexanol	23546	1.90	5.25	6	0	0	0	0	0	1
methylanisole	28031	1.60	6.25	1	6	0	0	0	0	1
methylcyclohexane	31394	1.43	7.00	7	0	0	0	0	0	0
methylcyclohexanols	28031	1.60	6.25	7	0	0	0	0	0	1
phenol	23546	1.90	5.25	0	6	0	0	0	0	1
toluene	31394	1.43	7.00	1	6	0	0	0	0	0
xylenol	32516	1.38	7.25	2	6	0	0	0	0	1

Abreviations: r.f.: response factor; ECN: effective carbon number; aliph.: aliphatic; arom: aromatic; olef.: olefinic; carb.: carbonyl; alcoh.: alcohol; BPE: benzyl phenyl ether; DPE: diphenyl ether; DHBF: dihydrobenzofuran; PPE: 2-phenylethyl phenyl ether; BP: biphenyl.

Table B3. BPE consumption and product formation for reaction with Cu_{20}PMO catalysts (300 °C).

A.

Conditions	**Cu_{20}PMO[a]/ BPE[b] / MeOH[c] / 300 °C**						
	Reaction Time (h) / Yield (μmol)						
Compound	**0**	**1**	**2**	**3**	**4**	**5**	**6**
BPE	1041	373	33	0	0	0	0
anisole	0	3	30	72	103	102	96
benzene	0	0	2	1	1	1	1
cresol (ortho)	0	0	60	105	84	84	54
cresol (para/meta)	0	0	0	0	3	2	2
cyclohexane	0	0	0	0	0	0	0
cyclohexanol	0	3	40	350	540	560	583
methylanisole	0	0	1	3	8	7	9
methylcyclohexane	0	0	0	0	0	0	0
methylcyclohexanols	0	0	2	38	160	165	223
phenol	0	676	824	504	90	68	16
toluene	0	687	977	1000	987	1027	1018
xylenol	0	0	2	6	12	12	21

[a] 100 mg Cu_{20}PMO. [b] 192 mg (1.04 mmol). [c] 3.0 mL

B.

Conditions	**Cu_{20}PMO+FA[a] / BPE[b] / MeOH[c]/ 300 °C**						
	Reaction Time (h) / Yield (μmol)						
Compound	**0**	**1**	**2**	**3**	**4**	**5**	**6**
BPE	1041	983	478	309	128	0	0
anisole	0	0	12	25	37	61	63
benzene	0	0	1	3	3	4	4
cresol (ortho)	0	2	45	94	138	188	187
cresol (para/meta)	0	0	5	7	8	8	8
cyclohexane	0	0	0	0	0	0	0
cyclohexanol	0	0	5	7	11	37	29
methylanisole	0	0	0	1	2	4	4
methylcyclohexane	0	0	0	0	0	0	0
methylcyclohexanols	0	0	0	2	5	16	12
phenol	0	125	540	667	594	547	540
toluene	0	119	593	782	873	983	1040
xylenol	0	1	2	6	15	26	26

[a] 100 mg Cu_{20}PMO; 50 mL 88% aq. formic acid (1.17 mmol). [b] 192 mg (1.04 mmol). [c] 3.0 mL

C.

Conditions	$Cu_{20}PMO+Sm^{3+}$ [a] / BPE[b] / MeOH[c] / 300 °C						
	Reaction Time (h) / Yield (μmol)						
Compound	**0**	**1**	**2**	**3**	**4**	**5**	**6**
BPE	1041	153	9	0	0	0	0
anisole	0	2	15	31	41	63	60
benzene	0	1	2	2	2	3	3
cresol (ortho)	0	58	138	207	280	292	351
cresol (para/meta)	0	2	3	4	5	5	6
cyclohexane	0	0	0	0	0	0	0
cyclohexanol	0	2	24	34	57	102	37
methylanisole	0	0	1	3	5	11	14
methylcyclohexane	0	0	0	0	0	0	0
methylcyclohexanols	0	0	11	15	27	86	56
phenol	0	683	730	579	470	312	252
toluene	0	738	941	945	938	937	1009
xylenol	0	2	9	22	53	75	153

[a] 100 mg $Cu_{20}PMO$; 5 mg $Sm(CF_3SO_3)_3 \bullet 9H_2O$ (6.7 μmol Sm^{3+}). [b] 192 mg (1.04 mmol) [c] 3.0 mL

D.

Conditions	$Cu_{20}Sm_5PMO$ [a] / BPE[b] / MeOH[c] / 300 °C						
	Reaction Time (h) / Yield (μmol)						
Compound	**0**	**1**	**2**	**3**	**4**	**5**	**6**
BPE	1041	90	2	0	0	0	0
anisole	0	10	39	51	65	58	68
benzene	0	2	4	5	4	6	8
cresol (ortho)	0	71	123	116	104	66	16
cresol (para/meta)	0	3	4	4	4	4	10
cyclohexane	0	0	0	0	0	0	8
cyclohexanol	0	15	201	369	402	455	279
methylanisole	0	0	3	5	9	9	26
methylcyclohexane	0	0	0	0	0	0	8
methylcyclohexanols	0	5	29	98	166	239	474
phenol	0	681	458	215	89	22	1
toluene	0	714	787	784	847	897	958
xylenol	0	3	10	15	22	23	28

[a] 100 mg $Cu_{20}Sm_5PMO$. [b] 192 mg (1.04 mmol). [c] 3.0 mL

E.

Conditions	Cu_{20}PMO+AA[a] / BPE[b] / MeOH[c] / 300 °C	
	Yield (μmol)	
Compound	**0 h**	**6 h**
BPE	997	0
anisole	0	137
benzene	0	7
cresol (ortho)	0	142
cresol (para/meta)	0	1
cyclohexane	0	1
cyclohexanol	0	240
methylanisole	0	1
methylcyclohexane	0	0
methylcyclohexanols	0	98
phenol	0	266
toluene	0	973
xylenol	0	20

[a] 100 mg Cu_{20}PMO; 71 mg acetic acid (1.17 μmol). [b] 192 mg (1.04 mmol). [c] 3.0 mL.

Table B4. PPE consumption and product formation for reaction with Cu_{20}PMO catalysts (300 °C).

A.

Conditions	**Cu_{20}PMO[a] / PPE[b] / MeOH[c] / 300 °C**						
	Reaction Time (h) / Yield (μmol)						
Compound	**0**	**1**	**2**	**3**	**4**	**5**	**6**
PPE	530	306	231	167	70	63	21
anisole	0	7	12	16	21	25	19
benzene	0	10	21	29	34	35	42
2-ethylcyclohexanol	0	0	0	0	0	0	0
ethylbenzene	0	144	250	325	402	414	447
ethylcyclohexane	0	0	1	1	2	3	5
benzyl alcohol	0	0	0	1	1	2	2
cresol (ortho)	0	5	7	8	7	8	3
cresol (para/meta)	0	0	0	1	1	1	2
cyclohexane	0	1	2	4	5	6	9
cyclohexanol	0	66	153	204	253	232	227
methylanisole	0	1	1	2	2	2	1
methylcyclohexane	0	0	0	1	1	2	3
methylcyclohexanols	0	8	29	52	97	111	142
phenol	0	51	42	34	20	17	6
toluene	0	1	1	1	2	2	2
xylenol	0	5	8	9	7	6	2

[a] 100 mg Cu_{20}PMO. [b] 105.1mg (530 μmol). [c] 3.0 mL

B.

Conditions	**Cu_{20}PMO+FA[a] / PPE[b] / MeOH[c]/ 300 °C**						
	Reaction Time (h) / Yield (μmol)						
Compound	**0**	**1**	**2**	**3**	**4**	**5**	**6**
PPE	530	474	360	321	287	228	120
anisole	0	4	6	10	14	16	23
benzene	0	5	10	14	18	25	31
2-ethylcyclohexanol	0	0	0	0	0	0	0
ethylbenzene	0	80	113	158	197	254	354
ethylcyclohexane	0	0	0	0	0	1	1
benzyl alcohol	0	0	0	0	0	1	3
cresol (ortho)	0	5	4	7	8	7	7
cresol (para/meta)	0	0	0	0	0	1	2
cyclohexane	0	0	1	1	2	3	4
cyclohexanol	0	30	55	83	112	146	197
methylanisole	0	1	1	1	2	3	4
methylcyclohexane	0	0	0	0	1	1	1
methylcyclohexanols	0	4	9	21	37	53	125
phenol	0	43	27	27	26	23	17
toluene	0	1	0	1	1	2	2
xylenol	0	4	0	1	1	2	3

[a] 100 mg Cu_{20}PMO plus 25 μL 88% aq. FA (0.58 mmol). [b] 105.1 mg (530 μmol). [c] 3.0 mL

C.

Conditions	**$Cu_{20}PMO+Sm^{3+}$ [a] / PPE[b] / MeOH[c] / 300 °C**						
	Reaction Time (h) / Yield (μmol)						
Compound	**0**	**1**	**2**	**3**	**4**	**5**	**6**
PPE	530	435	387	365	360	338	326
anisole	0	4	5	7	11	14	17
benzene	0	5	6	9	9	10	11
2-ethylcyclohexanol	0	0	0	0	0	0	0
ethylbenzene	0	90	121	138	146	161	168
ethylcyclohexane	0	0	0	0	0	0	0
benzyl alcohol	0	0	0	0	0	1	1
cresol (ortho)	0	12	13	19	25	31	33
cresol (para/meta)	0	0	0	0	0	0	0
cyclohexane	0	0	0	1	1	1	2
cyclohexanol	0	20	27	31	32	37	33
methylanisole	0	1	1	1	2	2	3
methylcyclohexane	0	0	0	0	0	0	0
methylcyclohexanols	0	3	7	6	10	14	15
phenol	0	55	67	61	58	61	51
toluene	0	1	1	1	1	1	1
xylenol	0	1	1	3	7	8	8

[a] 100 mg $Cu_{20}PMO$; 5 mg $Sm(CF_3SO_3)_3 \bullet 9H_2O$ (6.7 μmol). [b] 105.1 mg (530 μmol). [c] 3.0 mL

D.

Conditions	**$Cu_{20}Sm_5PMO$ [a] / PPE [b] / MeOH [c] / 300 °C**						
	Reaction Time (h) / Yield (μmol)						
Compound	**0**	**1**	**2**	**3**	**4**	**5**	**6**
PPE	530	415	291	204	100	65	5
anisole	0	6	13	22	24	26	33
benzene	0	6	13	22	30	33	38
2-ethylcyclohexanol	0	0	0	0	0	0	0
ethylbenzene	0	99	193	292	374	417	476
ethylcyclohexane	0	0	0	1	2	3	5
benzyl alcohol	0	0	0	1	2	3	15
cresol (ortho)	0	7	14	20	15	11	0
cresol (para/meta)	0	0	0	0	1	2	6
cyclohexane	0	0	1	2	5	7	8
cyclohexanol	0	33	70	136	181	197	104
methylanisole	0	1	1	2	2	2	1
methylcyclohexane	0	0	0	1	1	2	7
methylcyclohexanols	0	8	18	53	89	122	253
phenol	0	50	62	55	32	19	2
toluene	0	1	1	1	2	2	3
xylenol	0	4	2	9	4	5	7

[a] 100 mg $Cu_{20}Sm_5PMO$. [b] 105.1mg (530 μmol). [c] 3.0 mL

Table B5. Diphenyl ether consumption and product formation with Cu_{20}PMO catalysts (300 °C).

A.

Conditions	**Cu_{20}PMO[a]/ DPE[b] / MeOH[c]/ 300 °C**						
Compound[d]	**Reaction Time (h) / Yield (μmol)**						
	0	**1**	**2**	**3**	**4**	**5**	**6**
DPE	311	306	293	261	237	265	247
benzene	0	6	4	9	22	28	24
cyclohexanol	0	3	1	4	11	17	14
methylcyclohexanols	0	0	0	1	3	4	3
phenol	0	1	1	2	2	3	2

[a] 100 mg Cu_{20}PMO. [b] 52.9 mg (311 μmol). [c] 3.0 mL. [d]The GC-FID analysis did not show any signals for the following: anisole, cresol (ortho,meta,para), cyclohexane, methylanisole, methylcyclohexanol, toluene or xylenol.

B.

Conditions	**Cu_{20}PMO+FA[a] / DPE[b] / MeOH[c] / 300 °C**						
Compound	**Reaction Time (h) / Yield (μmol)**						
	0	**1**	**2**	**3**	**4**	**5**	**6**
DPE	311	292	279	260	268	232	227
anisole	0	0	1	0	1	3	2
benzene	0	3	24	32	30	64	61
cresol (ortho)	0	1	0	0	0	1	0
cyclohexanol	0	1	15	20	20	64	42
methylcyclohexanols	0	0	3	5	3	26	12
phenol	0	1	2	2	2	4	2

[a] 100 mg Cu_{20}PMO plus 12.5 μL 88% FA (292 μmol). [b] 52.9 mg (311 μmol). [c] 3.0 mL. [d]The GC-FID analysis did not show signals for the following: cresol (meta,para), cyclohexane or methylanisole

C.

Conditions	$Cu_{20}PMO+Sm^{3+}$ [a] / DPE[b] / MeOH[c] / 300 °C						
Compound[d]	Reaction Time (h) / Yield (μmol)						
	0	1	2	3	4	5	6
DPE	311	274	295	284	282	284	280
anisole	0	0	0	0	1	1	1
benzene	0	2	5	5	7	10	8
cresol (ortho)	0	0	0	1	0	1	1
cyclohexanol	0	0	2	1	2	2	2
methylcyclohexanols	0	0	0	0	1	1	1
phenol	0	1	2	2	2	2	2

[a] 100 mg $Cu_{20}PMO$; 5 mg $Sm(CF_3SO_3)_3 \bullet 9H_2O$ (6.7 μmol). [b] 52.9 mg; (311 μmol). [c] 3.0 mL. [d]The GC-FID analysis did not show signals for the following: cresol (meta,para), cyclohexane or methylanisole.

D.

Conditions	$Cu_{20}Sm_5PMO$[a] / DPE[b] / MeOH[c] / 300 °C						
Compound[d]	Reaction Time (h) / Yield (μmol)						
	0	1	2	3	4	5	6
DPE	311	282	278	254	243	218	191
anisole	0	0	0	0	1	1	2
benzene	0	3	7	25	42	61	88
cresol (ortho)	0	0	0	0	0	1	1
cyclohexane	0	0	0	0	0	0	1
cyclohexanol	0	1	3	17	28	42	54
methylanisole	0	0	0	0	0	0	2
methylcyclohexane	0	0	0	0	0	0	1
methylcyclohexanols	0	0	0	2	7	12	22
phenol	0	1	2	2	3	3	3
toluene	0	1	0	0	1	0	1

[a] 100 mg $Cu_{20}Sm_5PMO$. [b] 52.9 mg (311 μmol). [c] 3.0 mL. [d]The GC-FID analysis did not show signals for cresol (meta/para) or xylenol.

Table B6. DPE consumption and product formation with Cu_{20}PMO catalysts (100 mg in each case) in sc-MeOH (3.0 mL) after 6 hours at 330 °C . Product yields are in mmol.

Compound [a]	Catalysts			
	FA[b]	Sm^{3+} [c]	Cu_{20}	$Cu_{20}Sm_5$
DPE [d]	89	269	51	25
anisole	4	2	4	3
benzene	168	11	214	271
cresol (para/meta)	1	0	3	0
cyclohexane	7	0	12	25
cyclohexanol	69	0	43	4
methylanisole	0	0	7	18
methylcyclohexane	5	0	16	25
methylcyclohexanols	66	2	102	125
phenol	2	1	1	1
toluene	1	0	1	2

[a] The GC-FID analysis did not detect o- cresol or xylenol. [b] 12.5 μL 88% FA (292 μmol)
[c] 5 mg $Sm(CF_3SO_3)_3 \cdot 9H_2O$ (6.7 μmol). [d] DPE(initial) = 47.5 mg (279 μmol).

Table B7. Temporal data for diphenyl ether reaction with $Cu_{20}Sm_5$PMO at 330 °C in sc-MeOH .

Conditions	**Cu20Sm5PMOa/ DPEb / MeOHc / 330 °C**						
	Reaction Time (h) / Yield (μmol)						
Compound	**0**	**1**	**2**	**3**	**4**	**5**	**6**
DPE	279	244	142	87	53	28	25
anisole	0	1	2	3	3	2	3
benzene	0	26	116	173	203	229	271
cresol (ortho)	0	0	0	0	0	0	0
cresol (para/meta)	0	0	1	1	2	3	0
cyclohexane	0	1	6	11	14	18	25
cyclohexanol	0	2	6	9	9	8	4
methylanisole	0	0	3	6	9	11	18
methylcyclohexane	0	0	3	5	8	10	25
methylcyclohexanols	0	4	35	65	83	100	125
phenol	0	3	3	2	2	1	1
toluene	0	0	1	1	1	1	2
xylenol	0	0	0	0	0	0	0

[a] **Conditions**: 100 mg catalyst, DPE(initial) = 47.5 mg (279 mmol), 3.0 mL MeOH, decane as internal standard, T = 330 °C. Products quantified by GC-FID. The mass balance (the sum of products divided twice the DPE consumed) at 6 hours was 93.4%. These data represent the average of two catalysis experiments under identical conditions.

Table B8. DHBF consumption and product formation with Cu_{20}PMO catalysts (300 °C).

A.

Conditions	**Cu_{20}PMO[a] / DHBF[b] / MeOH[c]**						
Compound[d]	**Reaction Time (h) / Yield (μmol)**						
	0	**1**	**2**	**3**	**4**	**5**	**6**
DHBF	512	508	474	446	430	413	326
ethoxybenzene	0	0	1	1	1	1	1
2-ethylphenol	0	0	3	7	6	7	7
2-ethylcyclohexanol	0	0	34	41	51	75	135
ethylbenzene	0	0	5	6	9	11	20
ethylcyclohexane	0	0	0	0	0	0	1
cresol (ortho)	0	0	4	5	4	4	5
cyclohexanol	0	0	2	3	2	3	3
methylcyclohexane	0	0	0	0	0	0	1
methylcyclohexanols	0	2	3	4	4	5	6
toluene	0	0	0	0	1	1	1

[a] 100 mg Cu_{20}PMO. [b] 61.5 mg (512 μmol). [c] 3.0 mL. [d] The GC-FID analysis did not show any signals for the following: methylethylcyclohexane, benzene, benzyl alcohol, cresol (meta/para), cyclohexane, methylanisole, phenol or methylethylphenol.

B.

Conditions	**Cu_{20}PMO+FA [a]/ DHBF [b]/ MeOH[c]**						
Compound	**Reaction Time (h) / Yield (mmol)**						
	0	**1**	**2**	**3**	**4**	**5**	**6**
DHBF	512	529	501	493	486	455	408
ethoxybenzene	0	0	1	1	1	1	1
2-ethylphenol	0	0	4	3	4	1	3
2-ethylcyclohexanol	0	0	4	19	19	37	42
ethylbenzene	0	0	1	3	3	5	4
cresol (ortho)	0	0	7	1	1	4	2
cyclohexanol	0	0	2	5	5	4	3
methylanisole	0	0	1	1	1	1	1
methylcyclohexanols	0	0	3	5	5	6	6
phenol	0	3	1	0	0	0	0
toluene	0	0	0	0	0	0	1

[a] 100 mg Cu_{20}PMO plus 25 μL 88% aq. FA (0.58 mmol). [b] 61.5 mg (512 μmol). [b] 61.5 mg (512 μmol). [c] 3.0 mL [d] The GC-FID analysis did not show any signals for the following: methylethylcyclohexane, benzene, benzyl alcohol, cresol (meta/para), cyclohexane, methylanisole, phenol or methylethylphenol

C.

Conditions	Cu20PMO+Sm^{3+} [a] / DHBF [b] / MeOH [c] / 300 °C						
Compound	**Reaction Time (h) / Yield (mmol)**						
	0	**1**	**2**	**3**	**4**	**5**	**6**
DHBF	512	512	503	471	467	438	435
ethoxybenzene	0	1	1	1	1	1	1
2-ethylphenol	0	3	3	4	11	9	11
2-ethylcyclohexanol	0	1	13	9	21	25	25
ethylbenzene	0	0	2	2	4	5	5
cresol (ortho)	0	7	7	7	7	7	7
cyclohexanol	0	1	3	2	2	2	2
methylcyclohexanols	0	0	2	1	3	4	4
methylethylphenol	0	0	0	0	0	0	1

[a] 100 mg Cu_{20}PMO plus 5 mg $Sm(CF_3SO_3)_3 \cdot 9H_2O$ (6.7 μmol). [b] 61.5 mg (512 μmol). [c] 3.0 mL

D.

Conditions	$Cu_{20}Sm_5$PMO [a] / DHBF [b] / MeOH [c] / 300 °C						
Compound	**Reaction Time (h) / Yield (μmol)**						
	0	**1**	**2**	**3**	**4**	**5**	**6**
DHBF	512	501	496	436	397	283	160
ethoxybenzene	0	0	1	1	1	0	2
2-ethylphenol	0	8	8	4	5	3	4
2-ethylcyclohexanol	0	7	17	35	34	98	233
ethylbenzene	0	1	3	5	4	15	28
ethylcyclohexane	0	0	0	0	0	2	6
benzyl alcohol	0	0	0	0	0	0	2
cresol (ortho)	0	2	7	6	7	3	4
cyclohexane	0	0	0	0	0	0	1
cyclohexanol	0	1	2	2	1	2	2
methylcyclohexanols	0	1	2	4	4	5	7
toluene	0	0	0	0	0	1	1
methylethylphenol	0	0	0	4	20	55	53

[a] 100 mg $Cu_{20}Sm_5$PMO [b] 61.5 mg (512 μmol). [c] 3.0 mL

Table B9. DHBF consumption and product formation with Cu_{20}PMO catalysts (100 mg) in sc-MeOH (3.0 mL) after 6 hours at 330 °C. Product yields are in mmol.

Compound [a]	Cu_{20}PMO	Cu_{20}PMO+FA	Cu_{20}PMO+Sm^{3+}	$Cu_{20}Sm_5$PMO
DHBF [b]	91	99	409	42
methylethylcyclohexane	6	5	0	23
benzene	0	0	0	1
ethoxybenzene	2	2	0	2
2-ethylphenol	23	25	23	17
2-ethylcyclohexanol	186	216	0	157
ethylbenzene	24	6	0	37
ethylcyclohexane	23	24	0	69
benzyl alcohol	2	5	4	6
cyclohexane	1	1	0	2
cyclohexanol	3	9	0	4
methylanisole	0	0	0	3
methylcyclohexane	0	1	0	2
methylcyclohexanols	7	10	1	8
phenol	3	2	0	1
toluene	2	2	1	3
methylethylphenol	86	58	9	96

[a] The GC-FID analysis did not show signals for cresol (ortho, meta, para). [b] DHBF(initial) 60.3 mg (502 μmol)

Table B10. Temporal data for DHBF reaction with $Cu_{20}Sm_5$PMO at 330 °C.

Conditions	**$Cu_{20}Sm_5$PMO [a] / DHBF[b] / MeOH[c] / 330 °C**						
	Reaction Time (h) / Yield (μmol)						
Compound	**0**	**1**	**2**	**3**	**4**	**5**	**6**
DHBF	502	450	320	170	89	84	42
2-ethyl(methyl)cyclohexane	0	0	0	2	7	9	23
benzene	0	0	0	1	2	2	1
benzyl phenyl ether	0	0	0	0	0	0	0
diphenyl ether	0	0	0	0	0	0	0
ethoxybenzene	0	0	1	2	2	2	2
2-ethylphenol	0	43	37	51	26	22	17
2-ethylcyclohexanol	0	12	84	188	187	184	157
ethylbenzene	0	2	13	27	35	33	37
ethylcyclohexane	0	0	2	11	30	38	69
benzyl alcohol	0	0	0	1	2	3	6
cresol (ortho)	0	0	0	0	0	0	0
cresol (para/meta)	0	0	0	0	0	0	0
cyclohexane	0	0	0	1	2	2	2
cyclohexanol	0	0	1	3	3	4	4
methylanisole	0	0	0	0	1	2	3
methylcyclohexane	0	0	0	1	1	1	2
methylcyclohexanols	0	3	7	8	8	12	8
phenol	0	1	1	0	0	0	1
toluene	0	1	1	2	3	2	3
2-ethyl(methyl)phenol	0	10	16	57	73	78	96

[a] 100 mg $Cu_{20}Sm_5$PMO. [b] 60.3 mg (502 μmol). [c] 3.0 mL

Table B11. Temporal data for biphenyl (BP) reaction with $Cu_{20}Sm_5PMO$ (330 °C)

Conditions	**$Cu_{20}Sm_5PMO$ [a] / BP[b] / MeOH[c] / 330 °C**						
	Reaction Time (h) / Yield (μmol)						
Compound	**0**	**1**	**2**	**3**	**4**	**5**	**6**
BP	309	223	67	12	4	0	0
anisole	0	0	0	0	0	0	0
benzene	0	1	1	2	3	4	5
bicyclohexane	0	0	3	10	19	34	41
phenylcyclohexane	0	70	229	280	269	266	252
cresol (ortho)	0	0	0	0	0	0	0
cresol (para/meta)	0	0	0	0	0	0	0
cyclohexane	0	1	5	10	14	19	23
cyclohexanol	0	0	0	0	0	0	0
methylanisole	0	0	0	0	0	0	0
methylcyclohexane	0	0	2	4	5	6	8
methylcyclohexanols	0	0	0	0	0	0	0
phenol	0	0	0	0	0	0	0
toluene	0	0	0	0	0	0	0
xylenol	0	0	0	0	0	0	0

[a] 100 mg $Cu_{20}Sm_5PMO$. [b] 47.7 mg (309 μmol). [c] 3.0 mL

Table B12. Average molecular weight (M_w) extracted from GPC data for organosolv poplar lignin depolymerization for reactions at different time intervals at 300 °C.[a]

Catalyst	$Cu_{20}PMO$	$Cu_{20}PMO+FA$	$Cu_{20}Sm_5PMO$	$Cu_{20}PMO+Sm^3$
Time (h)	M_W (g mol^{-1})			
1	1000	1080	860	440
2	550	450	490	450
3	340	360	230	410
4	360	180	210	270
5	440	200	250	230
6	340	270	300	280
OPL	2800	2800	2800	2800

[a]Conditions: 100 mg catalyst, 3 mL of MeOH and 100 mg of OPL. For FA, 100 mL of 88% aq. formic acid was added. For Sm^{3+} was added 5% of $Sm(OTf)_3$ regarding to catalyst weighted mass.

Table B13. ^{1}H MNR data for temporal dependent catalytic reactions of organosolv poplar lignin disassembly at 300 °C.[a]

Catalyst	$Cu_{20}PMO$			$Cu_{20}PMO+FA$			$Cu_{20}Sm_5PMO$			$Cu_{20}PMO+Sm^{3+}$		
Time (h)	H_E	O_E	A_E	H_E	O_E	A_E	H_E	O_E	A_E	H_E	O_E	A_E
1	39	41	20	41	41	19	36	42	22	42	36	22
2	39	39	22	44	36	21	44	36	20	43	35	22
3	51	31	18	52	29	19	53	39	18	50	31	20
4	55	28	17	61	24	15	58	26	16	57	27	16
5	49	39	12	63	23	14	58	26	16	54	28	18
6	68	20	12	64	22	14	60	25	15	60	25	15
OPL	20	41	38	20	41	38	20	41	38	20	41	38

[a]Conditions: 100 mg catalyst, 3 mL of MeOH and 100 mg of OPL. For FA, 100 mL 88% aq, formic acid (1.17 mmols) was added. For Sm^{3+} was added 5% of $Sm(OTf)_3$ regarding to catalyst weighted mass. [b] Values in the Table correspond to the integral of the areas for the regions H_E: aliphatic, O_E: near oxygen and A_E: aromatic compounds.

Table B14. NMR and GPC data for the recycling experiments using organosolv poplar lignin and $Cu_{20}Sm_5$PMO catalyst at 300 °C after 6 hours of reaction.[a]

Cycle	NMR			GPC
	H_E	O_E	A_E	M_w (g mol^{-1})
1	61	25	14	210
2	72	17	11	280
3	67	21	12	300
4	67	20	13	290
Average	67±4	21±3	12±1	271±35
OPL	20	41	38	2800

[a]Conditions: 100 mg of $Cu_{20}Sm_5$PMO, 100 mg of OPL in each cycle, 3.0 mL of MeOH. Values are the average of two distinct reactions sets.

Table B15. Catalyst metals leaching from $Cu_{20}Sm_5$PMO at 300 °C as determined from ICP analysis of the methanolic reaction solutions.[a]

Metal	Cycle / Leaching (%)[b]				S (each metal)
	1st	2nd	3rd	4th	
Mg	0.35	0.20	0.14	0.12	0.81
Cu	0.02	0.05	0.03	0.09	0.19
Al	0.02	0.01	0.00	0.00	0.03
Sm	0.01	0.00	0.00	0.00	0.01
S (each cycle)	0.39	0.26	0.17	0.21	-
S (total)	-	-	-	-	1.03

[a] Conditions: 100 mg of $Cu_{20}Sm_5$PMO, 3 mL of MeOH and 1 mmol of BPE. Values are the average of two distinct reactions sets. [b] Percent of the original metal of interest that is leached in a specific cycle.

Appendix C

C1. Synthesis and Characterization of Cu_{10}HTC

Figure C1: Powder X-Ray Diffraction pattern for Cu_{10}HTC

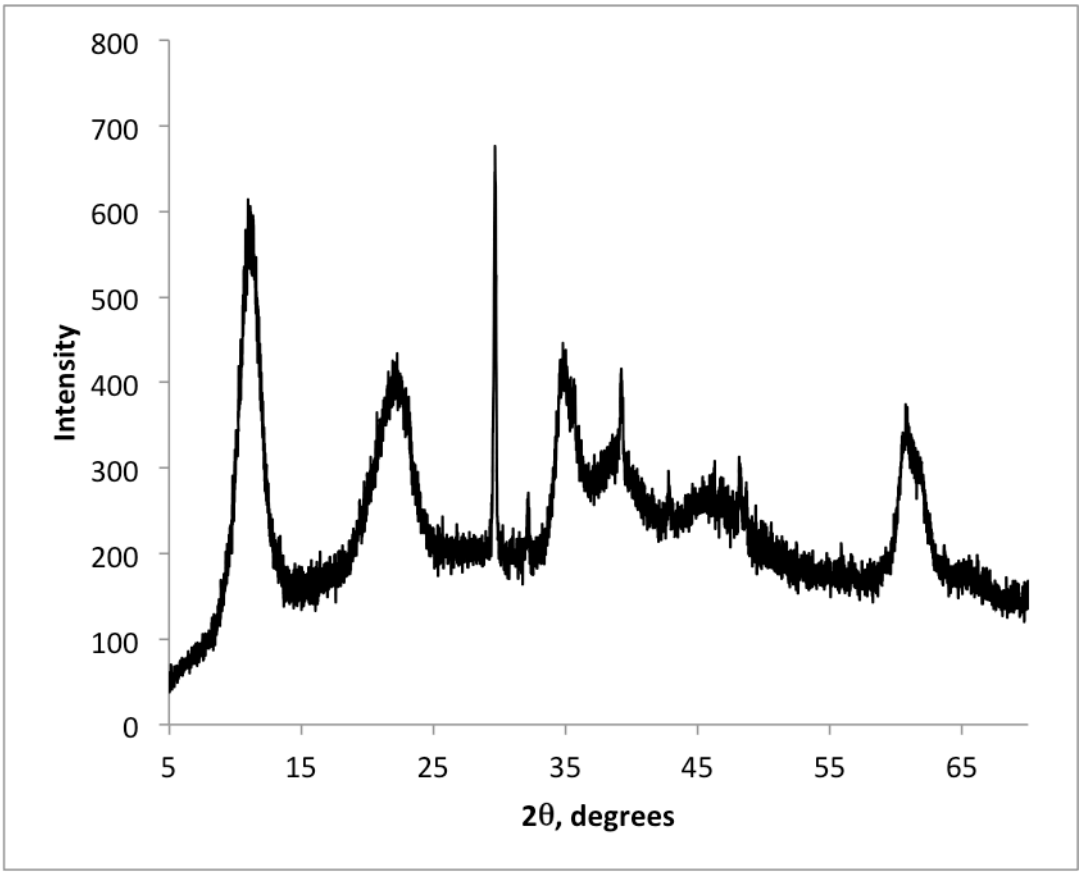

Cu_{10} HTC was synthesized by a modified coprecipitation method. 2.91 g Na_2CO_3 was added to 375 mL of DI H_2O in a 1000 mL beaker. In a 500 mL beaker, 38.08 g of $Mg(NO_3)_2 \cdot 6H_2O$ and 3.99 g $Cu(NO_3)_2 \cdot 3H_2O$ was added to 200 mL of DI H_2O. A second solution of 20.63 g $Al(NO_3)_3 \cdot 9H_2O$ was added to 200 mL of DI H_2O. The two metal solutions were combined and added dropwise to the to the vigorously stirring Na_2CO_3 solution and a light blue precipitate instantly formed. A pH of ~10 for the solution must be maintained for accurate synthesis. This was achieved by alternating aliquots of 1 M NaOH

and the metal solution and checked with pH paper. The final solution was covered and left to age while stirring for one day between 60-65 °C. The catalyst was filtered in a Buchner funnel and added to a solution of 2.91 g Na_2CO_3 in 1000 mL of DI H_2O. The catalyst was stirred at room temperature for a minimum of 4 hours and then filtered in a Buchner funnel. When only a thin layer of water remained over the catalyst cake during filtration, 1000 mL of DI H_2O was gently added to thoroughly wash the catalyst. The light blue catalyst was transferred to an evaporating dish and placed in an oven at 110 °C overnight. The solid was then analyzed though powder XRD, TGA, and BET.

C2. Synthesis and Characterization of $Cu_{10}Nb_{1.25}$HTC

Figure C2: Powder X-Ray Diffraction pattern for $Cu_{10}Nb_{1.25}$HTC

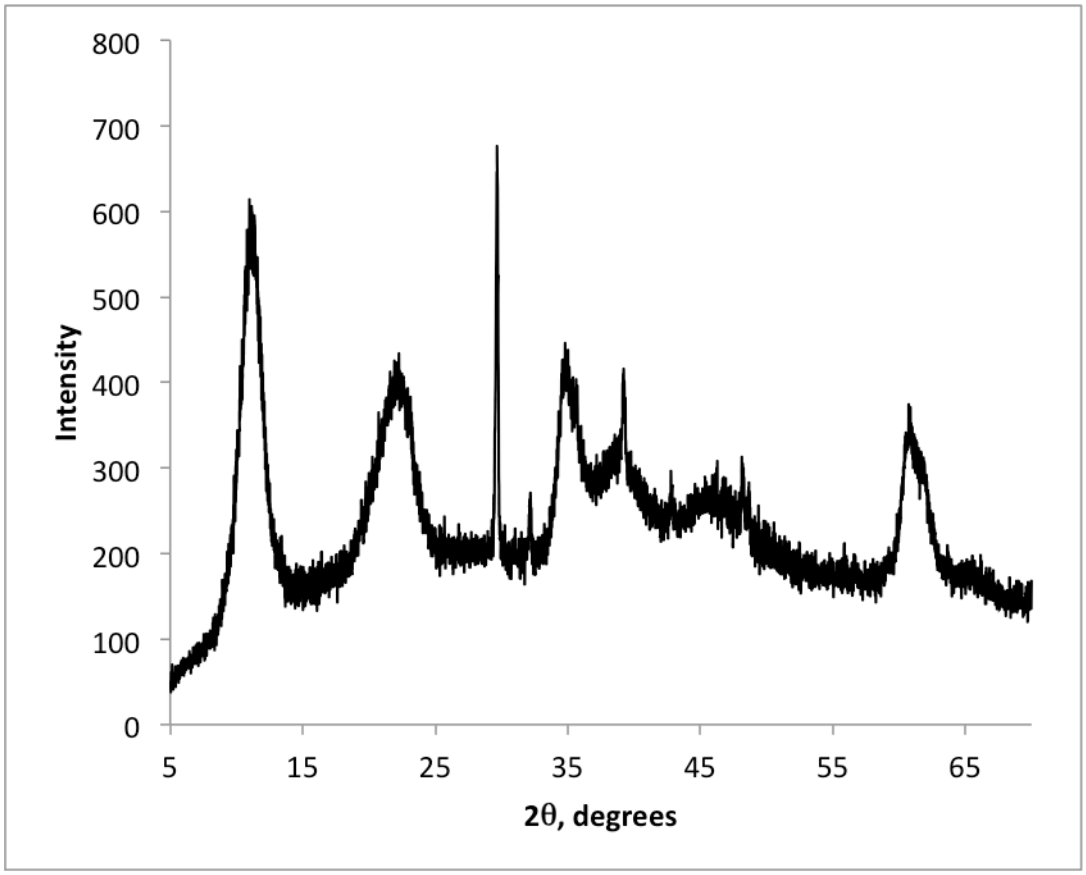

$Cu_{10}Nb_{1.25}$ HTC was synthesized by a modified coprecipitation method. 2.97 g Na_2CO_3 was added to 375 mL of DI H_2O in a 1000 mL beaker. In a 500 mL beaker, 38.08 g of $Mg(NO_3)_2 \cdot 6H_2O$ and 3.99 g $Cu(NO_3)_2 \cdot 3H_2O$ was added to 200 mL of MeOH. A second solution of 20.63 g $Al(NO_3)_3 \cdot 9H_2O$ was added to 200 mL of MeOH. A third solution of 0.26 g $NbCl_5$ was dissolved in a minimal amount of MeOH (5-10 mL) to obtain 1.25 weight % of niobium in the final PMO. The three metal solutions were combined and added dropwise to the Na_2CO_3 solution under sonication and a light blue precipitate instantly formed. A pH of ~10 for the solution must be maintained for accurate synthesis. This was achieved by alternating aliquots of 1 M NaOH and the metal solution and checked with pH paper. The

final solution was covered and left to age while stirring for one day between 60-65 °C. The catalyst was filtered in a Buchner funnel and added to a solution of 2.97 g Na_2CO_3 in 1000 mL of DI H_2O. The catalyst was stirred at room temperature for a minimum of 4 hours and then filtered in a Buchner funnel. When only a thin layer of water remained over the catalyst cake during filtration, 1000 mL of DI H_2O was gently added to thoroughly wash the catalyst. The light blue catalyst was transferred to an evaporating dish and placed in an oven at 110 °C overnight. The solid was then analyzed though powder XRD, TGA, and BET.

C3. Synthesis and Characterization of $Cu_{10}Nb_{2.5}$HTC

Figure C3: Powder X-Ray Diffraction pattern for $Cu_{10}Nb_{2.5}$HTC

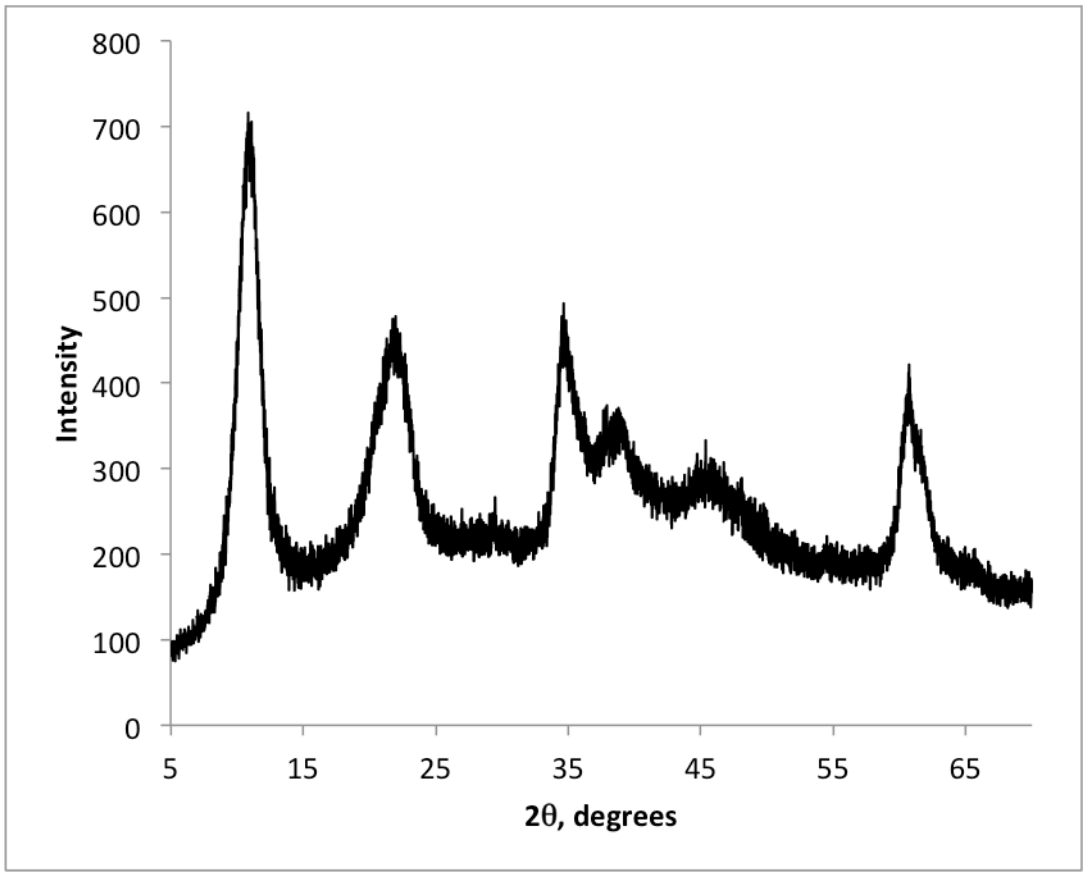

$Cu_{10}Nb_{2.5}$ HTC was synthesized by a modified coprecipitation method. 3.02 g Na_2CO_3 was added to 375 mL of DI H_2O in a 1000 mL beaker. In a 500 mL beaker, 38.08 g of $Mg(NO_3)_2 \cdot 6H_2O$ and 3.99 g $Cu(NO_3)_2 \cdot 3H_2O$ was added to 200 mL of MeOH. A second solution of 20.63 g $Al(NO_3)_3 \cdot 9H_2O$ was added to 200 mL of MeOH. A third solution of 0.51 g $NbCl_5$ was dissolved in a minimal amount of MeOH (5-10 mL) to obtain 2.5 weight % of niobium in the final PMO. The three metal solutions were combined and added dropwise to the Na_2CO_3 solution under sonication and a light blue precipitate instantly formed. A pH of ~10 for the solution must be maintained for accurate synthesis. This was achieved by alternating aliquots of 1 M NaOH and the metal solution and checked with pH paper. The

final solution was covered and left to age while stirring for one day between 60-65 °C. The catalyst was filtered in a Buchner funnel and added to a solution of 3.02 g Na_2CO_3 in 1000 mL of DI H_2O. The catalyst was stirred at room temperature for a minimum of 4 hours and then filtered in a Buchner funnel. When only a thin layer of water remained over the catalyst cake during filtration, 1000 mL of DI H_2O was gently added to thoroughly wash the catalyst. The light blue catalyst was transferred to an evaporating dish and placed in an oven at 110 °C overnight. The solid was then analyzed though powder XRD, TGA, and BET.

C4. Synthesis and Characterization of $Cu_{10}Nb_5HTC$

Figure C4: Powder X-Ray Diffraction pattern for $Cu_{10}Nb_5HTC$

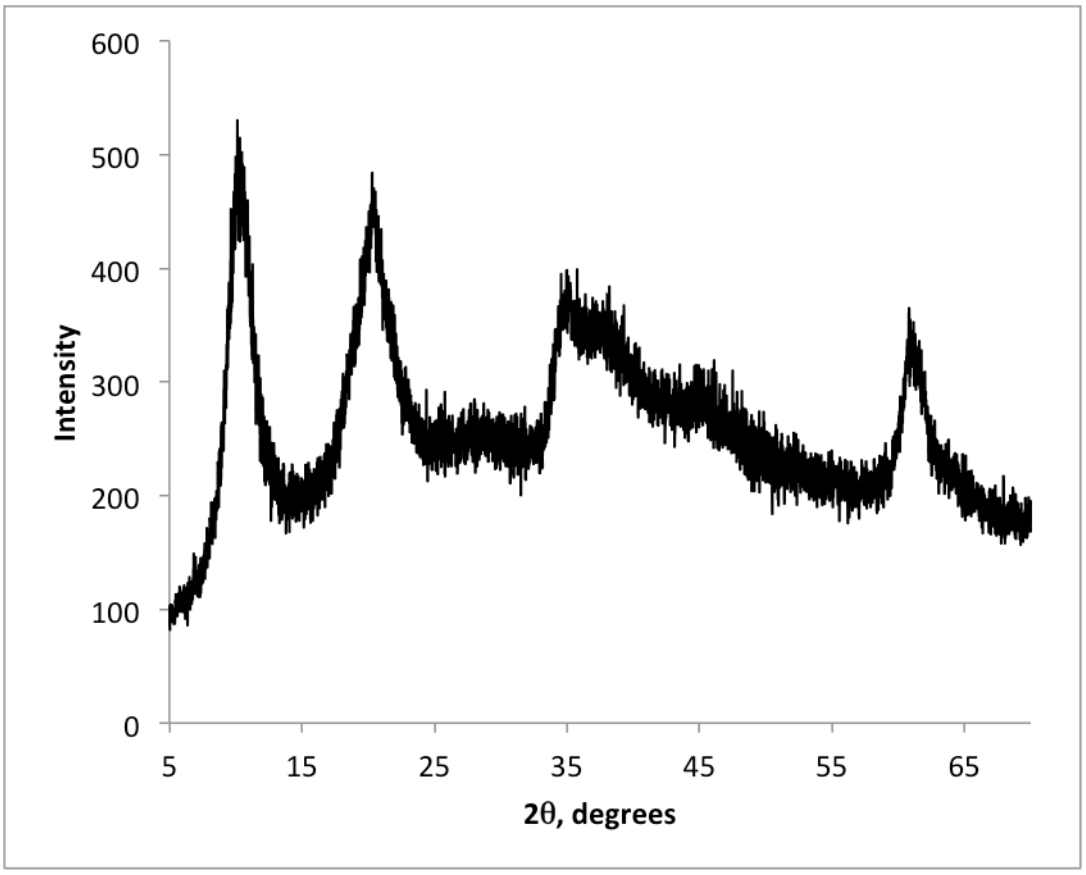

$Cu_{10}Nb_5$ HTC was synthesized by a modified coprecipitation method. 3.12 g Na_2CO_3 was added to 375 mL of DI H_2O in a 1000 mL beaker. In a 500 mL beaker, 38.08 g of $Mg(NO_3)_2 \cdot 6H_2O$ and 3.99 g $Cu(NO_3)_2 \cdot 3H_2O$ was added to 200 mL of MeOH. A second solution of 20.63 g $Al(NO_3)_3 \cdot 9H_2O$ was added to 200 mL of MeOH. A third solution of 1.03 g $NbCl_5$ was dissolved in a minimal amount of MeOH (5-10 mL) to obtain 5 weight % of niobium in the final PMO. The three metal solutions were combined and added dropwise to the Na_2CO_3 solution under sonication and a light blue precipitate instantly formed. A pH of ~10 for the solution must be maintained for accurate synthesis. This was achieved by alternating aliquots of 1 M NaOH and the metal solution and checked with pH paper. The

final solution was covered and left to age while stirring for one day between 60-65 °C. The catalyst was filtered in a Buchner funnel and added to a solution of 3.12 g Na_2CO_3 in 1000 mL of DI H_2O. The catalyst was stirred at room temperature for a minimum of 4 hours and then filtered in a Buchner funnel. When only a thin layer of water remained over the catalyst cake during filtration, 1000 mL of DI H_2O was gently added to thoroughly wash the catalyst. The light blue catalyst was transferred to an evaporating dish and placed in an oven at 110 °C overnight. The solid was then analyzed though powder XRD, TGA, and BET.

Table C1. Phenol consumption and product formation for reaction with Cu_{10}PMO catalyst

Conditions	**Cu10 100mg / Phenol / 3 ml MeOH / 300 °C**				
	Reaction Time (h) / Yield (mmol)				
Compound	**0**	**1**	**2**	**3**	**4**
anisole	0	9	29	48	69
benzene	0	0	0	0	1
benzyl phenyl ether	0	0	0	0	0
diphenyl ether	0	0	0	0	0
cresol (ortho)	0	69	111	141	163
cresol (para/meta)	0	3	4	5	7
cyclohexane	0	0	0	0	0
cyclohexanol	0	0	6	16	33
methylanisole	0	0	0	0	0
methylcyclohexane	0	0	0	9	0
methylcyclohexanols	0	0	2	0	23
phenol	1037	661	408	314	217
toluene	0	0	0	0	0
xylenol	0	4	14	27	44

Table C2. Phenol consumption and product formation for reaction with Cu_{10} $Nb_{1.25}$PMO catalyst

Conditions	Cu10Nb1.25 100mg / Phenol / 3 ml MeOH / 300 °C				
	Reaction Time (h) / Yield (mmol)				
Compound	0	1	2	3	4
anisole	0	7	18	30	42
benzene	0	0	0	0	0
benzyl phenyl ether	0	0	0	0	0
diphenyl ether	0	0	0	0	0
cresol (ortho)	0	37	60	75	98
cresol (para/meta)	0	3	4	6	9
cyclohexane	0	0	0	0	0
cyclohexanol	0	0	2	5	11
methylanisole	0	0	0	0	0
methylcyclohexane	0	0	0	0	0
methylcyclohexanols	0	0	0	2	7
phenol	1037	552	320	240	197
toluene	0	0	0	0	0
xylenol	0	2	7	13	6

Table C3. O-cresol consumption and product formation for reaction with Cu_{10}PMO catalyst

Conditions	Cu10 100mg / o-cresol / 3 ml MeOH / 300 °C				
	Reaction Time (h) / Yield (mmol)				
Compound	0	1	2	3	4
cresol	1004	598	331	278	192
dimethylanisole	0	0	3	11	13
dimethylphenol	0	74	137	191	167
methylanisole	0	0	0	1	3
methylcyclohexanol	0	0	7	19	39
trimethylphenol	0	1	6	12	11

Table C4. O-cresol consumption and product formation for reaction with Cu_{10} $Nb_{1.25}$PMO catalyst

Conditions	Cu10Nb1.25 100mg / o-cresol / 3 ml MeOH / 300 °C				
	Reaction Time (h) / Yield (mmol)				
Compound	0	1	2	3	4
cresol	1004	640	385	263	192
dimethylanisole	0	0	4	10	16
dimethylphenol	0	84	205	210	202
methylanisole	0	0	0	1	1
methylcyclohexanol	0	0	0	0	10
trimethylphenol	0	3	23	26	29

Table C5. M-cresol consumption and product formation for reaction with Cu_{10}PMO catalyst

Conditions	Cu10 100mg / m-cresol / 3 ml MeOH / 300 °C				
	Reaction Time (h) / Yield (mmol)				
Compound	0	1	2	3	4
cresol	791	240	83	35	2
dimethylanisole	0	1	7	16	29
dimethylphenol	0	187	210	197	160
tetramethylphenol	0	3	20	38	16
trimethylphenol	0	45	132	196	141

Table C6. M-cresol consumption and product formation for reaction with Cu_{10} $Nb_{1.25}$PMO catalyst

Conditions	Cu10Nb1.25 100mg / m-cresol / 3 ml MeOH / 300 °C				
	Reaction Time (h) / Yield (mmol)				
Compound	0	1	2	3	4
cresol	791	125	48	22	17
dimethylanisole	0	0	4	8	14
dimethylphenol	0	82	135	133	135
tetramethylphenol	0	6	31	63	74
trimethylphenol	0	35	121	189	217

Table C7. Dimethylanisole consumption and product formation for reaction with Cu_{10}PMO catalyst

Conditions	Cu10 100mg / Dimethylanisole / 3 ml MeOH / 300 °C				
	Reaction Time (h) / Yield (mmol)				
Compound	0	1	2	3	4
dimethylanisole	1179	1106	1066	1023	970
dimethylbenzene	0	0	4	8	14
dimethylphenol	0	1	8	14	22
trimethyl benzene	0	0	7	14	27

Table C8. Dimethylanisole consumption and product formation for reaction with Cu_{10} $Nb_{1.25}$PMO catalyst

Conditions	Cu10Nb1.25 100mg / Dimethylanisole / 3 ml MeOH / 300 °C				
	Reaction Time (h) / Yield (mmol)				
Compound	0	1	2	3	4
dimethylanisole	1179	1108	1131	984	991
dimethylbenzene	0	0	2	5	7
dimethylphenol	0	1	9	13	19
trimethyl benzene	0	0	4	15	23

Table C9. Dimethylphenol consumption and product formation for reaction with Cu_{10}PMO catalyst

Conditions	Cu10 100mg / Dimethylphenol / 3 ml MeOH / 300 °C				
	Reaction Time (h) / Yield (mmol)				
Compound	0	1	2	3	4
dimethylanisole	0	1	1	1	1
dimethylbenzene	0	0	0	1	4
dimethylcyclohexanol	0	1	1	5	19
dimethylphenol	1366	1116	1047	1001	1024
methylanisole	0	0	0	0	0
trimethylphenol	0	25	40	57	56

Table C10. Dimethylohenol consumption and product formation for reaction with Cu_{10} $Nb_{1.25}$PMO catalyst

Conditions	Cu10Nb1.25 100mg / Dimethylphenol / 3 ml MeOH / 300 °C				
	Reaction Time (h) / Yield (mmol)				
Compound	**0**	**1**	**2**	**3**	**4**
dimethylanisole	0	10	42	82	114
dimethylbenzene	0	0	0	1	2
dimethylcyclohexanol	0	1	1	5	11
dimethylphenol	1366	1062	946	928	915
methylanisole	0	0	0	0	0
trimethylphenol	0	40	63	74	84

Table C11. BPE consumption and product formation for reaction with Cu_{10}PMO catalyst

Conditions	Cu10 100mg / BPE / 3 ml MeOH / 300 °C				
	Reaction Time (h) / Yield (mmol)				
Compound	**0**	**1**	**2**	**3**	**4**
anisole	0	24	113	171	189
benzene	0	2	4	4	4
benzyl phenyl ether	827	426	20	1	7
diphenyl methane	0	9	17	21	16
cresol (ortho)	0	46	87	117	102
cresol (para/meta)	0	0	0	3	2
cyclohexane	0	0	0	0	0
cyclohexanol	0	0	0	0	0
methylanisole	0	0	23	50	53
methylcyclohexane	0	0	0	0	0
methylcyclohexanols	0	0	19	46	65
phenol	0	289	337	243	102
toluene	0	502	834	760	709
xylenol	0	6	12	24	32

Table C12. BPE consumption and product formation for reaction with $Cu_{10}Nb_{1.25}$PMO catalyst

Conditions	Cu10Nb1.25 100mg / BPE / 3 ml MeOH / 300 °C				
	Reaction Time (h) / Yield (mmol)				
Compound	0	1	2	3	4
anisole	0	14	73	127	158
benzene	0	2	5	5	6
benzyl phenyl ether	827	596	88	9	1
diphenyl methane	0	10	23	24	28
cresol (ortho)	0	24	54	76	78
cresol (para/meta)	0	0	0	2	2
cyclohexane	0	0	0	0	0
cyclohexanol	0	0	0	0	0
methylanisole	0	0	7	17	24
methylcyclohexane	0	0	0	0	0
methylcyclohexanols	0	0	6	16	24
phenol	0	211	296	225	136
toluene	0	328	725	778	742
xylenol	0	2	7	15	22

Appendix D

D1. Synthesis and Characterization of $Cu_{20}Mo_{1.25}$HTC

Figure D1: Powder X-Ray Diffraction pattern for $Cu_{20}Mo_{1.25}$HTC

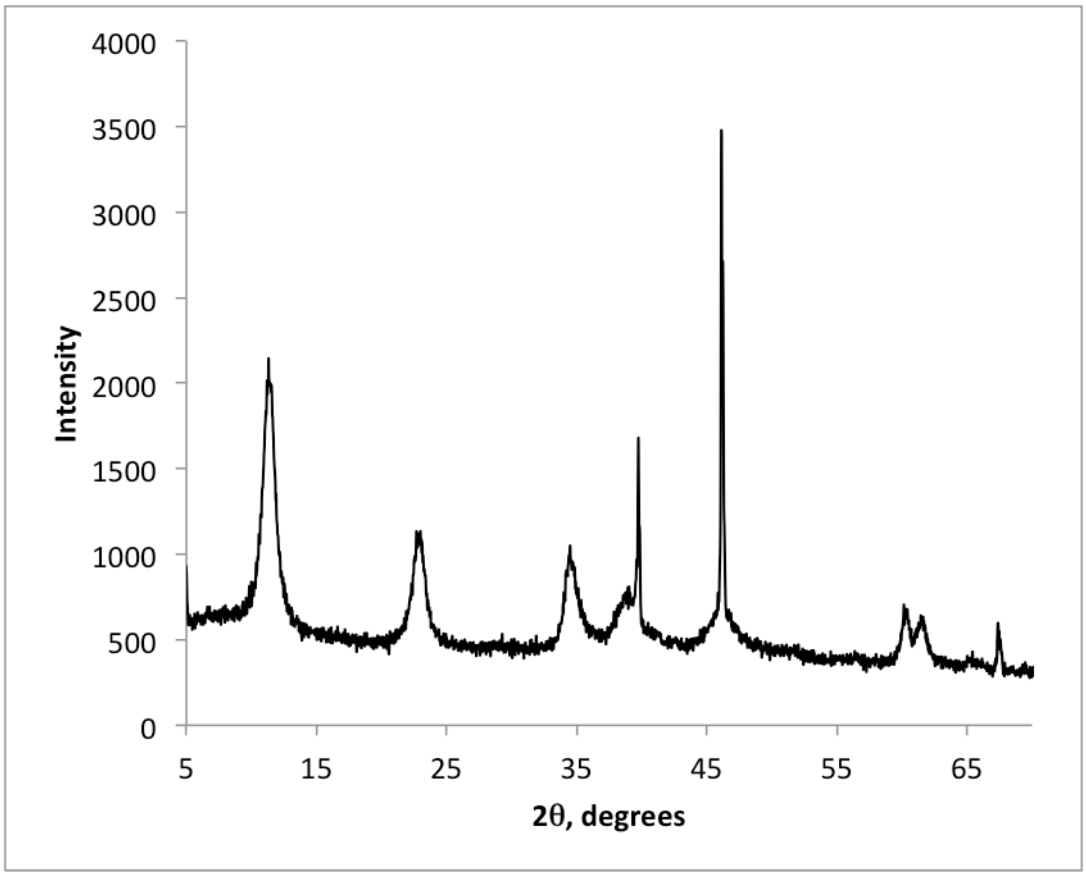

$Cu_{20}Mo_{1.25}$ HTC was synthesized by a modified coprecipitation method. 5.32 g Na_2CO_3 was added to 375 mL of DI H_2O in a 1000 mL beaker with stirring and heated to 60 °C. In a 500 mL beaker, 30.78 g of $Mg(NO_3)_2 \cdot 6H_2O$ and 7.27 g $Cu(NO_3)_2 \cdot 3H_2O$ was added to 200 mL of DI H_2O. A second solution of 18.83 g $Al(NO_3)_3 \cdot 9H_2O$ was added to 200 mL of DI H_2O. The two metal solutions were combined and added dropwise to the vigorously stirring Na_2CO_3 solution and a light blue precipitate instantly formed. A pH of ~10 for the solution must be maintained for accurate synthesis. This was achieved by alternating aliquots of 1 M

NaOH and the metal solution and checked with pH paper. The final solution was covered and left to age while stirring for one day between 60-65 °C. The catalyst was filtered in a Buchner funnel and added to a solution of 5.32 g Na_2CO_3 in 500 mL of DI H_2O. The catalyst was stirred at room temperature for a minimum of 4 hours and then filtered in a Buchner funnel. When only a thin layer of water remained over the catalyst cake during filtration, 1000 mL of DI H_2O was gently added to thoroughly wash the catalyst. The light blue catalyst was transferred to an evaporating dish and placed in an oven at 110 °C overnight. The next step in catalyst synthesis was molybdenum surface deposition onto the hydrotalcite via equilibrium deposition filtration. A molybdenum stock solution was created by combining 2.165 g of ammonium molybdate tetrahydrate ($(NH_4)_4Mo_7O_{24}•4H_2O$) in a 100 mL volumetric flask with deionized water. 1.25 % molybdenum was deposited onto the Cu-doped hydrotalcite by combining 4.0g of Cu-doped hydrotalcite with 2.5 mL of the $(NH_4)_4Mo_7O_{24}•4H_2O$ solution. The slurries were allowed to stir at room temperature for several days, and the Mo-doped hydrotalcites were collected via frit funnel and dried for 2.5 hours in an oven (110 °C). After completely dried, the catalyst was ground in a mortar and pestle and stored. The solid was then analyzed though powder XRD resulting in a pattern characteristic of an undoped hydrotalcite.

D2. Synthesis and Characterization of $Cu_{20}Mo_{2.5}$HTC

Figure D2: Powder X-Ray Diffraction pattern for $Cu_{20}Mo_{2.5}$HTC

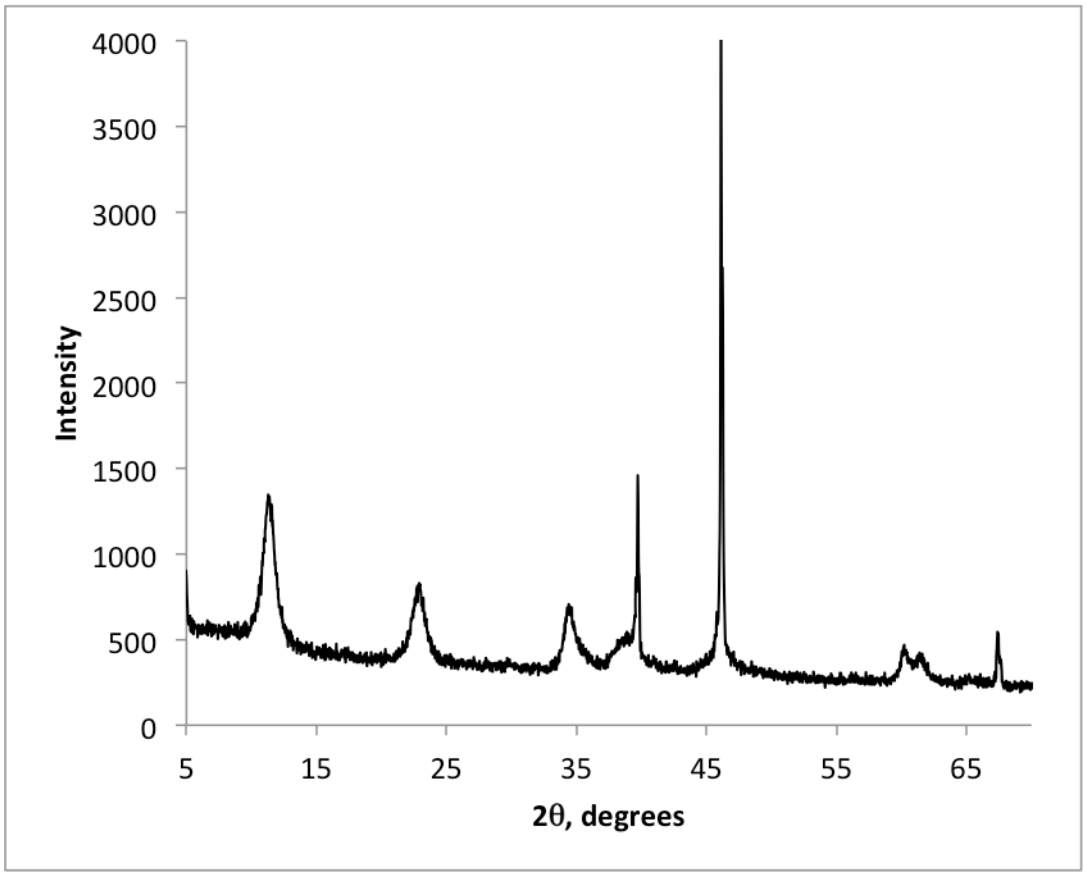

$Cu_{20}Mo_{2.5}$ HTC was synthesized by a modified coprecipitation method. 5.32 g Na_2CO_3 was added to 375 mL of DI H_2O in a 1000 mL beaker with stirring and heated to 60 °C. In a 500 mL beaker, 30.78 g of $Mg(NO_3)_2 \cdot 6H_2O$ and 7.27 g $Cu(NO_3)_2 \cdot 3H_2O$ was added to 200 mL of DI H_2O. A second solution of 18.83 g $Al(NO_3)_3 \cdot 9H_2O$ was added to 200 mL of DI H_2O. The two metal solutions were combined and added dropwise to the vigorously stirring Na_2CO_3 solution and a light blue precipitate instantly formed. A pH of ~10 for the solution must be maintained for accurate synthesis. This was achieved by alternating aliquots of 1 M NaOH and the metal solution and checked with pH paper. The final solution was covered and left to age while stirring for one day between 60-65 °C. The catalyst was filtered in a

Buchner funnel and added to a solution of 5.32 g Na_2CO_3 in 500 mL of DI H_2O. The catalyst was stirred at room temperature for a minimum of 4 hours and then filtered in a Buchner funnel. When only a thin layer of water remained over the catalyst cake during filtration, 1000 mL of DI H_2O was gently added to thoroughly wash the catalyst. The light blue catalyst was transferred to an evaporating dish and placed in an oven at 110 °C overnight. The next step in catalyst synthesis was molybdenum surface deposition onto the hydrotalcite via equilibrium deposition filtration. A molybdenum stock solution was created by combining 2.165 g of ammonium molybdate tetrahydrate ($(NH_4)_4Mo_7O_{24}•4H_2O$) in a 100 mL volumetric flask with deionized water. 2.5 % molybdenum was deposited onto the Cu-doped hydrotalcite by combining 4.0g of Cu-doped hydrotalcite with 5 mL of the $(NH_4)_4Mo_7O_{24}•4H_2O$ solution. The slurries were allowed to stir at room temperature for several days, and the Mo-doped hydrotalcites were collected via frit funnel and dried for 2.5 hours in an oven (110 °C). After completely dried, the catalyst was ground in a mortar and pestle and stored. The solid was then analyzed though powder XRD resulting in a pattern characteristic of an undoped hydrotalcite.

D3. Synthesis and Characterization of $Cu_{20}Mo_5$HTC

Figure D3: Powder X-Ray Diffraction pattern for $Cu_{20}Mo_5$HTC

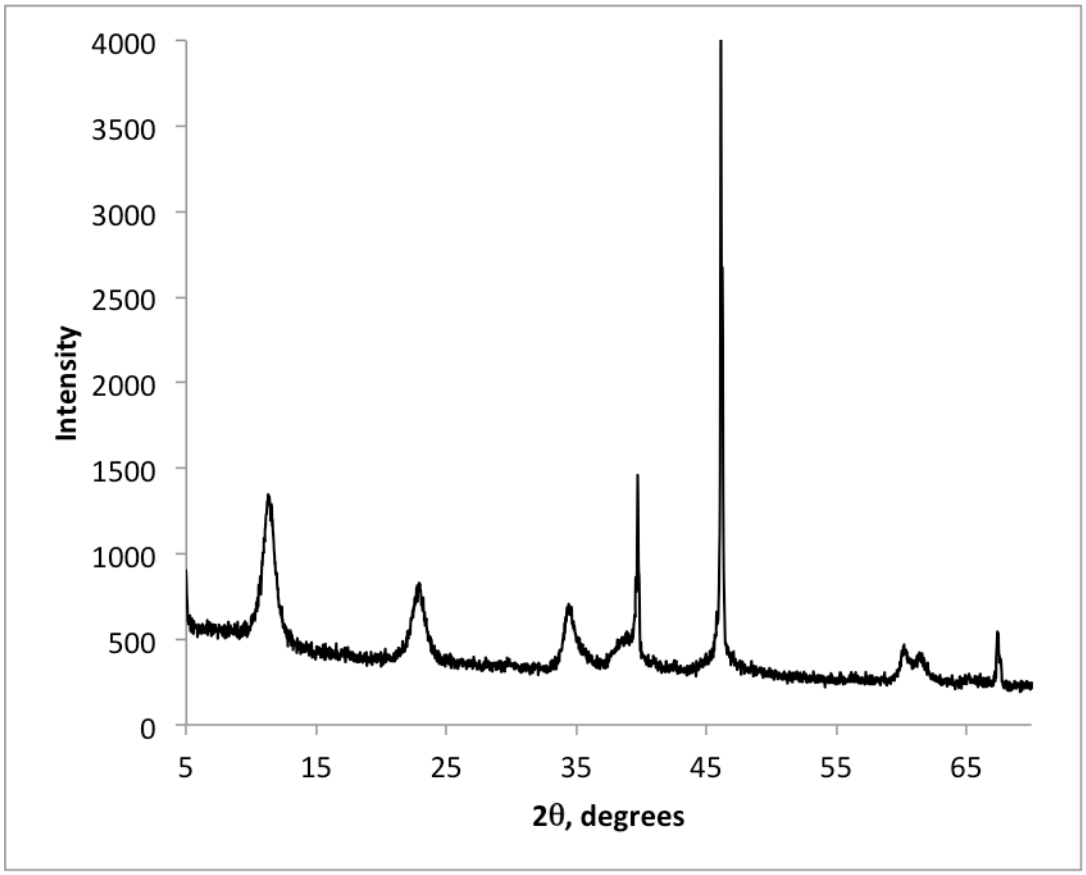

$Cu_{20}Mo_5$ HTC was synthesized by a modified coprecipitation method. 5.32 g Na_2CO_3 was added to 375 mL of DI H_2O in a 1000 mL beaker with stirring and heated to 60 °C. In a 500 mL beaker, 30.78 g of $Mg(NO_3)_2 \cdot 6H_2O$ and 7.27 g $Cu(NO_3)_2 \cdot 3H_2O$ was added to 200 mL of DI H_2O. A second solution of 18.83 g $Al(NO_3)_3 \cdot 9H_2O$ was added to 200 mL of DI H_2O. The two metal solutions were combined and added dropwise to the vigorously stirring Na_2CO_3 solution and a light blue precipitate instantly formed. A pH of ~10 for the solution must be maintained for accurate synthesis. This was achieved by alternating aliquots of 1 M NaOH and the metal solution and checked with pH paper. The final solution was covered and left to age while stirring for one day between 60-65 °C. The catalyst was filtered in a

Buchner funnel and added to a solution of 5.32 g Na_2CO_3 in 500 mL of DI H_2O. The catalyst was stirred at room temperature for a minimum of 4 hours and then filtered in a Buchner funnel. When only a thin layer of water remained over the catalyst cake during filtration, 1000 mL of DI H_2O was gently added to thoroughly wash the catalyst. The light blue catalyst was transferred to an evaporating dish and placed in an oven at 110 °C overnight. The next step in catalyst synthesis was molybdenum surface deposition onto the hydrotalcite via equilibrium deposition filtration. A molybdenum stock solution was created by combining 2.165 g of ammonium molybdate tetrahydrate ($(NH_4)_4Mo_7O_{24}•4H_2O$) in a 100 mL volumetric flask with deionized water. 5 % molybdenum was deposited onto the Cu-doped hydrotalcite by combining 4.0g of Cu-doped hydrotalcite with 10 mL of the $(NH_4)_4Mo_7O_{24}•4H_2O$ solution. The slurries were allowed to stir at room temperature for several days, and the Mo-doped hydrotalcites were collected via frit funnel and dried for 2.5 hours in an oven (110 °C). After completely dried, the catalyst was ground in a mortar and pestle and stored. The solid was then analyzed though powder XRD resulting in a pattern characteristic of an undoped hydrotalcite.

D4. Synthesis and Characterization of $Cu_{20}Mo_{10}$HTC

Figure D4: Powder X-Ray Diffraction pattern for $Cu_{20}Mo_{10}$HTC

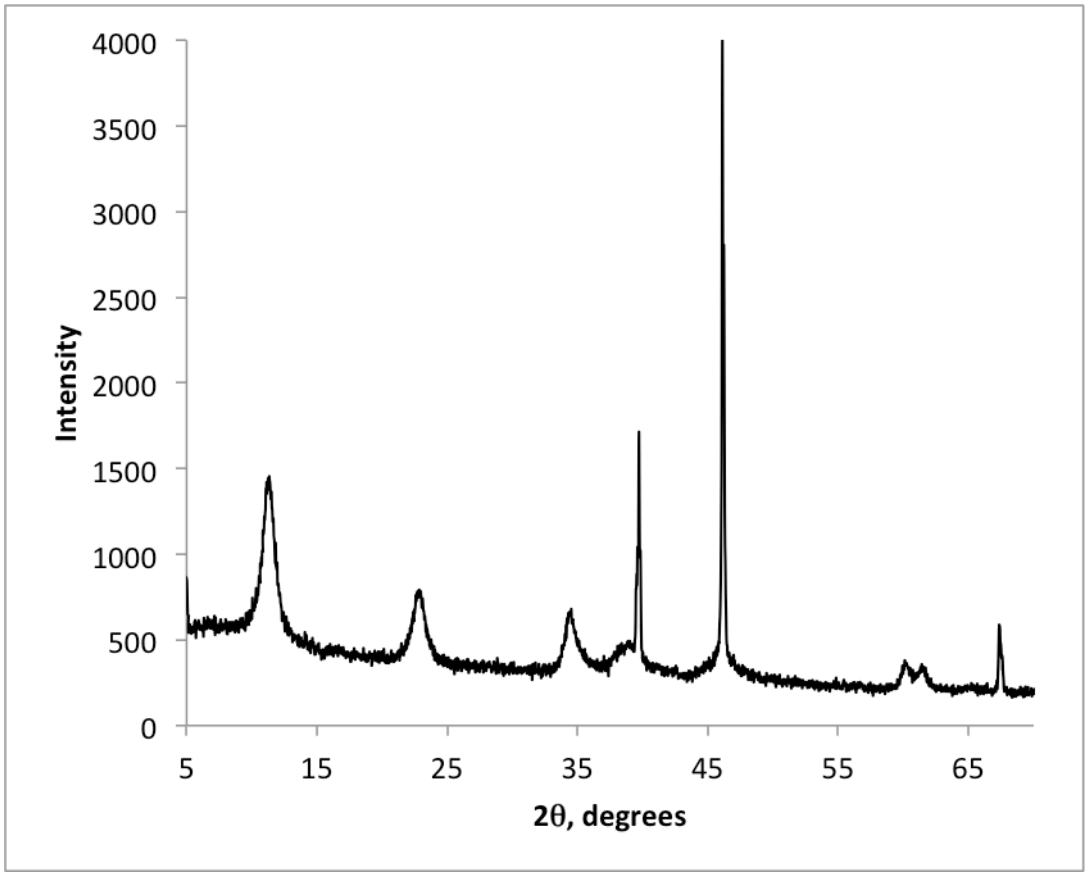

$Cu_{20}Mo_{10}$ HTC was synthesized by a modified coprecipitation method. 5.32 g Na_2CO_3 was added to 375 mL of DI H_2O in a 1000 mL beaker with stirring and heated to 60 °C. In a 500 mL beaker, 30.78 g of $Mg(NO_3)_2 \cdot 6H_2O$ and 7.27 g $Cu(NO_3)_2 \cdot 3H_2O$ was added to 200 mL of DI H_2O. A second solution of 18.83 g $Al(NO_3)_3 \cdot 9H_2O$ was added to 200 mL of DI H_2O. The two metal solutions were combined and added dropwise to the vigorously stirring Na_2CO_3 solution and a light blue precipitate instantly formed. A pH of ~10 for the solution must be maintained for accurate synthesis. This was achieved by alternating aliquots of 1 M NaOH and the metal solution and checked with pH paper. The final solution was covered and left to age while stirring for one day between 60-65 °C. The catalyst was filtered in a

Buchner funnel and added to a solution of 5.32 g Na_2CO_3 in 500 mL of DI H_2O. The catalyst was stirred at room temperature for a minimum of 4 hours and then filtered in a Buchner funnel. When only a thin layer of water remained over the catalyst cake during filtration, 1000 mL of DI H_2O was gently added to thoroughly wash the catalyst. The light blue catalyst was transferred to an evaporating dish and placed in an oven at 110 °C overnight. The next step in catalyst synthesis was molybdenum surface deposition onto the hydrotalcite via equilibrium deposition filtration. A molybdenum stock solution was created by combining 2.165 g of ammonium molybdate tetrahydrate ($(NH_4)_4Mo_7O_{24}•4H_2O$) in a 100 mL volumetric flask with deionized water. 10 % molybdenum was deposited onto the Cu-doped hydrotalcite by combining 4.0g of Cu-doped hydrotalcite with 20 mL of the $(NH_4)_4Mo_7O_{24}•4H_2O$ solution. The slurries were allowed to stir at room temperature for several days, and the Mo-doped hydrotalcites were collected via frit funnel and dried for 2.5 hours in an oven (110 °C). After completely dried, the catalyst was ground in a mortar and pestle and stored. The solid was then analyzed though powder XRD resulting in a pattern characteristic of an undoped hydrotalcite.

Table D1. BPE consumption and product formation for reaction with Cu_{20}PMO catalyst

Conditions	**Cu20 100mg / BPE / 3 ml MeOH / 300 °C**						
	Reaction Time (h) / Yield (mmol)						
Compound	**0**	**1**	**2**	**3**	**4**	**5**	**6**
anisole	0	3	30	72	103	102	96
benzene	0	0	2	1	1	1	1
Benzyl phenyl ether	1041	373	33	0	0	0	0
Diphenyl ether	0	0	0	0	0	0	0
cresol(o)	0	0	60	105	84	84	54
cresol (m/p)	0	0	0	0	3	2	2
cyclohexane	0	0	0	0	0	0	0
cyclohexanol	0	3	40	350	540	560	583
methylanisole	0	0	1	3	8	7	9
methylcyclohexane	0	0	0	0	0	0	0
methylcyclohexanol	0	0	2	38	160	165	223
phenol	0	676	824	504	90	68	16
toluene	0	687	977	1000	987	1027	1018
xylenol	0	0	2	6	12	12	21
BPE Conversion (%)		64.2	96.8	100	100	100	100
BPE Mass Balance (mmol)	2083	2117	2003	2078	1988	2030	2022
(%)		102	96	100	95	97	97

Table D2. BPE consumption and product formation for reaction with $Cu_{10}Mo_{1.25}$PMO catalyst

Conditions	Cu20Mo1.25 100mg / BPE / 3 ml MeOH / 300 °C						
	Reaction Time (h) / Yield (mmol)						
Compound	**0**	**1**	**2**	**3**	**4**	**5**	**6**
Anisole	0	4	18	24	22	31	37
Benzene	0	2	8	10	12	14	15
Benzyl phenyl ether	1056	716	462	359	278	229	212
Diphenyl ether	0	0	0	0	0	0	0
2-ethylcyclohexanol	0	0	0	0	0	0	0
Ethyl benzene	0	0	0	0	0	0	1
Ethyl cyclohexane	0	0	0	0	0	0	0
Benzyl alcohol	0	3	9	12	15	17	18
cresol(o)	0	16	58	66	48	70	80
cresol (m/p)	0	1	2	2	1	2	2
cyclohexane	0	0	0	0	0	0	0
cyclohexanol	0	0	0	0	0	0	0
methylanisole	0	1	1	1	1	1	1
methylcyclohexane	0	0	0	0	0	0	0
methylcyclohexanol	0	0	1	1	0	0	0
phenol	0	124	242	235	167	141	155
toluene	0	154	373	392	178	360	396
2,3 xylenol	0	1	8	9	10	25	27
Phenylethylalchol	0	1	6	8	7	7	7
2,4 xylenol	0	0	1	1	2	3	4
2,3,5 trimethyl phenol	0	0	0	0	0	0	0
Biphenyl	0	2	13	21	22	30	45
1,2-diphenylethane	0	1	0	0	0	0	0
methoxymethylene dibenzene	0	1	2	3	2	5	6
benzophenone	0	13	0	0	0	0	0
2-phenyl methyl phenol	0	14	39	38	59	46	40
4-methyl-2-benzyl phenol	0	4	20	24	24	26	29
4-phenylmethylphenol	0	4	10	13	18	18	21
1-methoxy-4-phenyl methyl benzene	0	1	2	3	2	5	6
4,(1-methyl-1phenylethyl) phenol	0	1	32	5	8	7	11
unknown monomers	0	316	16	22	35	53	61

unknown dimers	0	4	5	5	7	8	21
BPE Conversion (%)		32	56	66	74	78	80
BPE Mass Balance (mmol)	2113	2099	1794	1618	1290	1332	1409
(%)		99	85	77	61	63	67

Table D3. BPE consumption and product formation for reaction with $Cu_{20}Mo_{2.5}$PMO catalyst

Conditions	**Cu20Mo2.5 100mg / BPE / 3 ml MeOH / 300 °C**						
	Reaction Time (h) / Yield (mmol)						
Compound	**0**	**1**	**2**	**3**	**4**	**5**	**6**
Anisole	0	1	1	10	7	14	14
Benzene	0	2	3	14	8	17	17
Benzyl phenyl ether	1056	861	751	502	395	267	229
Diphenyl ether	0	0	0	0	0	0	0
2-ethylcyclohexanol	0	0	0	0	0	0	0
Ethyl benzene	0	0	0	0	0	0	0
Ethyl cyclohexane	0	0	0	0	0	0	0
Benzyl alcohol	0	3	6	16	15	21	19
cresol(o)	0	6	12	45	43	61	60
cresol (m/p)	0	0	0	1	1	1	1
cyclohexane	0	0	0	0	0	0	0
cyclohexanol	0	0	0	0	0	0	0
methylanisole	0	1	1	1	1	1	1
methylcyclohexane	0	0	0	0	0	0	0
methylcyclohexanol	0	0	1	1	0	0	0
phenol	0	38	48	155	102	146	139
toluene	0	44	44	234	155	341	349
xylenol	0	1	3	10	18	27	24
Phenylethylalchol	0	1	2	9	4	5	6
2,4 xylenol	0	0	0	1	3	5	4
2,3,5 trimethyl phenol	0	0	0	0	0	0	0
Biphenyl	0	0	2	14	19	23	25
1,2-diphenylethane	0	1	0	0	0	0	0
methoxymethylene dibenzene	0	1	2	8	6	11	10
benzophenone	0	0	0	0	0	0	0
2-phenyl methyl phenol	0	19	40	73	64	72	63
4-methyl-2-benzyl phenol	0	5	8	30	27	36	34
4-phenylmethylphenol	0	5	5	17	18	26	27
1-methoxy-4-phenyl methyl benzene	0	3	0	5	2	7	12

4,(1-methyl-1phenylethyl) phenol	0	1	2	5	6	11	19
unknown monomers	0	40	19	36	18	86	75
unknown dimers	0	5	1	13	9	18	52
BPE Conversion (%)		19	29	53	63	75	78
BPE Mass Balance (mmol)	2113	1899	1702	1702	1317	1462	1410
(%)		90	81	81	67	69	67

Table D4. BPE consumption and product formation for reaction with $Cu_{20}Mo_5$PMO catalyst

Conditions	Cu20Mo5 100mg / 1056 umol BPE / 3 ml MeOH / 300 C						
	Reaction Time (h) / Yield (μmol)						
Compound	**0**	**1**	**2**	**3**	**4**	**5**	**6**
Anisole	0	1	6	8	8	12	10
Benzene	0	2	12	14	8	18	16
Benzyl phenyl ether	1056	871	592	496	338	247	340
Diphenyl ether	0	0	0	0	0	0	0
2-ethylcyclohexanol	0	0	0	0	0	0	0
Ethyl benzene	0	0	0	0	0	0	0
Ethyl cyclohexane	0	0	0	0	0	0	0
Benzyl alcohol	0	3	13	17	13	22	22
cresol(o)	0	6	29	41	47	54	47
cresol (m/p)	0	0	1	1	1	1	1
cyclohexane	0	0	0	0	0	0	0
cyclohexanol	0	0	0	0	0	0	0
methylanisole	0	1	1	1	1	1	1
methylcyclohexane	0	0	0	0	0	0	0
methylcyclohexanol	0	0	1	1	0	0	0
phenol	0	38	129	141	123	164	134
toluene	0	48	184	229	186	345	284
xylenol	0	1	7	10	13	19	14
Phenylethylalchol	0	1	7	7	5	6	5
2,4 xylenol	0	0	1	1	2	4	3
2,3,5 trimethyl phenol	0	0	1	1	0	1	0
Biphenyl	0	7	5	9	24	22	21
1,2-diphenylethane	0	0	0	0	0	0	0
methoxymethylene dibenzene	0	1	6	8	6	11	9
benzophenone	0	0	0	0	0	0	0
2-phenyl methyl phenol	0	19	40	73	64	72	63
4-methyl-2-benzyl phenol	0	21	71	85	46	72	69
4-phenylmethylphenol	0	4	14	17	4	25	23
1-methoxy-4-phenyl methyl benzene	0	3	3	5	1	6	13
4,(1-methyl-1phenylethyl)	0	2	2	4	5	8	15

phenol							
unknown monomers	0	10	17	79	26	86	88
unknown dimers	0	3	3	6	23	14	80
BPE Conversion (%)		18	44	53	66	77	68
BPE Mass Balance (mmol)	2113	1904	1716	1706	1244	1427	1570
(%)		90	81	81	63	68	74

Table D5. BPE consumption and product formation for reaction with $Cu_{20}Mo_{10}$PMO catalyst

Conditions	Cu20Mo10 100mg / BPE / 3 ml MeOH / 300 °C						
	Reaction Time (h) / Yield (mmol)						
Compound	**0**	**1**	**2**	**3**	**4**	**5**	**6**
Anisole	0	1	5	7	6	11	9
Benzene	0	3	13	15	11	18	12
Benzyl phenyl ether	1056	863	583	492	271	217	198
Diphenyl ether	0	0	0	0	0	0	0
2-ethylcyclohexanol	0	0	0	0	0	0	1
Ethyl benzene	0	0	0	0	0	0	0
Ethyl cyclohexane	0	0	0	0	0	0	0
Benzyl alcohol	0	3	14	18	20	20	16
cresol(o)	0	5	24	36	33	46	46
cresol (m/p)	0	0	1	1	1	1	1
cyclohexane	0	0	0	0	0	0	0
cyclohexanol	0	0	0	0	0	0	0
methylanisole	0	1	1	1	1	1	1
methylcyclohexane	0	0	0	0	0	0	0
methylcyclohexanol	0	0	0	0	0	0	0
phenol	0	34	126	151	104	170	126
toluene	0	42	178	231	181	356	235
xylenol	0	1	5	8	10	13	16
Phenylethylalchol	0	1	7	8	6	6	5
2,4 xylenol	0	0	1	1	1	3	4
2,3,5 trimethyl phenol	0	0	1	1	1	1	1
Biphenyl	0	0	4	8	14	22	24
1,2-diphenylethane	0	0	0	0	0	0	0
methoxymethylene dibenzene	0	1	6	8	6	10	8
benzophenone	0	0	0	0	0	0	0
2-phenyl methyl phenol	0	23	79	94	49	53	49
4-methyl-2-benzyl phenol	0	0	24	34	21	35	33
4-phenylmethylphenol	0	4	12	18	11	19	22
1-methoxy-4-phenyl methyl benzene	0	0	3	5	4	5	5

4,(1-methyl-1phenylethyl) phenol	0	1	2	4	3	5	5
unknown monomers	0	23	23	26	49	31	91
unknown dimers	0	5	4	8	4	11	13
BPE Conversion (%)		18	45	53	74	79	80
BPE Mass Balance (mmol)	2113	1874	1698	1668	1079	1275	1118
(%)		89	80	79	51	60	57

Table D6. DHBF consumption and product formation for reaction with Cu_{20}PMO catalyst

Conditions	**Cu20 100mg / DHBF / 3 ml MeOH / 300 °C**						
	Reaction Time (h) / Yield (mmol)						
Compound	**0**	**1**	**2**	**3**	**4**	**5**	**6**
Anisole	0	0	0	0	0	0	0
Benzene	0	0	0	0	0	0	0
DHBF	512	508	474	446	430	413	326
Ethoxy benzene	0	0	1	1	1	1	1
2-ethylphenol	0	0	3	7	6	7	7
2-ethylcyclohexanol	0	0	34	41	51	75	135
Ethyl benzene	0	0	5	6	9	11	20
Ethyl cyclohexane	0	0	0	0	0	0	1
Benzyl alcohol	0	0	0	0	0	0	0
cresol(o)	0	0	4	5	4	4	5
cresol (m/p)	0	0	0	0	0	0	0
cyclohexane	0	0	0	0	0	0	0
cyclohexanol	0	0	2	3	2	3	3
methylanisole	0	0	0	0	0	0	0
methylcyclohexane	0	0	0	0	0	0	0
methylcyclohexanol	0	2	3	4	4	5	6
phenol	0	0	0	0	0	0	0
toluene	0	0	0	0	1	1	1
Methyl-ethyl phenol	0	0	0	0	0	0	0
DHBF Conversion (%)		1	7	13	16	19	36
DHBF Mass Balance (mmol)	512	510	526	514	509	521	505
(%)		99	103	100	99	101	98

Table D7. DHBF consumption and product formation for reaction with $Cu_{20}Mo_{1.25}$PMO catalyst

Conditions	**Cu20Mo1.25 100mg / DHBF / 3 ml MeOH / 300 °C**						
	Reaction Time (h) / Yield (mmol)						
Compound	**0**	**1**	**2**	**3**	**4**	**5**	**6**
Anisole	0	0	0	0	0	0	0
Benzene	0	0	0	0	0	0	0
DHBF	545	483	479	492	479	492	423
Ethoxy benzene	0	0	0	0	0	0	0
2-ethylphenol	0	0	0	0	0	0	0
2-ethylcyclohexanol	0	0	0	0	0	0	0
Ethyl benzene	0	0	0	0	0	0	0
Ethyl cyclohexane	0	0	0	0	0	0	0
Benzyl alcohol	0	0	0	0	0	0	0
cresol(o)	0	3	3	4	3	4	3
cresol (m/p)	0	0	0	0	0	0	0
cyclohexane	0	0	0	0	0	0	0
cyclohexanol	0	0	0	0	0	0	0
methylanisole	1	1	1	1	0	1	1
methylcyclohexane	0	0	0	0	0	0	0
methylcyclohexanol	0	0	0	0	0	0	0
phenol	0	0	2	2	2	2	1
toluene	0	0	0	0	0	0	0
2,3 xylenol	0	1	2	2	2	3	3
2,4 xylenol	0	2	3	3	3	4	3
Unknown monomer	0	26	18	24	32	40	35
DHBF Conversion (%)		11	12	10	12	10	22
DHBF Mass Balance (mmol)	545	516	509	501	523	501	431
(%)		95	93	92	96	92	79

Table D8. DHBF consumption and product formation for reaction with $Cu_{20}Mo_{2.5}$PMO catalyst

Conditions	**Cu20Mo2.5 100mg / DHBF / 3 ml MeOH / 300 °C**						
	Reaction Time (h) / Yield (mmol)						
Compound	**0**	**1**	**2**	**3**	**4**	**5**	**6**
Anisole	0	0	0	0	0	0	0
Benzene	0	0	0	0	0	0	0
DHBF	545	546	516	482	542	512	509
Ethoxy benzene	0	0	0	0	0	0	0
2-ethyl phenol	0	0	0	0	0	0	0
2-ethylcyclohexanol	0	0	0	0	0	0	0
Ethyl benzene	0	0	0	0	0	0	0
Ethyl cyclohexane	0	0	0	0	0	0	0
Benzyl alcohol	0	0	0	0	0	0	0
cresol(o)	0	4	3	3	4	3	3
cresol (m/p)	0	0	0	0	0	0	0
cyclohexane	0	0	0	0	0	0	0
cyclohexanol	0	0	0	0	0	0	0
methylanisole	0	1	1	1	1	1	1
methylcyclohexane	0	0	0	0	0	0	0
methylcyclohexanol	0	0	0	0	0	0	0
phenol	0	2	1	1	1	1	0
toluene	0	0	0	0	0	0	0
Methyl-ethyl phenol	0	0	0	0	0	0	0
2,3 xylenol	0	1	2	2	3	4	5
2,4 xylenol	0	0	0	0	0	0	0
Unknown monomer	0	14	26	21	33	31	42
DHBF Conversion (%)		0	5	12	1	6	7
DHBF Mass Balance (mmol)	545	568	552	512	588	520	565
(%)		104	101	94	108	95	104

Table D9. DHBF consumption and product formation for reaction with $Cu_{20}Mo_5$PMO catalyst

Conditions	**Cu20Mo5 100mg / DHBF / 3 ml MeOH / 300 °C**						
	Reaction Time (h) / Yield (mmol)						
Compound	**0**	**1**	**2**	**3**	**4**	**5**	**6**
Anisole	0	0	0	0	0	0	0
Benzene	0	0	0	0	0	0	0
DHBF	545	512	484	523	498	510	484
Ethoxy benzene	0	0	0	0	0	0	0
2-ethylphenol	0	0	0	0	0	0	0
2-ethylcyclohexanol	0	0	0	0	0	0	0
Ethyl benzene	0	0	0	0	0	0	0
Ethyl cyclohexane	0	0	0	0	0	0	0
Benzyl alcohol	0	0	0	0	0	0	0
cresol(o)	0	3	2	3	2	2	1
cresol (m/p)	0	0	0	0	0	0	0
cyclohexane	0	0	0	0	0	0	0
cyclohexanol	0	0	0	0	0	0	0
methylanisole	0	1	1	1	1	1	1
methylcyclohexane	0	0	0	0	0	0	0
methylcyclohexanol	0	0	0	0	0	0	0
phenol	0	1	0	0	0	0	0
toluene	0	0	0	0	0	0	0
Methyl-ethyl phenol	0	0	0	0	0	0	0
2,3 xylenol	0	1	3	5	6	6	7
2.4 xylenol	0	0	0	0	0	0	0
Unknown monomers	0	19	36	79	58	57	67
DHBF Conversion (%)		6	11.2	4	8.7	6.5	11.2
DHBF Mass Balance (mmol)	545	538	530	616	571	582	567
(%)		99	97	113	105	107	104

Table D10. DHBF consumption and product formation for reaction with $Cu_{20}Mo_{10}$PMO catalyst

Conditions	**Cu20Mo10 100mg / DHBF / 3 ml MeOH / 300 °C**						
	Reaction Time (h) / Yield (mmol)						
Compound	**0**	**1**	**2**	**3**	**4**	**5**	**6**
Anisole	0	0	0	0	0	0	0
Benzene	0	0	0	0	0	0	0
DHBF	545	509	542	472	446	534	495
Ethoxy benzene	0	0	0	0	0	0	0
2-ethylphenol	0	0	0	0	0	0	0
2-ethylcyclohexanol	0	0	0	0	0	0	0
Ethyl benzene	0	0	0	0	0	0	0
Ethyl cyclohexane	0	0	0	0	0	0	0
Benzyl alcohol	0	0	0	0	0	0	0
cresol(o)	0	3	3	2	4	2	3
cresol (m/p)	0	0	0	0	0	0	0
cyclohexane	0	0	0	0	0	0	0
cyclohexanol	0	0	0	0	0	0	0
methylanisole	0	1	1	1	1	1	1
methylcyclohexane	0	0	0	0	0	0	0
methylcyclohexanol	0	0	0	0	0	0	0
phenol	0	1	1	1	2	0	0
toluene	0	0	0	0	0	0	0
Methyl-ethyl phenol	0	0	0	0	0	0	0
2,3 xylenol	0	1	3	4	4	6	6
2,4 xylenol	0	0	0	0	0	1	1
Unknown monomer	0	18	32	32	38	53	49
DHBF Conversion (%)		7	1	14	18	2	9
DHBF Mass Balance (mmol)	545	534	582	511	454	597	555
(%)		98	107	94	83	109	102

Table D11. Methyl P-Toluene Sulfonate (MPTS) consumption and product formation for reaction with Cu_{20}PMO catalyst

Conditions	**Cu20 100mg / MPTS / 3 ml MeOH / 300 °C**			
	Reaction Time (h) / Yield (mmol)			
Compound	**0**	**2**	**4**	**6**
Anisole	0	0	0	0
Benzene	0	0	0	0
MPTS	636	0	0	0
Ethoxy benzene	0	0	0	0
2-ethylphenol	0	0	0	0
2-ethylcyclohexanol	0	0	0	0
Ethyl benzene	0	0	0	0
Ethyl cyclohexane	0	0	0	0
Benzyl alcohol	0	0	0	0
cresol(o)	0	0	0	0
cresol (m/p)	0	0	0	0
cyclohexane	0	0	0	0
cyclohexanol	0	0	0	0
methylanisole	0	1	1	1
methylcyclohexane	0	0	0	0
methylcyclohexanol	0	0	0	0
phenol	0	0	0	0
toluene	0	0	1	1
2,3-xylenol	0	0	0	0
2,4-xylenol	0	0	0	0
1,2- diphenyl ethane	0	2	1	1
Unknown monomer	0	40	72	72
MPTS Conversion (%)		N/A	N/A	N/A
MPTS Mass Balance (mmol)	1272	43	75	75
(%)		3	6	6

Table D12. Methyl P-Toluene Sulfonate (MPTS) consumption and product formation for reaction with $Cu_{20}Mo_{10}$PMO catalysts

Conditions	**Cu20Mo10 100mg / MPTS / 3 ml MeOH / 300 C**			
	Reaction Time (h) / Yield (mmol)			
Compound	**0**	**2**	**4**	**6**
Anisole	0	0	0	0
Benzene	0	0	0	0
MPTS	636	0	0	0
Ethoxy benzene	0	0	0	0
2-ethylphenol	0	0	0	0
2-ethylcyclohexanol	0	0	0	0
Ethyl benzene	0	0	1	0
Ethyl cyclohexane	0	0	0	0
Benzyl alcohol	0	0	0	0
cresol(o)	0	0	0	0
cresol (m/p)	0	0	0	0
cyclohexane	0	0	0	0
cyclohexanol	0	0	0	0
methylanisole	0	1	1	1
methylcyclohexane	0	0	0	0
methylcyclohexanol	0	0	0	0
phenol	0	0	0	0
toluene	0	0	1	2
2,3-xylenol	0	0	0	0
2,4-xylenol	0	0	0	0
1,2- diphenyl ethane	0	0	1	1
Unknown monomer	0	55	74	122
MPTS Conversion (%)		N/A	N/A	N/A
MPTS Mass Balance (mmol)	1272	56	78	122
(%)		4.4	6.2	9.6

Table D13. Benzyl Mercaptan (MPTS) consumption and product formation for reaction with Cu_{20} and $Cu_{20}Mo_xPMO$ catalyst

Conditions	**Catalyst 100mg / BM / 3 ml MeOH / 300 C / 6 hrs**					
	Catlalyst / Yield (μmol)					
Compound	**stock**	**Cu_{20}**	**$Cu_{20}Mo_{1.25}$**	**$Cu_{20}Mo_{2.5}$**	**$Cu_{20}Mo_{5.0}$**	**$Cu_{20}Mo_{10}$**
***Decane (Standard)**	103	103	103	103	103	103
Anisole	0	0	0	0	0	0
Benzene	0	1	0	0	0	0
Benzyl Mercaptan	1224	69	28	80	60	31
Ethoxy benzene	0	0	1	0	0	0
Phenylethyl alcohol	0	2	2	0	0	2
2-ethylcyclohexanol	0	0	0	0	0	0
Ethyl benzene	0	1	1	2	2	2
Ethyl cyclohexane	0	0	0	0	0	0
Benzyl alcohol	0	112	345	130	231	263
cresol(o)	0	0	0	0	0	0
cresol (m/p)	0	0	0	0	0	0
cyclohexane	0	0	0	0	0	0
cyclohexanol	0	1	1	1	1	1
methylanisole	0	1	1	1	1	1
methylcyclohexane	0	0	0	0	0	0
methylcyclohexanol	0	0	0	0	0	0
phenol	0	0	0	0	0	0
toluene	0	599	575	581	664	629
Methyl-ethyl phenol	0	0	0	0	0	0
2,3 xylenol	0	0	0	0	0	6
methoxymethylenedibenzene	0	9	2	5	4	6
Unknown monomers	0	255	335	240	348	555
Unknown dimers	0	64	18	46	34	46
BM Conversion (%)		94	98	93.5	95.1	98
BM Mass Balance (mmol)	2448	1045	1281	93.5	1288	1240
(%)		42.7	52.4	41.1	52.6	50.7

Appendix E Calcium

Table E1. BPE consumption and product formation for reaction with $Cu_{20}Ca_5$PMO catalyst at 290 °C

Conditions	Cu20Ca5 100mg / BPE / 3 ml MeOH / 290 C			
	Reaction Time (h) / Yield (mmol)			
Compound	0	1	2	3
anisole	0	26	96	123
benzene	0	2	5	6
benzyl phenyl ether	855	195	10	0
diphenyl ether	0	0	0	0
cresol (ortho)	0	34	62	67
cresol (para/meta)	0	0	0	1
cyclohexane	0	0	0	0
cyclohexanol	0	47	223	270
methylanisole	0	0	0	0
methylcyclohexane	0	0	0	0
methylcyclohexanols	0	9	41	106
phenol	0	469	379	81
toluene	0	725	890	872
xylenol	0	1	4	11

Table E2. BPE consumption and product formation for reaction with $Cu_{20}Ca_5$PMO catalyst at 300 °C

Conditions	Cu20Ca5 100mg / BPE / 3 ml MeOH / 300 C			
	Reaction Time (h) / Yield (mmol)			
Compound	0	1	2	3
anisole	0	43	104	108
benzene	0	4	7	8
benzyl phenyl ether	855	134	2	0
diphenyl ether	0	0	0	0
cresol (ortho)	0	52	70	50
cresol (para/meta)	0	0	0	1
cyclohexane	0	0	0	0
cyclohexanol	0	76	258	300
methylanisole	0	0	0	1
methylcyclohexane	0	0	0	0
methylcyclohexanols	0	21	89	116
phenol	0	494	187	25
toluene	0	788	862	825
xylenol	0	3	9	12

Table E3. DPE consumption and product formation for reaction with $Cu_{20}Ca_5$PMO catalyst at 290 °C

Conditions	Cu20Ca5 100mg / DPE / 3 ml MeOH / 290 C			
	Reaction Time (h) / Yield (mmol)			
Compound	**0**	**1**	**2**	**3**
anisole	0	0	1	1
benzene	0	3	24	54
diphenyl ether	314	345	355	294
cyclohexanol	0	0	12	36
methylcyclohexanols	0	0	0	6
phenol	0	1	1	1
toluene	0	1	0	0

Table E4. DPE consumption and product formation for reaction with $Cu_{20}Ca_5$PMO catalyst at 300 °C

Conditions	Cu20Ca5 100mg / DPE / 3 ml MeOH / 300 C			
	Reaction Time (h) / Yield (mmol)			
Compound	**0**	**1**	**2**	**3**
***Decane (Standard)**	103	103	103	103
anisole	0	0	2	2
benzene	0	0	80	81
diphenyl ether	314	325	251	276
cyclohexanol	0	0	48	49
methylcyclohexanols	0	0	15	15
phenol	0	0	1	1
toluene	0	0	0	0

Table E5. DHBF consumption with $Cu_{20}Ca_5$PMO catalyst at 290 °C

Conditions	Cu20 100mg / 500 umol DHBF / 3 mL MeOH / 290 C			
	Reaction Time (h) / Yield (mmol)			
Compound	**0**	**1**	**2**	**3**
DHBF	325	327	306	266

Table E6. DHBF consumption with $Cu_{20}Ca_5$PMO catalyst at 300 °C

Conditions	Cu20 100mg / 500 umol DHBF / 3 mL MeOH / 300 C			
	Reaction Time (h) / Yield (mmol)			
Compound	**0**	**1**	**2**	**3**
DHBF	325	313	254	217